

DOKUZ EYLÜL UNIVERSITY
GRADUATE SCHOOL OF NATURAL AND APPLIED
SCIENCES

OMNI-DIRECTIONAL VISION BASED
ENVIRONMENT SENSING FOR MOVEMENT
CONTROL OF MOBILE ROBOTS

by
Kali GÜRKAHRAMAN

June, 2011
İZMİR

**OMNI-DIRECTIONAL VISION BASED
ENVIRONMENT SENSING FOR MOVEMENT
CONTROL OF MOBILE ROBOTS**

**A Thesis Submitted to the
Graduate School of Natural and Applied Sciences of Dokuz Eylül University
In Partial Fulfillment of the Requirements for the Degree of Doctor of
Philosophy in Computer Engineering, Computer Engineering Program**

**by
Kali GÜRKAHRAMAN**

**June, 2011
İZMİR**

Ph.D. THESIS EXAMINATION RESULT FORM

We have read the thesis entitled “OMNI-DIRECTIONAL VISION BASED ENVIRONMENT SENSING FOR MOVEMENT CONTROL OF MOBILE ROBOTS” completed by **KALİ GÜRKAHRAMAN** under supervision of **PROF. DR. YALÇIN ÇEBİ** and we certify that in our opinion it is fully adequate, in scope and in quality, as a thesis for the degree of Doctor of Philosophy.


Prof. Dr. Yalçın ÇEBİ

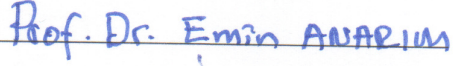
Supervisor


Prof. Dr. Erol UYAR

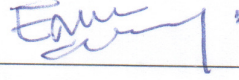

Yrd. Doç. Dr. Gökhan DALKILIÇ

Thesis Committee Member

Thesis Committee Member


Prof. Dr. Emin ANARIM


Yrd. Doç. Dr. Adil ALPKOÇAK


Prof. Dr. Emin ANARIM


Yrd. Doç. Dr. Adil ALPKOÇAK

Thesis Committee Member

Thesis Committee Member


Prof. Dr. Mustafa SABUNCU

Director

Graduate School of Natural and Applied Sciences

ACKNOWLEDGMENTS

The author extends his sincere thanks to his supervisor Prof. Dr. Yalçın ÇEBİ for his advice and guidance. This document has been produced through a thesis of degree of doctor of philosophy to Graduate School of Natural and Applied Sciences, Dokuz Eylül University, and this study has been supported partially by Dokuz Eylül University Scientific Research Project Coordination Unit (Project Number: 2009-KB-FEN-001) and Turkish Scientific and Technological Research Council, TÜBİTAK (Project Number: 108E156). The name of this TÜBİTAK Project is “Development of an Omni-Directional Vision System by Using Curved Mirror and Matrix Pattern Laser Dots”.

I am grateful for working together with Emre ÜNSAL in the TÜBİTAK Project whose subject is the part of this thesis.

Special thanks to Prof. Dr. Erol UYAR for his guidance in my research.

I am greatly indebted to Tuğrul SÜRÜCÜ, the owner of Alron Electronics for the support in developing the electronic and mechanical parts of my project in his company.

I am also greatly indebted to Mustafa KAYABAŞI for the support in developing the mechanical part of my project.

The work would have been more difficult to complete without the support of my students Utku İŞLER, Cüneyt YEŞİLKAYA, Sinan GÖKER, Ali ÖZDAŞ and Göksu YÖRÜK.

Kali GÜRKAHRAMAN

OMNI-DIRECTIONAL VISION BASED ENVIRONMENT SENSING FOR MOVEMENT CONTROL OF MOBILE ROBOTS

ABSTRACT

In this thesis, a mobile robot which is equipped with an omni-directional stereo vision system using laser dots and a tilt sensor in order to achieve autonomy is presented. The proposed steps of development of the omni-directional vision system are finding the laser dot centers, developing a mathematical model for computing the depth of points in the environment, finding the feature correspondences, and error analysis for distance calculation.

The vision system was comprised with two rectilinear curved mirrors and two Charge Coupled Device (CCD) cameras fitted in front of the mirrors to sense the environment in a stereo approach manner. The feature matching in stereo images was carried out by using dot-matrix laser pattern, and the pattern was obtained by using a Fiber Grating Device (FGD) scattering the laser light beam.

A polynomial based algorithm was developed to find the feature pixel matching in stereo images. A mathematical model based on triangulation method was developed and used to calculate the three dimensional locations of the real points in the environment by using matched pixel pairs in two images with the help of the matching algorithm.

An error calculation model based on the locations of pixels in the images was developed in order to test the vision system according to noisy data. With the help of the developed mathematical and error estimation models, the distances between the points on the objects in the environment and the vision system were determined; and by using synthetic data, the effects of noise on the error rates were analyzed.

According to the results of the experiments carried out with synthetic data, it was seen that errors were occurred depending on the limitation in the resolution of the image sensors for the pixels in the images without noisy locations. After the pixel locations were corrupted by adding noise to any values of their row and column values, the resultant errors were increased.

Although the error rates of X , Y and Z axes were increased according to the distance between the obstacle and the center of the vision system for the same horizontal/vertical plane, the average error rates for X (range) and Z (height) were decreased to 3.14% and 2.02%, respectively with the increasing distance between the vision system and horizontal/vertical planes for real world. In common, the main reasons of errors were the size and location of the laser points, reflection errors on the mirrors, sensitivity of the refractive lenses, misalignment of the mirror-camera pairs and limitation of the image resolution.

An interface between the user and the mobile robot consisting of two control options which were joystick and tilt sensor was used to obtain the user command for movement of the robot.

The system was combined with the vision system and tested in an environment having different sized and located obstacles. It was seen that, by using omni-directional vision system on a mobile robot, the obstacles can be easily detected and the mobile robot can easily pass between the obstacles.

Keywords: mobile robot, localization, mapping, curved mirror, omni-directional vision, stereo vision, fiber grating, tilt sensor

GEZGİN ROBOTLARIN HAREKET KONTROLÜ İÇİN TÜM-YÖNLÜ GÖRÜNTÜLEME TABANLI ORTAM ALGILAMASI

ÖZ

Bu tez çalışmasında, otonom davranabilmesi için lazer noktaları kullanan tümyönlü bir çiftli görüntüleme sistemi ve tilt sensörü ile donatılmış bir gezgin robot ele alınmıştır. Tümyönlü görüntüleme sisteminin geliştirilmesi amacıyla lazer noktalarının merkezlerinin bulunması, çevredeki noktalarının derinliğinin bulunması için matematiksel bir model geliştirilmesi, nokta eşleştirme ve uzaklık hesaplanmasında oluşan hataların analizinin yapılması planlanmıştır.

Çevreyi çiftli mantığı ile algılamak üzere karşılına iki adet kamera yerleştirilmiş iki adet eğrisel ayna ile görüntüleme sistemi oluşturulmuştur. Çiftli görüntülerde nokta eşleştirilmesi, matris desenli lazer noktaları kullanılarak gerçekleştirilmiş ve bu desen lazer ışığını saçan Fiber Izgaralı Aygıt kullanılarak elde edilmiştir.

Çiftli görüntülerdeki noktaların eşlenmesi için polinom tabanlı bir algoritma geliştirilmiştir. Üçlü metoduna dayanan bir matematiksel model geliştirilmiş ve eşleme algoritması yardımıyla bulunan iki görüntüdeki piksel çiftleri bu modelde kullanılarak çevredeki gerçek noktaların üç boyutlu konumları bulunmuştur.

Görüntüleme sistemini gürültü içeren veriler kullanarak test etmek için, görüntülerdeki piksel konumlarını kullanan bir hata hesaplama modeli geliştirilmiştir. Geliştirilen matematiksel ve hata modelleri yardımıyla, çevredeki cisimlerin üzerinde bulunan noktalar ile görüntüleme sistemi arasındaki mesafeler hesaplanmıştır ve sentetik veriler kullanılarak gürültünün hata oranları üzerindeki etkisi analiz edilmiştir.

Sentetik verilerle yapılan deney sonuçlarına göre, gürültü olmayan piksel konumlarıyla yapılan denemelerde hata oranlarının görüntü sensörlerinin

özünürlüklerinin sınırlı olmasından kaynaklandığı görülmüştür. Satır ve kolon değerlerine gürültü eklenerek bozulan piksel konumları hata oranlarının artmasına neden olmuştur.

Gerçek veriler kullanıldığında, aynı yatay / dikey düzlemler için, engel ile görüntüleme sisteminin merkezi arasındaki uzaklığa bağı olarak X , Y ve Z eksenindeki hatalar artmış olsa da, görüntüleme sistemi ile yatay / dikey düzlem arasındaki uzaklığın artmasına bağı olarak X (yatay uzaklık) ve Z (yükseklik) ortalama hata oranları sırasıyla %3,14 ve %2,02 değerlerine düşmüştür. Genel olarak, hataların ana sebepleri lazer noktalarının boyutları ve konumları, aynalardaki yansıma hataları, kırıcı lenslerin hassasiyeti, ayna-kamera ikililerinin doğrultusundaki sapma ve görüntü çözünürlüğünün sınırlı olması olarak sıralanmıştır.

Kullanıcı ile gezgin robot arasında bulunan ve kumanda kolu ve tilt sensörü olarak iki seçenek içeren bir ara yüz yardımıyla kullanıcı komutu elde edilerek robot hareket ettirilmiştir.

Görüntüleme sistemi gezgin robota monte edilmiş ve farklı boyutlarda ve konumlarda yerleşik engellerin bulunduğu bir ortamda test edilmiştir. Tümyönlü görüntüleme sistemi kullanan bir gezgin robotun engelleri kolayca tespit edebildiği ve engeller arasından kolayca geçebildiği görülmüştür.

Anahtar Sözcükler: gezgin robot, konumlandırma, haritalama, eğrisel ayna, tümyönlü görüntüleme, çiftli görüntüleme, fiber ızgaralama, tilt sensörü

CONTENTS

	Page
Ph.D. THESIS EXAMINATION RESULT FORM.....	ii
ACKNOWLEDGEMENTS.....	iii
ABSTRACT	iv
ÖZ.....	vi
CHAPTER ONE - INTRODUCTION	1
1.1 Overview	1
1.2 Aim of the Study and Contributions.....	3
1.3 Road Map.....	4
CHAPTER TWO - RELATED WORKS.....	6
2.1 Human Computer Interface.....	6
2.2 Localization and Mapping of The Environment	11
CHAPTER THREE - MAPPING AND MOVEMENT TECHNIQUES	19
3.1 Omni-Directional Vision Systems for Localization and Mapping.....	19
3.1.1 Omni-Directional Vision Techniques	21
3.1.1.1 Rotating Camera	21
3.1.1.2 Multiple Cameras	21
3.1.1.3 Special Lens and Curved Mirror	22
3.1.2 Central and Noncentral Omni-Directional Vision Systems	23
3.1.2.1 Mirrors with Central Projection	24
3.1.2.2 Mirrors with Noncentral Projection.....	28
3.2 Control Techiques	33
3.2.1 Joysticks	34
3.2.2 Tilt Sensors.....	34
3.3 Movement of a Mobile Robot with Two Actuators	35
CHAPTER FOUR - MOBILE ROBOT SYSTEM.....	39
4.1 General Overview of Mobile Robot System.....	39
4.1.1 Human Computer Interface (HCI)	40

4.1.2 Computer	40
4.1.3 Base Part.....	41
4.1.4 Vision System.....	42
4.1.5 Energy Supply/Batteries.....	42
4.2 Human Computer Interface (HCI)	42
4.2.1 Joystick for Hand Based Control.....	42
4.2.2 Tilt Sensor for Hands Free Control.....	43
4.2.2.1 Communication Between Computer and Tilt Sensor.....	44
4.3 Base Part	45
4.3.1 Control Unit and Drivers.....	45
4.3.1.1 Communication Between Computer and Control Unit.....	45
4.3.1.2 Driving The Motors	46
4.3.1.3 Driving The Laser Light Source.....	47
4.3.2 Navigation Platform.....	48
4.3.2.1 Mechanical Properties of The Platform.....	48
4.3.2.2 Motors.....	49
4.3.2.3 Proximity Sensors.....	50
4.4 Vision System	51
4.4.1 Basic System.....	51
4.4.2 System Components.....	53
CHAPTER FIVE - DETECTION OF LASER DOTS IN 2D IMAGE.....	57
5.1 Separation of Laser Dots from The Background	57
5.2 Finding The Locations of Laser Dots.....	59
5.3 Circular Neighborhood Structure of Laser Dots	60
5.4 Finding The Centers of Laser Dots	61
CHAPTER SIX - OMNI-DIRECTIONAL VISION SYSTEM.....	66
6.1 Determination of 3D Locations of Laser Dots in The Environment.....	67
6.2 Error Calculation According to Row and Column Values	69
6.3 Calculating The Locations, Errors and Calibration.....	70
6.3.1 The Sources and Reasons of Errors	70
6.3.1.1 Matching The Pixels for Environment Without Obstacle.....	72

6.3.1.2 Matching The Pixels for Environment With Obstacle.....	77
6.3.1.3 Calculating The Distance and Height	78
CHAPTER SEVEN - EXPERIMENTS	85
7.1 Preliminary Work	85
7.1.1 Applications Without Matching Algorithm.....	85
7.1.2 Applications With Matching Algorithm.....	87
7.1.3 Problems and System Improvements	90
7.2 Experiments After Vision System Improvement	90
7.2.1 Experiments With Synthetic Data.....	90
7.2.2 Experiments With Real Data	95
7.3 Experiments for Mobile Robot.....	103
CHAPTER EIGHT - CONCLUSIONS	105
8.1 Omni-directional Vision System.....	105
8.2 Integrated Mobile Robot.....	108
8.3 Future Work.....	108
REFERENCES	110

CHAPTER ONE

INTRODUCTION

1.1 Overview

Researches on robotics have been carried out for many years. Although early researches usually focused on the development of the robots which were used in the production plants, studies on mobile robots have become widespread with the improvements in the computer technologies. Especially in the last decade, studies on autonomous mobile robots have been grown up.

Many researchers interest on robotics in order to build a robot as autonomous as possible. For a mobile robot, the autonomy can be defined as the ability of sensing its environment and navigating to the target area safely through the obstacles without any help. A wheelchair for disabled people is also a kind of autonomous robot. The wheelchairs are equipped with necessary devices including assistant software in order to provide mobility to the user in the environment. Many people with disabilities are not adequately served by traditional powered wheelchairs. Most of the disabled people can use powered wheelchair but find them hard to use in terms of physical and cognitive manner. By improving mobility and autonomy, the quality of daily life will be improved for disabled people.

For a safe navigation, the user should be able to interact with the robot by using an interface and structure of the environment should be obtained for localization and mapping. Localization and mapping are defined basically with the information of the current position of the robot and structure of the environment, respectively. Therefore researches in robotics can be classified as:

- *Advanced Interface*: Different methods enabling the user to give commands (“forward”, “stop”, “left” and “right”) to the robot such as voice (Komiya et al., 2000 and Simpson & Levine, 2002), head movement (Bauckhage et al., 2006) and facial expression (Faria et al., 2007) can be used. There may also be different interface techniques to monitor a specific user feature such as gaze information for

obtaining the user command. Gaze information can be taken by electrodes (Barea et al., 2000) connected to the face to get the Electroculography (EOG) signals which corresponds to gaze angle of the user as well as taken by image of the eyes with a camera system (Adachi et al., 2004).

- *Localization and Mapping*: Sensors such as odometry (Kriegman et al., 1989), laser/ultrasonic range finders (Gasparri et al., 2007 and Duan & Cai, 2008) and vision systems (Kriegman et al., 1989) or hybrid system using different sensor types together (Kriegman et al., 1989 and Chang et al., 2008) are used to find current position and to avoid obstacles for the mobile robot in order to navigate to a determined position.

Interactions between the users and the mobile robot can be hand-based control (e.g. joystick, keyboard, mouse, and touch screen), voice-based control (speech command), vision-based control and other sensor-based control such as tilt sensor and pressure sensor (Karray et al., 2008).

Since mapping of wider area of the environment can be made for a specific time period with respect to ultrasonic or laser range finder, the vision system is preferred in many studies. Although perspective cameras can provide more information about the surrounding environment, they have limited field of view. Omni-directional vision systems have been used to solve this problem (Nayar, 1997 and Baker & Nayar, 1999) by using curved mirror located in front of perspective camera.

Stereo omni-directional vision system can be used to obtain the three dimensional locations of points in the environment with a wide field of view (Southwell et al., 1996 and Gluckman et al., n.d.). In a stereo vision system, pairs of correspondences in two images are used to compute the depth of the related real points.

Structured light pattern which is projected to the interested area in real world has been used for matching of the correspondences in stereo images to reduce the computational cost and matching problems in image processing methods (Orghidan et al., 2005).

However, to the best of our knowledge, there has not been any study which combines mobile robot with omni vision and structured light obtained by using fiber grating device which is projected to the whole environment. Therefore, in order to fulfill of this lack, this study was proposed.

1.2 Aim of the Study and Contributions

The major aim of the study is to develop a stereo omni-directional vision-based mobile robot as an assistive technology to enhance the mobility of disabled people with less difficulty.

During this study, a mobile robot which consists of mainly an omni-directional stereo vision system with fiber grating device and tilt sensor will be developed. The robot will sense the locations of the obstacles by viewing a structured light of dot-matrix laser pattern projected to the environment and processing related images. The matrix pattern of laser light beam will be obtained by using the fiber grating device. The correspondence pairs of image points of laser dots in stereo images are used to calculate the three dimensional locations of the real laser dots in the world. The obstacles can be determined by computing the depths of sufficient number of points in the environment. The localization and mapping can be achieved by using the locations of points on the obstacles.

The vision system will be tested with real and synthetic data and the robustness of the system to noisy data will be analyzed by synthetically produced stereo images with the help of projection equations.

The user interacts with the mobile robot through a dual axis tilt sensor fixed to his / her head. The direction of user head indicates one of the commands which are “left”, “right”, “forward” and “stop” to control the movement of the robot.

The main contributions of the study are:

- In this work, a unique omni-directional vision system with dot-matrix laser pattern will be developed and applied. It is proposed to obtain the 3D structure of the environment with a wide field of view for localization and mapping.
- The dot-matrix laser pattern is assumed to be a solution of the problem of difference between the values of the pixels of different mirrors. The stereo matching is much easier and has much less computational cost with relatively low amount of error by using laser dots to be matched in two mirrors.
- A hands-free control of robotic wheelchair is aimed by using dual axis tilt sensor to determine the head direction of the user. The HCI including tilt sensor is considered to provide low computational cost and to be inexpensive to purchase for disabled people.

1.3 Road Map

In Chapter 2, the related works about the basic components of a mobile robot related to this study are presented. The researches on human computer interface methods and different omni-directional vision systems are given. The studies using structured light pattern are also mentioned.

Chapter 3 begins with the omni-directional vision techniques, then types of curved mirrors and their projection principles are detailed. The information about joystick and tilt sensor types is also given. Finally the kinematics of a mobile robot with two actuators is presented.

In Chapter 4, the detailed explanations of the components of the mobile robot developed in this study and their functions are given. The relations between the components and the flowchart of how the mobile robot works are explained.

In Chapter 5, the algorithm and image processing steps for isolating the laser dots from the background scene in the images and finding the laser dot centers are provided.

In Chapter 6, the mathematical model of finding 3 dimensional locations of a real point and its error calculation, and explanation of error sources in the system and algorithm for matching of laser dot centers in stereo images are given.

In Chapter 7, all the experiments and related results are presented.

Chapter 8 includes the conclusions and future work.

CHAPTER TWO

RELATED WORKS

The products developed in visual, audio and sensor fields; and with the increasing power of computational capacity in computer world, the role of human computer interface (HCI) has become widespread in robotics. Single type interface as well as hybrid systems using combination of different types of interface are used to control the robots through computer. With the help of the interfaces and environment sensing systems, the information of the current location of the robot and the route to the target place in the environment can be determined by a mobile robot for a safe navigation.

2.1 Human Computer Interface

Different methods are used by human to interact with computers. An HCI enables user to interact with the computer via its channels including inputs and outputs. The researches in developing new technologies enable to produce more reliable and high quality interfaces.

Functionality and usability are the basic criteria to evaluate the value of developed HCI systems (Fakhreddine et al., 2008). Functionality is the set of activity that the user can do efficiently by using the related interface system. Usability of an HCI is the degree of efficiency during usage of functions that the interface provides to the user to achieve some goals. Therefore, for a particular function to be performed, the value of functionality is related to the usability of that function.

The architectural content of an HCI system depends on the number and types of input and output it has. The interaction between the user and the computer is realized through these inputs and outputs. The single type interfaces are divided into three categories (Fakhreddine et al., 2008):

- Visual-based,
- Audio-based,

- Sensor-based.

One of the most interesting topics is hands-free control of the wheelchair. There have been many researches about the advanced interface between the user and the robotic wheelchair through which the commands of the user is obtained to hands-free control the motion of the wheelchair. In advanced interface researches the main topic is how the command of the user (such as “forward”, “stop”, “left”, “right” and “stop”) is obtained. The visual-based and audio-based categories and some sensor types in sensor-based category provide hands-free control facility to the user.

In visual-based interaction, the command and request of the user are recognized by visualization. The study of Faria et al. (2007) aims to obtain facial expression representing user command by using a digital camera for the users who are unable to move even their heads. The facial expression is obtained by image processing algorithms including edge detection and color segmentation for feature detection of the face. The user command is distinguished by neural network application to control the electric wheelchair.

Hu et al. (2010) also uses visual-based system; and comparison of lips location algorithm is used to recognize the head gesture for determining the user command (Figure 2.1). A search window is moved to scan all possible positions of the images for the lips. First, the lips are detected by an algorithm and marked as shown in green rectangular window. After the detection, the position of the lips is determined according to the rectangular red window centered in the middle of the image to determine the direction of the head. Another study including an algorithm of gesture analysis is made by Kang & Katupitiya (2004) to determine the hand direction in order to obtain the user command.

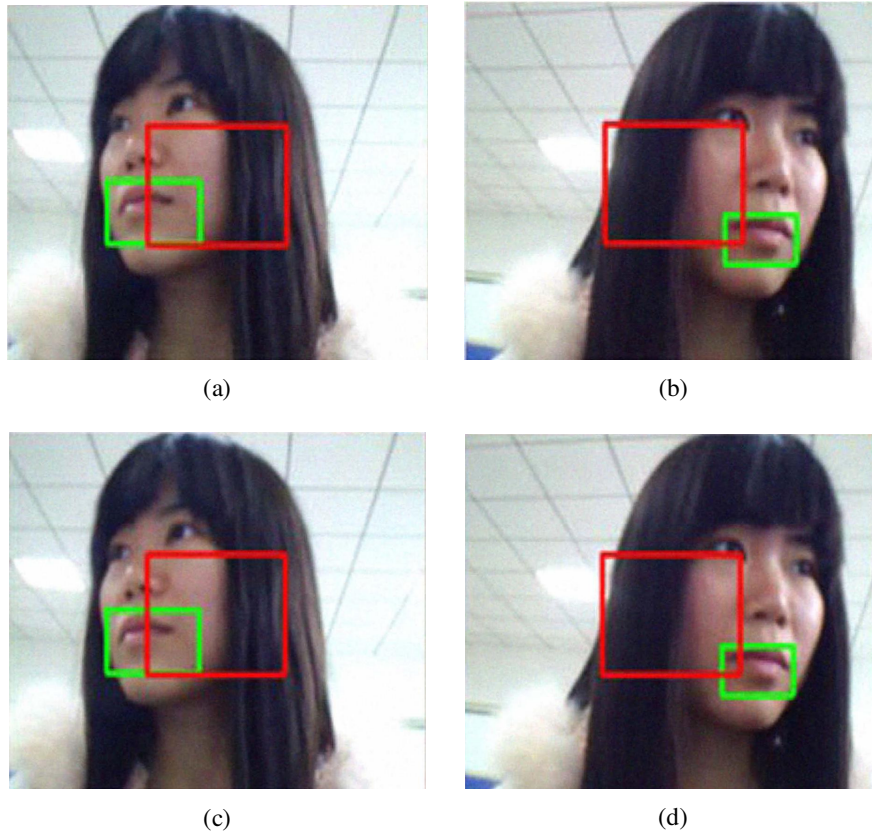


Figure 2.1 Head directions: left (a), right (b), up (c) and down (d) are determined according the position of the lips (Hu et al., 2010).

In the study of Bauckhage et al. (2006), a classification algorithm is used for face detection to follow the head movement of the user which is considered as body movement tracking subject, in order to control the motion of wheelchair. By using another visual-based method called gaze detection (eye movement tracking), not only the direction of the head is determined but also the attention of the user is known to reveal the insistence of the user. The study of Adachi et al. (2004) aims to detect gaze direction by using real-time stereo vision, a range sensor and a map to guess the attention point of the user in the environment.

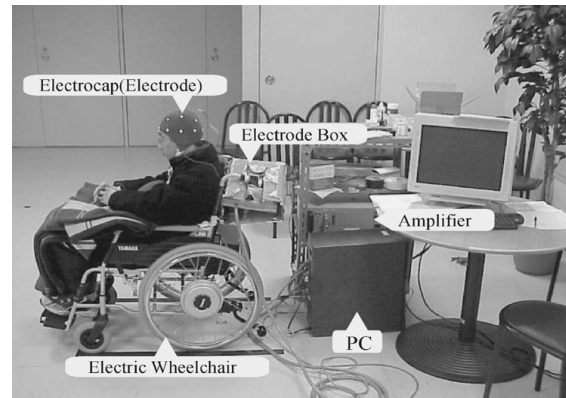
The researches based on the vision system for estimating the user command generally aims to develop smart interfaces. However the decision algorithms used in these systems, have some difficulties of image processing steps and need relatively more computational cost; and the hardware of the systems is more expensive products.

In the interaction of audio-based category, the user command is obtained from the voice of the user by using speech recognition algorithms. Komiya et al. (2000) and Simpson & Levine (2002) are the studies to guide the wheelchair by user voice. In the study of Komiya et al. (2000), experimental comparison of the commands obtained from a keyboard and user voice is carried out. In the other study of Simpson & Levine (2002), the wheelchair is controlled with voice in combination with a navigation assistance including sensors to sense the obstacles in the environment.

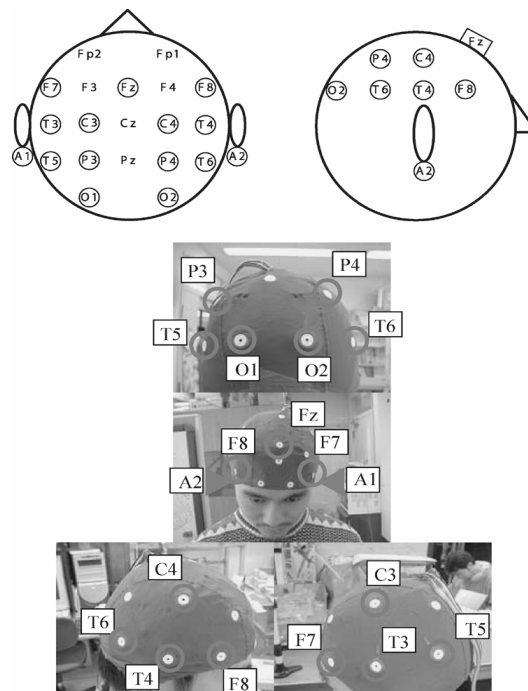
The voice signal may be more trustable than visual signal with respect to certainty of what the command is. However due to its limited bandwidth, and time delay and failure for speech recognition, there may be some problems in controlling a mobile robot especially in frequent small regulation in wheelchair speed Simpson & Levine (2002).

The sensor-based interface may include single or combination of different types of sensor. In different application areas, a variety of sensor types are used. Mouse, keyboard and joystick are the samples for sensor-based interfaces for HCI usage (Murata, 1991). Although these devices have widely used in powered wheelchair, some of the disabled people may find hard or impossible to use them due to the disability level of their body. Chen et al. (2003) uses a tilt sensor with analog output called Magneto Resistive Tilt Sensor fitted onto the user's head to determine the direction of the head and to control the direction and the speed of the wheelchair without using hands. A tilt sensor and a telemetry transmission system are used in the study of Joseph & Nyugen (1998) to transmit data of the head movement to the control unit in a wireless manner. A multilayer neural network is used to train the system for the head movement of the user.

Researches on EEG signal-based control systems have been made such as by Tanaka et al. (2005) (Figure 2.2a), Lakany & Conway (2005) and Edlinger & Guyer (2005).



(a)



(b)

Figure 2.2 Experimental system (a) and electrode placement (b) for wheelchair control with EEG signals (Tanaka et al., 2005)

These studies focus on analyzing the EEG signal to determine the user's desire for the direction of the wheelchair. Since several electrodes must be used to obtain the EEG signals from the brain (Figure 2.2b), there are several physical problems during the usage. There may be high error rates during the signal processing because the EEG signal is very sensitive to noise and to other activities of the human body. There have been other studies such as using EOG and EMG signals to detect the eye movement (Hashimoto et al., July 2009). These signals are also sensitive to noise and

the user command may not be determined with exact confidence. Montesano et al. (2010) uses touch screen as an input device to control the navigation of the wheelchair. However it still needs hand for navigation of the wheelchair.

There are also hybrid (multimodal) interface systems which are combination of multiple single type interfaces from any categories mentioned above. Moon et al. (2003) uses EMG signal, face directional gesture and voice to determine the user intention. In the study of Ronzhin & Karpov (2005) voice and head direction information are both used to estimate the user command. The hybrid interfaces may ensure the system to recognize the user command but still have problems of single type interfaces included.

2.2 Localization and Mapping of The Environment

In robotics, localization and mapping are the basic subjects relating to the operation of determining the place or point that the mobile robot is standing according to some reference points in the environment and the procedure of obtaining the two dimensional (2D) or three dimensional (3D) structure of the environment in which the mobile robot is present.

In 3D image construction from 2D images, different approaches have been used. Shape-from silhouettes, multi-view geometry and model-based methods are most known methods (McInerney & Terzopoluos, 1996; Hartley & Zisserman, 2003). 3D construction of objects by using 2D images uses a sequence of images taken from cameras to determine the structure of the scene. This can be achieved by using the silhouettes in 2D images of a non moving object with image segmentation (Azevedo et al., 2010). In multi-view geometry, which is a stereo-based method, image of an object is taken at different viewpoints to determine the structure and the position of the object by using some techniques such as triangulation (Hartley & Zisserman, 2003), epipolar geometry (Zhang, 2003) and rotation and translation technique (Hartley & Zisserman, 2003) which uses rotation and camera calibration matrices.

In multi-view geometry, structure from motion is another method used for moving objects (Dellaert et al., 2000). The images of the scene representing motion can be used in structure from motion method to construct the 3D structure or to determine position of the object. Other model-based methods use a prior geometry of the object as a reference data to interpret the presented images (Siebert & Marshall, 2000). In order to construct 3D structure of complicated shapes such as human body, volumetric methods have been used as alternative techniques. A volumetric method using voxels is used for 3D construction by Azevedo et al. (2010); another study (Azevedo et al., 2009) for comparison of structures from motion and volumetric method is also presented.

For the safe navigation of a mobile robot, the most critical factors are localization, mapping and distance measurements. For localization and mapping, single model methods such as using ultrasound (Gasparri et al., 2007), laser (Duan & Cai, 2008), cameras (Kriegman et al., 1989) or hybrid model (Chang et al., 2008) can be used as different kinds of sensory systems. In study of Gasparri et al. (2007), an algorithm was developed for localization of the robot without the feature-based knowledge of the environment by the help of encoders and sonar rangefinder. Duan & Cai (2008) designed an adaptive particle filter for simultaneous localization and mapping by using laser rangefinder. Kriegman et al. (1989) used a stereo vision system with odometry to develop an uncertainty model of uncertain sensor data for motion and stereo in previously unknown indoor environment.

A trajectory planning strategy was presented in the study of Chang et al. (2008) for a wheeled mobile robot equipped with a vision system and a laser rangefinder to navigate towards a goal in an environment with obstacles. The obstacle in the environment is detected first by laser rangefinder according to received laser beam reflected through a mirror (Figure 2.3).

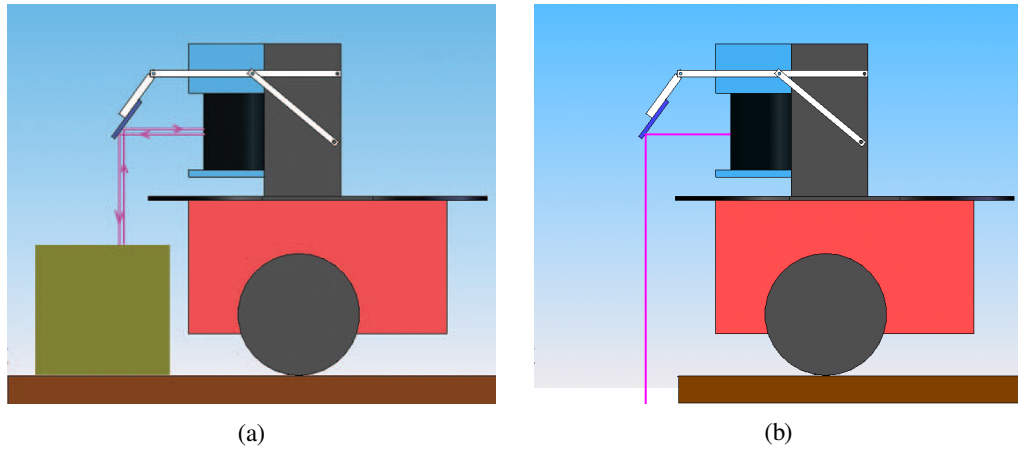


Figure 2.3 Applications of the proposed method (Chang et al., July 2008). Short obstacle (a) and missing floor (b)

In the same study, the size of the obstacle detected is determined by edge detection procedure applying on the image taken from the camera installed on mobile robot (Figure 2.4).

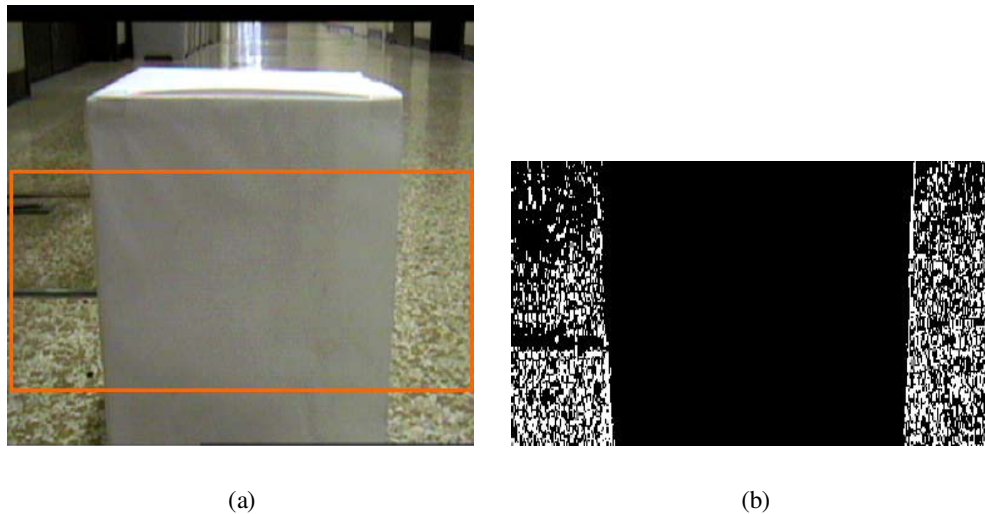


Figure 2.4 Original image (a) and detected edge (b) for edge detection procedure (Chang et al., July 2008)

Since perspective stereo cameras can provide more information of the surrounding environment, they are now widely used, but they have limited FOV (Figure 2.5a) and matching a pixel pair in the images obtained from both cameras has some difficulties in stereo visualization such as high computational cost (Wang & Hsiao, 1996).

Omni-directional vision systems have been used to solve the limited FOV problem (Nayar, 1997 and Baker & Nayar, 1999). In these systems, a classical camera with limited FOV (Figure 2.5a) is fixed in front of a curved mirror such as conical, hyperbolic or parabolic mirror (Figure 2.5c); therefore, a wider view of the environment is appeared in the curved mirror (Figure 2.5b).

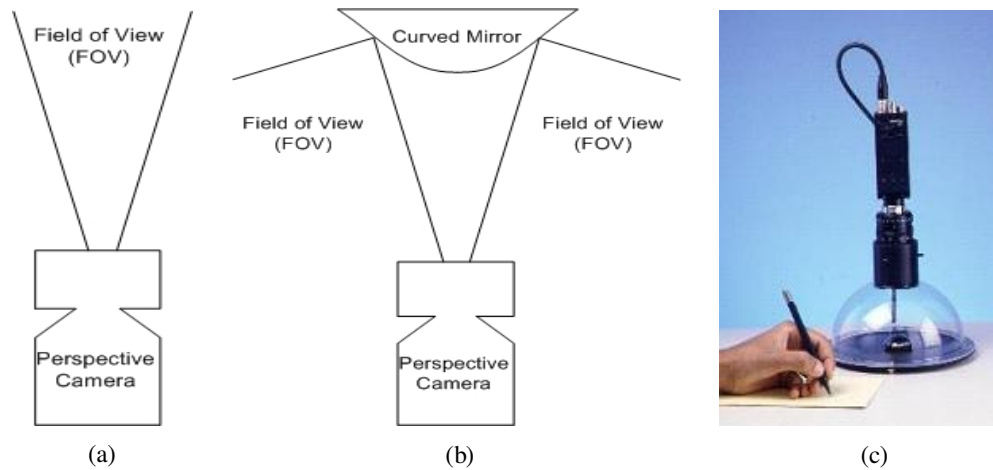


Figure 2.5 Limited FOV (a), wide FOV (b) and Omni-directional vision system (Nayar, 1997) (c)

As mentioned in the work published by Gluckman et al. (n.d.), two parabolic mirrors and two cameras fixed in front of each mirror were used. The distance of a point in the real world, P whose pair of image correspondences is p and p' (Figure 2.6), from the vision system was calculated by triangulation method. During the implementation with multiple cameras, the alignments of two cameras in the stereo system cannot be exactly the same and so can the focal distances. Since the image sensors of two cameras may differ, pixel values of a point in two sensors are not exactly the same.

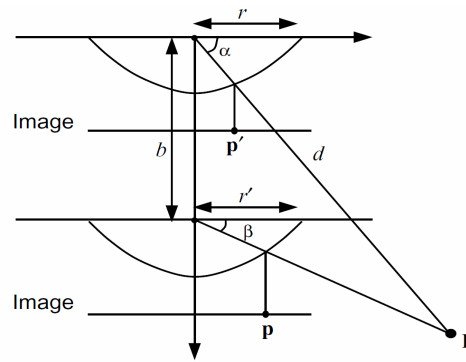


Figure 2.6 Triangulation and the computation depth (Gluckman et al., n.d.)

In order to have same characteristics such as response, gain and offset of the vision system, a number of studies have suggested the use of a single camera in the stereo systems (Nene & Nayar, 1998; Gluckman & Nayar, 1999; and Gluckman & Nayar, 2002; Southwell et al., 1996). In these studies, shapes and number of mirrors may differ (Figure 2.7). However, the common point in these studies is that the visualization is realized by using more than one image.

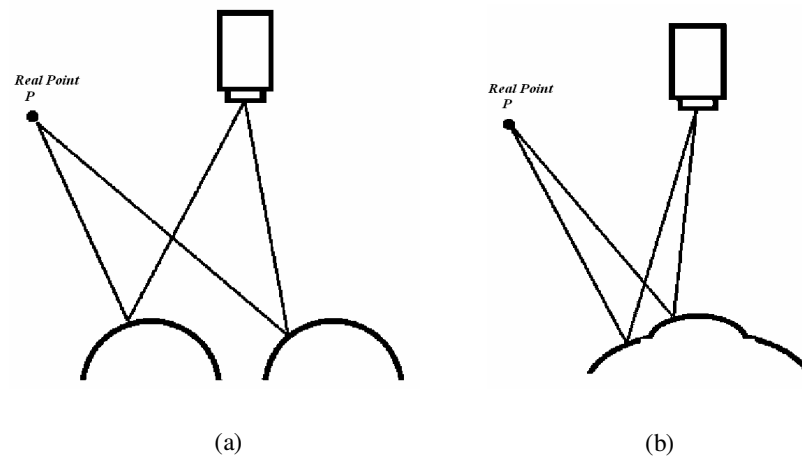


Figure 2.7 Single camera stereo systems with two spherical mirrors (a) and two stacked convex mirrors (b) (Gluckman & Nayar, 2002)

In a stereo system with a single camera, the calibration procedure is difficult and the stereo matching is much complex (Nene & Nayar, 1998). In stereo systems, pixels of an image in one mirror should be matched with the pixels of an image in the other mirror. This matching procedure is done with image processing algorithms

such as Sum of Squared Differences (SSD), Real-Time Correlation-Based Stereo method and Dynamic Programming method (Faugeras, 1993), but the computation cost and the amount of error are determined to be relatively high.

A hybrid system including omni-directional and perspective cameras was used (Bastanlar et al., 2010) to study on structure-from-motion by using feature matching and epipolar geometry between hybrid images. Since the image processing techniques such as epipolar geometry (Svoboda et al., 1998) can poorly find corresponding features in a pair of images of the same scene for omni-directional cameras due to the low resolution problem, structured light patterns (Orghidan et al., 2005; Orghidan et al., 2007) are used for matching. In the works carried out by Orghidan et al. (2005) and Orghidan et al. (2007), an omni-directional vision system with a laser beam reflected by a conic mirror as a structured light was developed (Figure 2.8a). Although the aim of this system was to develop full 3D model of an indoor environment, the sensor used in the system could recover only one line of 3D dots at a given position (Figure 2.8b).

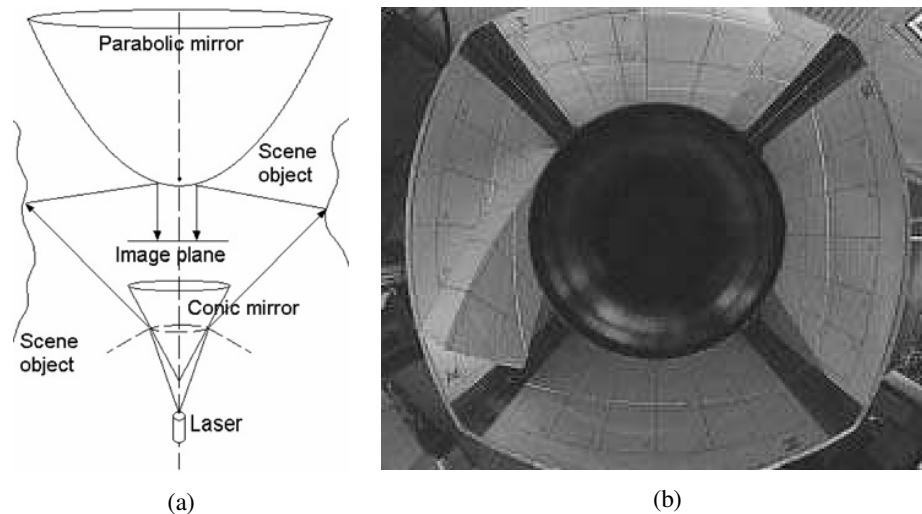


Figure 2.8 Omni-directional camera with structured light projector (a) and the scene image with laser pattern (b) (Orghidan et al., 2005)

The average distance calculation error rate was found as 7.69% in the work carried out by Orghidan et al. (2005) and the accuracy for detection of 3D points was improved in the work carried out by Orghidan et al. (2007). The experimental results

were for a range within 1000 mm in both studies. The error rates were increased with the increasing distance of the related points from the vision system.

There are some studies (Yamaguchi & Nakajima, November 1990; Habib, 2007; and Nakazawa & Suzuki, 1991) using Fiber Grating Device (FGD) and classical camera with limited FOV to detect obstacles, tracking and 3D construction of the environment (Figure 2.9c and Figure 2.9d). In these studies, a dot-matrix laser pattern is obtained by passing the laser through the FGD (Figure 2.9a and Figure 2.9b). However, to the best of our knowledge, for distance calculations, the usage of laser light scattered through FGD together with curved mirror has not been proposed in any of the previous studies.

In the study of Kim & Suga (2007), omni-directional vision-based moving obstacle detection for a mobile robot was defined by Kim and Suga. The method includes optical flow pattern on an omni-directional mirror. By using the method developed in this study, the direction of the movement can be determined.

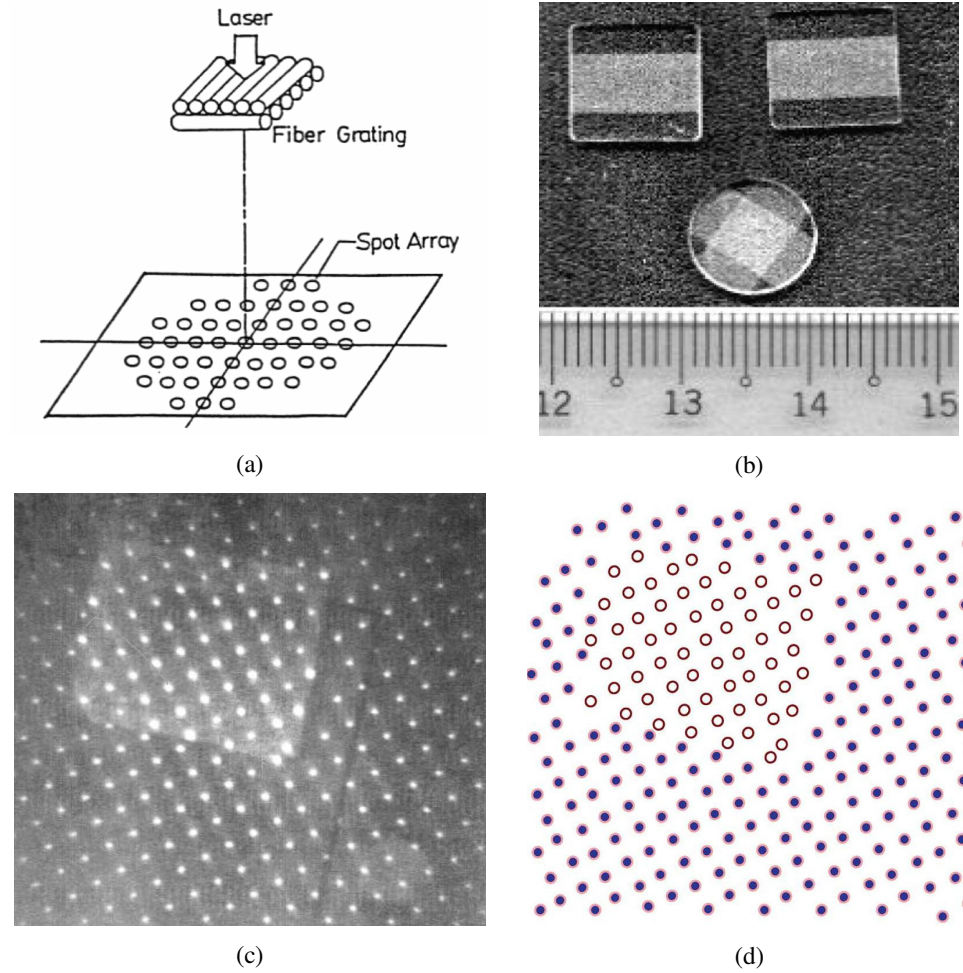


Figure 2.9 Generation of dot-matrix laser pattern with Fiber Grating Device (a), one-sheet and two-crossed-sheet samples of FG (b), image including object with laser pattern and highlight of displaced laser spots for obstacle detection (d) (Habib, 2007)

CHAPTER THREE

MAPPING AND MOVEMENT TECHNIQUES

In the mobile robot system, an omni-directional vision system and a tilt sensor can be used for localization of the mobile robot and mapping of the environment, and human computer interface, respectively. In this chapter, omni-directional vision techniques, types of tilt sensor and kinematics of a mobile robot with two actuator wheels are detailed in order to explain the basics of the components used in the work.

3.1 Omni-Directional Vision Systems for Localization and Mapping

For autonomous systems, especially mobile robots, there are two major information should be known to be able to navigate in the environment. First, the location of the mobile robot must be known and second, the path of the navigation must already be determined. The process to find the information about the localization of the robot is called localization. In this process, the position of the robot is determined with respect to the obstacles in the environment. The position can be defined by the distances between the mobile robot and the obstacles or a reference point in the environment. The route is the path which is wide enough for the mobile robot to pass through and without any obstacle to navigate safely. Also the slope of the floor must be suitable for safe navigation. The information for the localization and the obstacle for safe route must be acquired frequently. The frequency of the acquisition must be high enough for a mobile robot in order to process the information and update the route to navigate with a specific speed.

In mobile robotics, if localization is achieved by the robot, the distance and the direction of a target point to navigate can be determined. The localization of the point is the determination of the distances between the point and the objects in the environment. The directions such as angular positions of the objects with respect to the point are also important for the localization. A vision system fixed to the mobile robot can be used to obtain the 3D structure of the environment by using the distances and the directions of the objects in the environment with respect to the

mobile robot. The 3D structure of the environment is used for localization and finding the position of the obstacles for safe navigation.

Laser and ultrasonic sensors, vision sensor using cameras or hybrid systems including both sensor types have been used to find localization and route of the mobile robot (Biber et al., 2005 and Chang et al., 2008). The sensor types without camera system can only determine a section structure of the environment at a time. Although camera systems have been used in robotics for a long time, they have become relatively more important and used in wide field of robotics since the increase in processing speed of the computers in recent years.

The camera types and the secondary devices used in the vision system may vary. The numbers of cameras and mirrors can be different such as single camera and single mirror pair, single camera and two mirrors and two cameras and two mirrors. The laser light technologies have been used in limited fields of the vision system applications to obtain the structure of the environment.

For localization and mapping different techniques were developed, and in these techniques (Correa et al., 2006; Su et al., 2006; and Shimizuhiro & Maeda, 2003), the vision systems are comprised of a combination of video cameras and mirrors in order to achieve a safe navigation of the mobile robot.

Although perspective cameras are widely used in computer vision systems, they have limited Field Of View (FOV). However, curved mirrors used in the vision systems can have up to 180 degree of vertical and 360 degree of horizontal view. This wide FOV can be obtained by a visualization system called omni-directional, which has been widely used especially during last decade (Nayar, 1997; Gluckman & Nayar, 1999; Correa et al., 2006; Su et al., 2006 and Yagi & Yachida, 2002).

3.1.1 Omni-Directional Vision Techniques

Although perspective cameras are widely used in computer vision, they have a limited FOV. A wide FOV such as 360 degrees which is called panoramic view can be obtained using rotating camera, multiple cameras and special lenses such as fish-eye lens (Aizawa et al., April 2004). Panoramic view can also be obtained by a curved mirror across which a classical perspective camera is placed. The vision technique to obtain panoramic view is called omni-directional vision and has been widely used as the speed of processing in the hardware and the software technologies improved.

3.1.1.1 Rotating Camera

Rotating a camera around an axis is an ordinary method to obtain omni-directional view (Figure 3.1). Images are taken with the camera rotating with a constant angular speed and then the images taken frequently are combined to complete the panoramic view of the environment. The resolution of the horizontal axis is directly dependent to the angular resolution of the rotation (Aizawa et al., April 2004). It is possible to obtain images with high resolution by low angular velocity and controlling the rotation accurately.

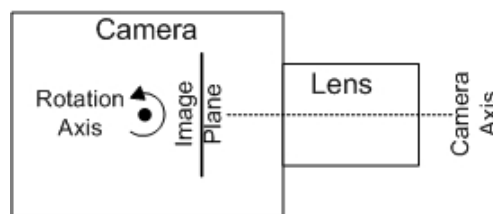


Figure 3.1 Rotating camera

3.1.1.2 Multiple Cameras

Using multiple cameras is an alternative technique to rotating the camera. The axes of the cameras must intersect at the same point in order to obtain single viewpoint projection (Figure 3.2) (Yagi, 1999).

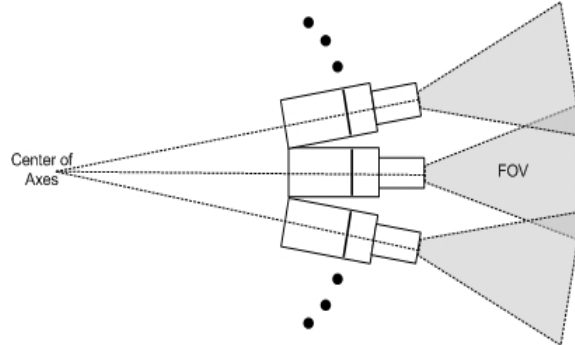


Figure 3.2 Multiple cameras

The differences in some properties such as offset and gray level of the cameras, cancellation of overlap of FOVs, alignment and calibration of all the cameras are the major difficulties of this method. A hardware requirement in order to record images obtained from multiple cameras is also a problem (Yagi, 1999).

3.1.1.3 Special Lens and Curved Mirror

In a dioptric system, which is one kind of omni-directional system, a special lens with wide angle view is used (Figure 3.3a and Figure 3.3b). Another kind of omni-directional vision system is catadioptric system in which a combination of some mirrors and lenses is used (Figure 3.4a and Figure 3.4b).



(a)



(b)

Figure 3.3 Omni-directional dioptric vision system with fish-eye lens (a) and image taken by a fish-eye lens (Court, 2008) (b)

The omni-directional vision can also be achieved by a curved mirror such as spherical, conical, parabolic or hyperbolic and a conventional camera pair (Baker & Nayar, 1999). In omni-directional vision system using such a mirror (Figure 3.4a), there is almost no need to rotate the camera while the objects in the environment can always be kept in sight as seen in Figure 3.4b.

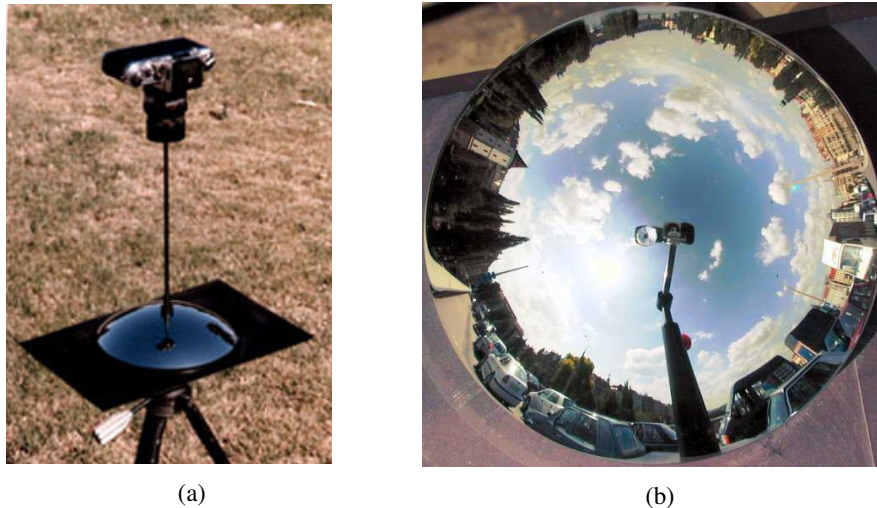


Figure 3.4 Omni-directional catadioptric vision system with a curved mirror (Charles, 1997) (a) and image obtained by a catadioptric system (Spacek, 2007) (b)

3.1.2 Central and Noncentral Omni-Directional Vision Systems

An omni-directional vision as a dioptric or a catadioptric system may also be classified whether it has central (Figure 3.5a) or noncentral projection (Figure 3.5b) according to the lens or mirror types used. While fish-eye lens ordinary uses central projection, a curved mirror may have central or noncentral projection depending on the mathematical equation related with its curvature.

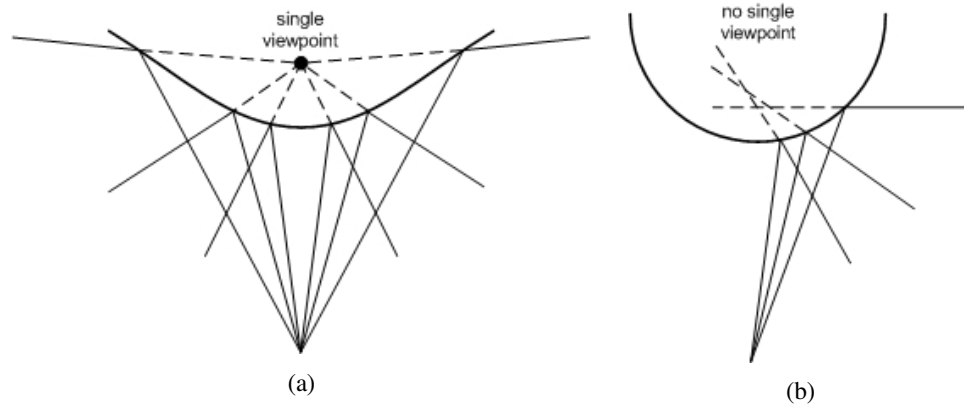


Figure 3.5 Curved mirrors with central projection (a) and noncentral projection (b)

The vision system with single viewpoint at which the incident light rays intersect has central projection and the one with no single viewpoint has noncentral projection.

3.1.2.1 Mirrors with Central Projection

Since hyperbolic and parabolic mirrors have single viewpoint as shown in Figure 3.6a and Figure 3.6b (Yagi, 1999) respectively, the omni-directional vision system using one of these mirrors across the perspective camera has central projection.

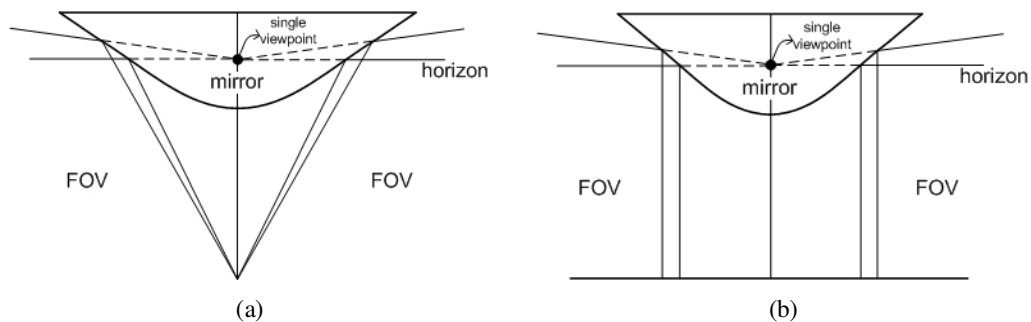


Figure 3.6 Curved mirror types of hyperbolic (a) and parabolic (b) mirrors with central projection

The 3D surface equation of hyperbolic mirror is (Ukida et al., 2008):

$$\frac{X^2 + Y^2}{a^2} - \frac{Z^2}{b^2} = -1$$

The focal point of the mirror and effective pinhole are located at $(0,0,c)$ and $(0,0,-c)$, respectively (Figure 3.7a), where $c = \sqrt{a^2 + b^2}$. The effective pinhole is the point at which the reflected light rays from the mirror surface intersect the rotational axis (Z). a and b are the parameters for mirror surface. The relation between the horizontal locations of real point and the image point is (Figure 3.7b):

$$\tan \theta = \frac{X}{Y} = \frac{x}{y}$$

where θ is the longitude angle.

The latitude angel α is used to estimate the vertical location of the real point at Z axis; and calculated as follows:

$$\alpha = \tan^{-1} \frac{(b^2 + c^2) \sin \gamma - 2bc}{(b^2 - c^2) \cos \gamma},$$

The angle γ can be calculated as:

$$\gamma = \tan^{-1} \frac{f}{\sqrt{x^2 + y^2}},$$

where f is focal length of the camera used. The longitude θ and latitude α angles are used to estimated the 3D location of the real point in the environment.

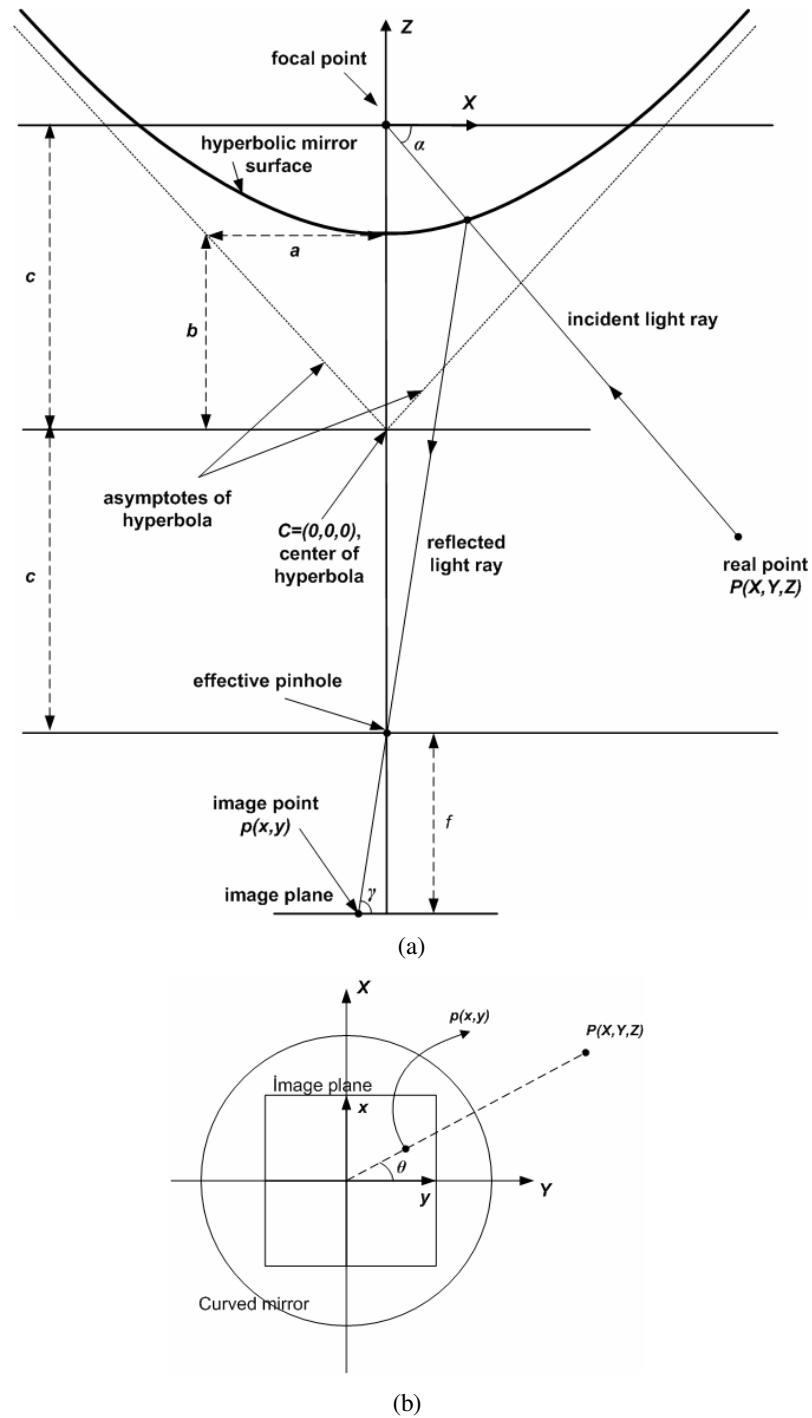


Figure 3.7 Vertical (a) and horizontal (b) views of projection principle for hyperbolic mirror

Parabolic mirrors are generally used to collimate the incoming parallel light rays to a point which is the focus of the mirror. This type of paraboloid is called concave mirror and the reflectivity is in its inner surface (Nayar, 1997). The paraboloid

concerning to omni-directional vision system is the type of convex mirror whose outer surface has reflective property. In the case of convex type, the incident light rays directed towards the focus (single viewpoint) of the paraboloid are orthographically reflected (parallel to the rotational axis) by the mirror (Figure 3.8). The equation defining the surface profile of the paraboloid shown in the figure is:

$$Z = \frac{h^2 - r^2}{2h},$$

where Z is the rotational axis, $r = \sqrt{x^2 + y^2}$, h is the radius of the paraboloid at $Z = 0$. The distance between the vertex of the paraboloid and the single viewpoint is $h/2$.

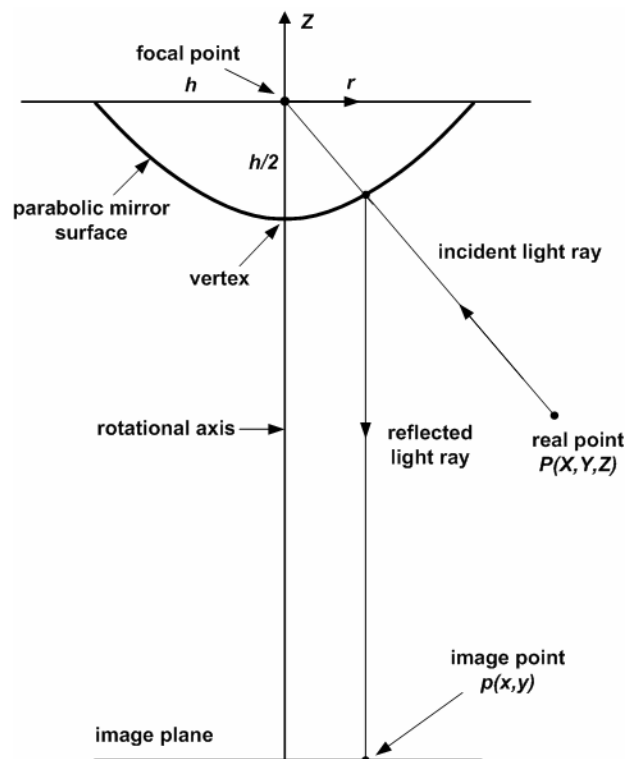


Figure 3.8 Projection principle of parabolic mirror

3.1.2.2 Mirrors with Noncentral Projection

The vision system consisting of spherical or conic mirror across the camera has noncentral projection because they have no single viewpoint as shown in Figure 3.9a and Figure 3.9b (Yagi, 1999).

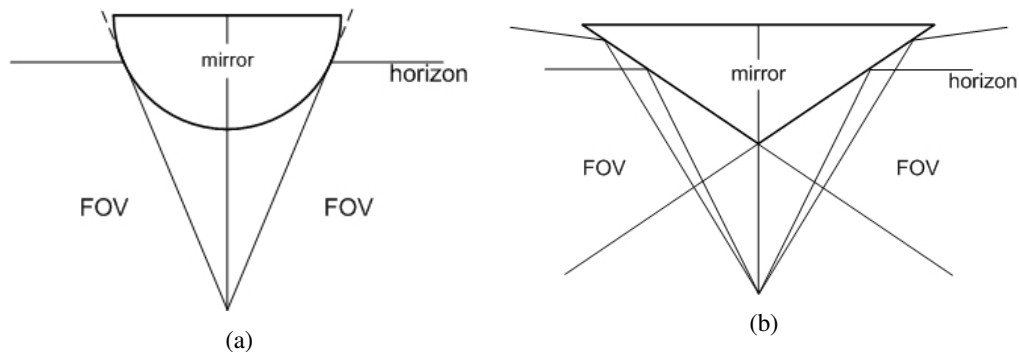


Figure 3.9 Samples of spherical (a) and conic (b) curved mirrors with noncentral projection

While hyperbolic and parabolic mirrors are preferably used as the curved mirror, spherical, elliptical and rectilinear mirrors are the other alternatives to be chosen for a special need. In fact, incorrect alignment of camera-mirror pair of system with central projection may cause the vision system to have non single viewpoint. Even though the reflection rule of incoming light is relatively easier on surface of the conic mirror since it is the same as in planar mirror, the projection principles of vision systems with non single viewpoint may be more complicated (Nayar, 1997).

Even though spherical mirror has no single viewpoint and the mathematical model is much more complicated to be developed, it is widely used in omni-directional visions system since some transfer functions and calibration procedures are used instead of generating the projection model.

In the case of conic profile, since the single viewpoint is at the vertex point of the mirror and practically useless, it is considered to have no central projection. The relation between the horizontal locations of real point and the image point is the same as in all the curved mirrors mentioned above such as hyperbolic mirror (Figure 3.7b):

$$\tan \theta = \frac{X}{Y} = \frac{x}{y}$$

According to the reflection principles and the geometric relation between the angles in Figure 3.10, the following equations can be written to determine the projection of the vision system (Yagi & Yachida, 1991):

$$\tan \alpha = \frac{L}{H - Z_p},$$

$$L = \sqrt{X_p^2 + Y_p^2},$$

$$\alpha = \pi - (\delta - \beta),$$

$$\beta = \tan^{-1} \frac{r}{f},$$

$$r = \sqrt{x^2 + y^2},$$

$$H = C \frac{\tan\left(\frac{\delta}{2}\right) [\tan(\delta - \beta) - \tan \beta]}{\tan(\delta - \beta) \left[\tan\left(\frac{\delta}{2}\right) - \tan \beta \right]}$$

where f is the focal length of the camera.

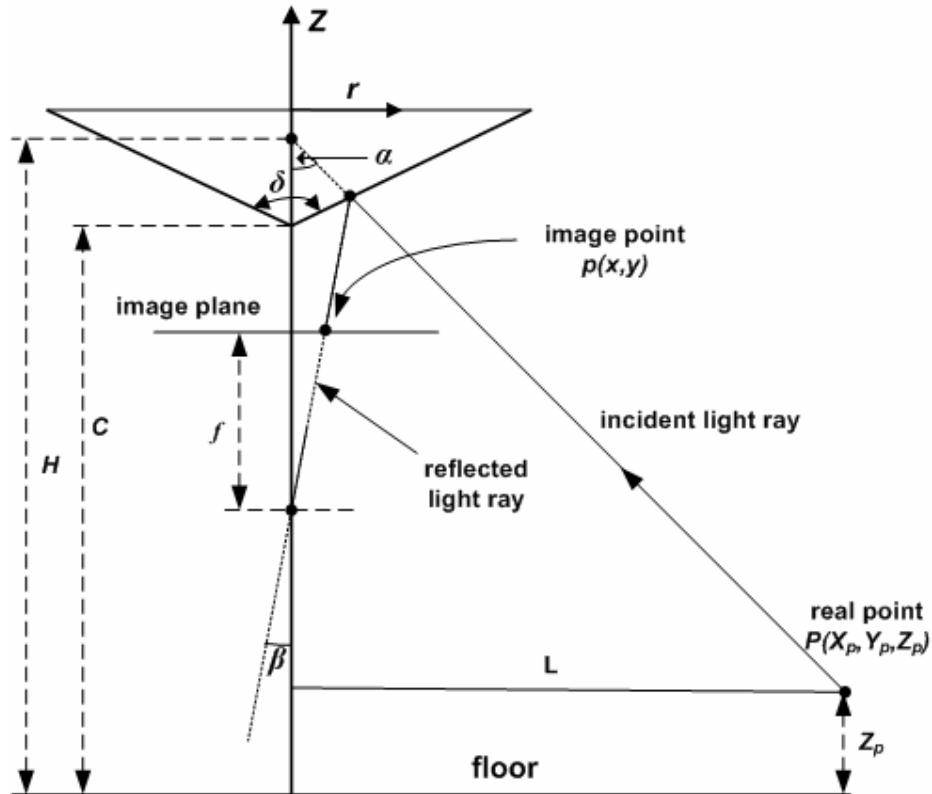


Figure 3.10 Projection principle of conic mirror

In order to obtain omni-directional vision, rectilinear mirrors, which have the principle of noncentral projection, can also be viewed. When this kind of mirror is used and if corresponding image point of real point $P(X, Y, Z)$ is $p(x, y)$ in the image plane, I , from similarity of vectors P and p , an equation can be formed as (Figure 3.7b is still valid):

$$\tan \theta = \frac{X}{Y} = \frac{x}{y} \quad (3.1)$$

In Figure 3.11, r and α are the radial distance and the polar angle in the spherical coordinate system and ρ and Z are the axial radius and the height in the cylindrical coordinate system respectively. ϕ and δ are the inclination angle of tangent plane T to the mirror at point of reflection and the incidence angle respectively. N is the nodal point at which the reflected lights intersect. f is the distance between the nodal point N (effective pinhole of the camera) and the image sensor I . ζ is the pixel distance with respect to the zenith angle α (Kweon et al., 2006).

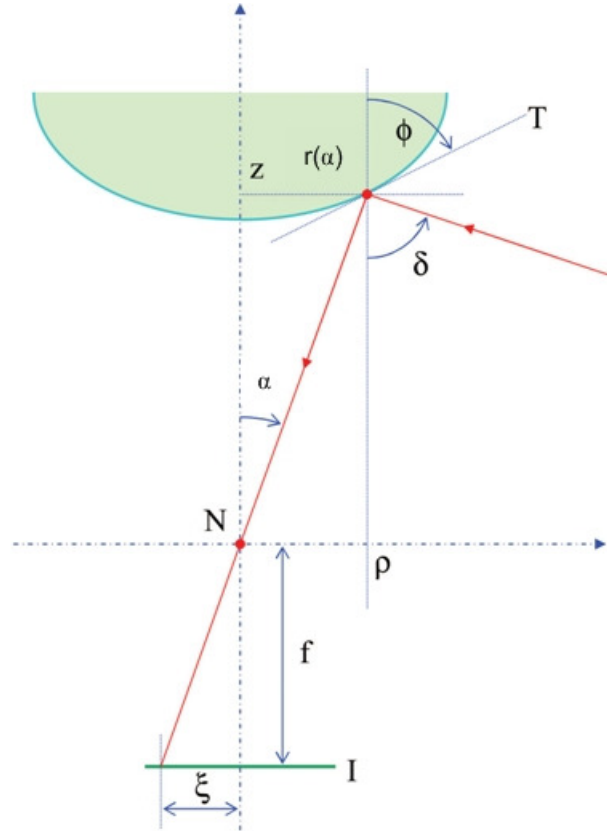


Figure 3.11 Projection principle of rectilinear mirror (section view) (Kweon et al., 2006)

To find the height of the real point in the environment, the angle (see angle of incidence δ in Figure 3.11) between the Z axis of the mirror and the incident light coming from the real point must be calculated. From the figure, the following equation can be written for the angle ϕ occurred by the tangent plane T at the reflection point and the Z axis (Kweon et al., 2006):

$$\tan \phi = \frac{d\rho}{dZ} \quad (3.2)$$

From equation (3.2), the cotangent equation can be written in spherical coordinates as in equation (3.3) (Kweon et al., 2006):

$$\cot \phi = \frac{r' \cos \alpha - r \sin \alpha}{r' \sin \alpha + r \cos \alpha} \quad (3.3)$$

where $r' = \frac{dr}{d\alpha}$.

While α is the zenith angle (i.e. polar angle) between the reflected light and the vertical axis of the mirror, r is the distance between the point N at which the reflected lights focused and the point at which the incident light reflected on the mirror (see Figure 3.11). Depending on above given assumptions, the ratio between r and r' can be written as equation (3.4) (Kweon et al., 2006):

$$\frac{r'}{r} = \frac{\sin \alpha + \cot \phi(\alpha) \cos \alpha}{\cos \alpha - \cot \phi(\alpha) \sin \alpha} \quad (3.4)$$

In order to calculate the value of δ to estimate the height of the real point, the derivative equation (3.4) must be solved. In order to solve this equation, at first, the relations between the angles ϕ , α and δ must be known. From the law of specular reflection, the equation (3.5) (Kweon et al., 2006):

$$\phi = \frac{\alpha + (\pi - \delta)}{2} \quad (3.5)$$

can be written. Also, the incident angle δ is calculated for each α angle depending on angles δ_r and α_r by equation (3.6) (Kweon et al., 2006):

$$\delta(\alpha) = \tan^{-1} \left(\frac{\tan \delta_r}{\tan \alpha_r} \tan \alpha \right) \quad (3.6)$$

Here, the constants δ_r and α_r are sensor size dependent reference reflection angles. α_r is the maximum reflection angle that the camera can take reflections from the mirror. For the National Television System Committee (NTSC) type Charge Coupled Device (CCD) camera of the developed system in this study, the width-to-height ratio is 4:3, and the angles δ_r and α_r are 80° and $26,565^\circ$ respectively (Kweon et al., 2006). The mirror constant for the rectilinear mirror used in the vision system in equation (3.6) is calculated as:

$$\frac{\tan \delta_r}{\tan \alpha_r} = 11.34259 \quad (3.7)$$

The distribution of ray trajectories for the rectilinear mirror is shown in Figure 3.12 (Kweon et al., 2006).

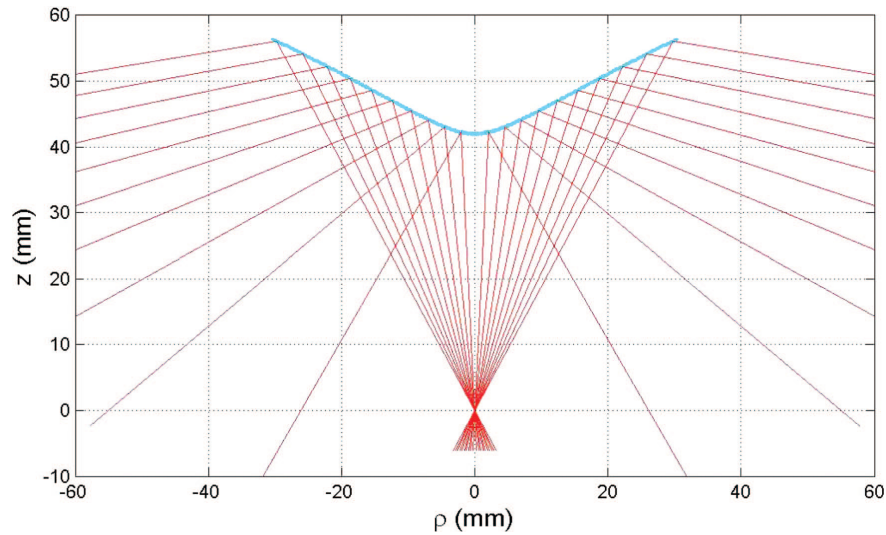


Figure 3.12 Ray trajectories of rectilinear mirror

In rectilinear projection, in a horizontal plane at a specific height from the floor the sequential lights with a constant distance between each other generate image points with a constant pixel distance between corresponding sequential points. Therefore on the same horizontal real plane with respect to the mirror, a specific distance is represented by a constant pixel distance in the image of the camera however the real distance is far from the vision system. This is known as “*equidistance*” property of the vision system (Kweon et al., 2004).

3.2 Control Techniques

Although there are various techniques as mentioned in Section 2.1, keyboard substituting for joystick and solid state dual axis tilt sensor for measuring the head movement were the methods used in this study.

3.2.1 Joysticks

There are different types of joysticks such as digital joystick, paddle controller and analog joystick. Digital joysticks are most common and generally used in personal computers as Atari-style. It has five switches; four for direction (up, down, left and right) and one for fire.

Paddle controller consists of one knob for controlling the game and it has an analog output as signal format. Analog joystick is a combination of ideas of digital and paddle. It has a potentiometer to determine the direction, instead of switches in digital joystick.

3.2.2 Tilt Sensors

Tilt sensors measure the angle of inclination with respect to gravity vector. The output of the sensor may be analog or digital signal and varies with angular orientation. There are two criteria for the types of a tilt sensor,

- According to its number of axis
- According to its sensor type to measure the tilt angle

For the first criterion, dual axis and single axis are the types of a tilt sensor. A sample of dual axis tilt sensor and its tilt angles are shown in Figure 3.13a and Figure 3.13b respectively. While tilt angle on one axis is called roll, the other is called pitch. Roll and pitch angles are perpendicular to each other. If a tilt angle occurred on a plane which is perpendicular to gravity vector is called *yaw* and cannot be measured by a tilt sensor. In another word, in order to be measured by a tilt sensor, an angle must be occurred relative to the gravity vector.

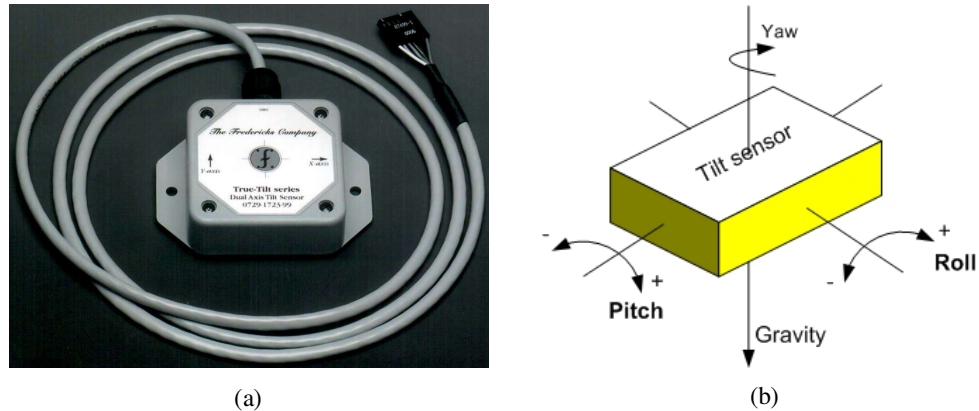


Figure 3.13 Dual axis tilt sensor (Dual axis tilt sensor, n.d.) (a) and tilt angles (b)

For the second criterion, many types of sensor may be classified into three major categories which are force balanced, solid state (Micro-Electro-Mechanical System, MEMS) and fluid-based. MEMS is fabrication of combining the mechanical and electronic components in silicon substrate on micrometer scale.

The force balanced sensors have better performance than other types but their cost are relatively higher. The MEMS-based sensors give integral signal conditioning and are easily installed. However compensation is required to get a suitable accuracy since their thermal coefficients are high. Electrolytic and capacitive are the types of fluid-based category. They are the most widely used in industry due to their low cost but are not preferred to be used in critical applications due to their poor response time.

3.3 Movement of a Mobile Robot with Two Actuators

The kinematics for a mobile robot (wheelchair) with two actuator wheels consists of velocities of left and right wheels as shown in Figure 3.14.

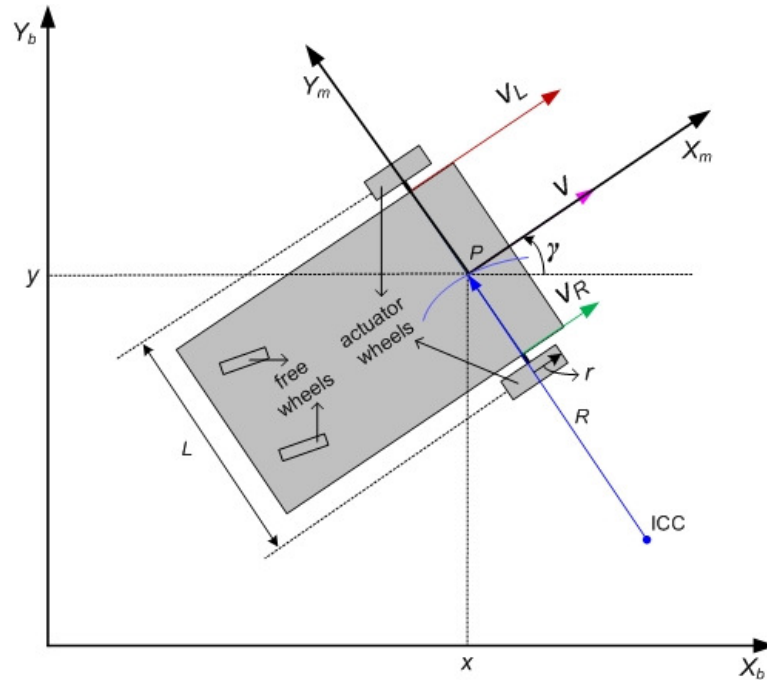


Figure 3.14 Kinematic model of a mobile robot with two actuator wheels

Where;

v_L and v_R - linear velocities of left and right wheels respectively,

v - linear velocity of mobile robot,

γ - orientation angle,

w - angular velocity of mobile robot in vertical Z axis,

R - instantaneous curvature radius of mobile robot with respect to instantaneous center of curvature (ICC),

r - radius of each wheel,

L - distance between two wheels,

$\{X_b, Y_b\}$ - coordinate axes of base frame,

$\{X_m, Y_m\}$ - coordinate axes of moving frame,

The angular velocity can be calculated by the equations (3.8) and (3.9):

$$w(t) = \frac{v_L(t)}{R + \frac{L}{2}} \quad (3.8)$$

$$w(t) = \frac{v_R(t)}{R - \frac{L}{2}} \quad (3.9)$$

where $R + \frac{L}{2}$ and $R - \frac{L}{2}$ are the curvature radii for left and right wheels respectively.

From equations (3.8) and (3.9), equations (3.10) and (3.11) are derived.

$$R = \frac{L(v_L(t) + v_R(t))}{2(v_L(t) - v_R(t))} \quad (3.10)$$

$$w(t) = \frac{v_L(t) - v_R(t)}{L} \quad (3.11)$$

By using equations (3.10) and (3.11), linear velocity of the mobile robot is written as in equation (3.12):

$$v(t) = w(t)R = \frac{1}{2}(v_L(t) + v_R(t)) \quad (3.12)$$

The position of the mobile robot in base frame is as in equation (3.13):

$$q = \begin{bmatrix} x(t) \\ y(t) \\ \gamma(t) \end{bmatrix} \quad (3.13)$$

where x and y are the horizontal position of the mobile robot in the base coordinate axis with respect to a reference point.

The equation (3.14) gives the kinematics in base frame:

$$\begin{bmatrix} \dot{x}(t) \\ \dot{y}(t) \\ \dot{\gamma}(t) \end{bmatrix} = \begin{bmatrix} \sin \gamma(t) & 0 \\ \cos \gamma(t) & 0 \\ 0 & 1 \end{bmatrix} \begin{bmatrix} v(t) \\ w(t) \end{bmatrix} \quad (3.14)$$

The kinematics in moving (robot) frame can be written as in the following equation:

$$\begin{bmatrix} V_x(t) \\ V_y(t) \\ \dot{j}(t) \end{bmatrix} = \begin{bmatrix} \frac{r}{2} & \frac{r}{2} \\ 0 & 0 \\ -\frac{r}{L} & \frac{r}{L} \end{bmatrix} \begin{bmatrix} w_L(t) \\ w_R(t) \end{bmatrix} \quad (3.15)$$

where $w_L(t)$ and $w_R(t)$ are left and right angular velocities respectively.

CHAPTER FOUR

MOBILE ROBOT SYSTEM

The mobile robot consists of different hardware and software components including Human Interaction devices, vision system to obtain the information about the environment, and a navigation platform on which the above mentioned components is installed. The main components and the flowchart are given in Figure 4.1.

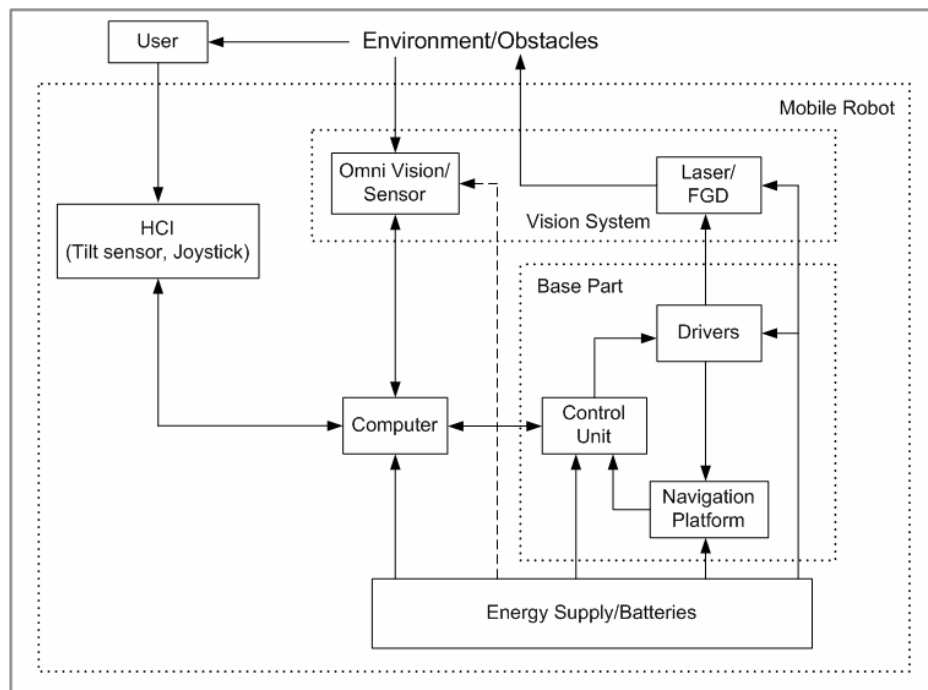


Figure 4.1 Detailed block diagram of mobile robot

4.1 General Overview of Mobile Robot System

Although User is the person holding the control of the mobile robot movement through HCI according to the target location and information of the environment structure obtained by human senses, the more the disability of the User more autonomous should be the mobile robot. The User is assumed probably not to be able to use his / her hands to control the mobile robot dependent on the disability of his / her body for the developed mobile robot. Therefore the HCI unit used by the

disabled user includes two options with and without hands of the user to control the robot.

4.1.1 Human Computer Interface (HCI)

The user command is translated to the Computer of the mobile robot through HCI via some electric signal types. In HCI unit, while keyboard is used as substituting for joystick to enable driving the robot by using hands, tilt sensor is also included as hands-free control option by fixing it to the user head in order to track head movement representing possible user commands. “Turn left”, “turn right”, “forward” and “stop” are the commands extracted from positions of head leaned to left, right, front and back respectively. Between the Computer and the solid state dual axis tilt sensor used for user control, half-duplex communication is used. In keyboard option, matching of the commands mentioned and the arrow keys is in a straightforward manner.

4.1.2 Computer

Briefly, option devices in HCI unit translate raw user command in digital signal format to the Computer which decides if the received signal is a real request of the User and/or it is reliable to execute. The decision is dependent on locations of obstacles in the environment which are determined after processing the images received from the vision system. The direction of the robot is determined according to both the user command and the free zone in the environment which is extracted by using the information about the obstacles.

The movement is allowed only if it is safe to pass through the free zone for the mobile robot. First a path passing through the free zone is generated. Then velocities of left and right wheels including directions (forward or backward) of motors are calculated according to the equations (3.8) through (3.12) in Section 3.3 in order to follow the desired path. The Computer sends digital signal representing velocity

information to the Control unit by using serial communication; and the Control unit activates the Drivers to rotate the motors connected to the wheels.

4.1.3 Base Part

In Base Part of mobile robot, Drivers, Control unit and Navigation Platform including proximity sensors and motors actuating the wheels exist.

- *Drivers*: The Drivers unit switches the power on and off to the left and right motors with separate circuitry by using Metal-oxide Semiconductor Field-effect Transistors (MOSFET). The laser light source in Laser/FGD unit is also driven by Drivers unit by using relay circuit.
- *Control unit*: Driving of both laser light source and motors is directed by Computer through Control unit by sending related on/off and velocity information signals, respectively. The Control unit generates necessary signals to the gates of the MOSFETs to drive the motors and necessary voltage for the laser light source. It also sends velocity information of two motors incoming from the proximity sensors as feedback data to the Computer.
- *Navigation Platform*: Location of the mobile robot is checked frequently by the Computer with processing the data representing the velocities of left and right wheels. The velocity values are taken from both of the proximity sensors through the Control unit. These velocity values are used in equations (3.13) through (3.15) in Section 3.3, to keep the mobile robot on the desired path. The proximity sensors are located on the Navigation Platform faced to left and right wheels to count the revolutions.

4.1.4 Vision System

The Vision System consisting of Laser unit with FGD and Omni Vision which is triggered by the Computer is an omni-directional stereo imaging system. The Computer activates the Omni Vision unit frequently to take the view of the environment in order to update the free zone. The image of the environment is processed first without laser pattern and then with laser pattern scattered by the Laser/FGD unit in sequence, while the mobile robot is in stationary position. An image obtained by subtracting of these images makes it possible to eliminate the background details which are undesirable in detection process of the free zone.

4.1.5 Energy Supply/Batteries

Power requirements of the all the electric and electronic components of mobile robot are supplied by Energy Supply/Batteries unit. Motors located in Navigation Platform use separate batteries in order to block their affect of the other units especially Control unit and proximity sensors with the noise occurred in power supply lines during mobile robot movement.

4.2 Human Computer Interface (HCI)

For interaction with the user, two different components, joystick and tilt sensor, are used. The user command is sent to the Computer by using some keys of the keyboard as joystick for hand based control and tilt sensor for hands free control of the mobile robot.

4.2.1 Joystick for Hand Based Control

The arrow keys up, right, left and down of the keyboard are used to move the mobile robot forward, right, left direction and finally to brake the robot, respectively.

4.2.2 Tilt Sensor for Hands Free Control

A dual axis solid state (Micro-Electro-Mechanical System, MEMS) tilt sensor is fixed on the user head in order to give commands to the mobile robot by head movements. The output of the tilt sensor corresponding to the angle of inclination with respect to gravity vector is used to determine the position of the user head. The tilt sensor used in the study is shown in Figure 4.2 and primary specifications of the tilt sensor are shown in Table 4.1 (Tilt sensors, n.d.),



Figure 4.2 Tilt sensor for HCI

Table 4.1 The specifications of the tilt sensor

Specifications	Typical
Linear angular range (degree)	± 45
Alignment Error (degree)	± 1
Bandwidth (Hz)	10 - 100
Operating Temp Range ($^{\circ}\text{C}$)	0 to 70
Supply Voltage by USB connector (Volts)	+ 3.3
Size (mm)	66.3 x 50 x 20
Output word length of reading (bits)	12
Sending the reading every (seconds)	0.01

Four adjustable threshold values are used to determine the angular positions of the head. The sign of the corresponding threshold values on roll and pitch axes and their corresponding commands are,

Forward : Negative threshold value on the roll axis,

Stop : Positive threshold value on the roll axis,

Right : Negative threshold value on the pitch axis,
Left : Positive threshold value on the pitch axis.

The head movement value within the intervals between the negative and positive threshold values on an axis is not considered as a command. Therefore the User feels comfortable to move his or her head for a particular angular space.

4.2.2.1 Communication Between Computer and Tilt Sensor

The tilt sensor is connected to the Computer via USB port. The communication protocol provides the Computer to communicate with the sensor through an RS-232 or RS-485 half duplex serial communication link. Each command sent from Computer should contain an ID in order to be recognized by the sensor. The response to the command should also include an ID to indicate the response type. As an example, the command sent from Computer to the sensor requesting the reading for the angular position of the sensor begins with the ID 0x50, while the response sent from sensor to the Computer begins with ID 0xA0. General format of the command or response is shown in Table 4.2 (Zhao, 2005).

Table 4.2 Command/Response format

No.	Length (byte)	Name	Explanation
1	1	ID	Command/Response ID
2	0 or any number	Data	Command/Response Data
3	1	Checksum	Checksum for ID and Data

The checksum is generated by adding the sum of data and the ID to allow the receiver side to check whether the packet is valid or not. The length of each command is constant. In another word, each packet which is in hexadecimal value format, consists of ID, data if exists and a checksum.

If the packet does not contain any data indicating the position of the sensor to send, the checksum should be equal to the ID. Therefore the packet contents of the command should be 0x50 0x50.

4.3 Base Part

Base Part consists of Control unit, Drivers and Navigation Platform including motors and proximity sensors. This part has mainly executive duty for the movement of the mobile robot according to the criteria decided by the computer.

4.3.1 Control Unit and Drivers

The user command from HCI is taken by the Computer. The Computer decides whether to perform the command after detection of the obstacles in the environment by processing the images of the environment obtained from the Omni Vision unit. Therefore the location of the wheelchair is obtained with respect to the obstacles. The safe route is established by the software in the Computer by using the localization information of the wheelchair and the structure of the surroundings.

4.3.1.1 Communication Between Computer and Control Unit

The communication between Computer and Control unit is in serial (RS-485) and the data formats to be sent and received are shown in Figure 4.3a and Figure 4.3b respectively.

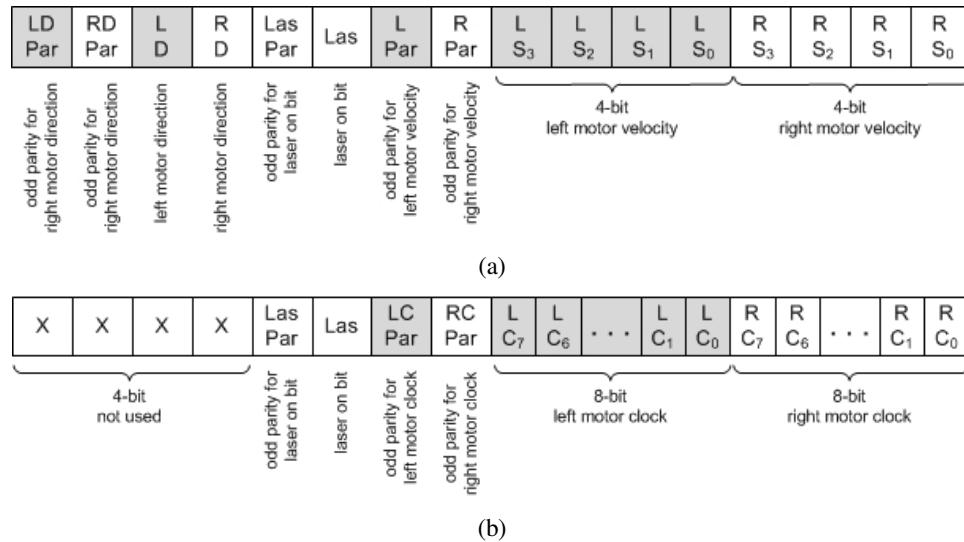


Figure 4.3 Data formats to be sent (a) and to be received (b) used in the communication with explanations of bit content

4.3.1.2 Driving The Motors

The velocities of right and left wheels are determined for the route and sent to the Control unit in a previously defined time slots by the Computer. The Control unit is shown in Figure 4.4.



Figure 4.4 Control unit and Drivers located in a box

The Control unit prepares Pulse Width Modulated (PWM) signals and rotates the left and right wheels by sending the signals to the gates of MOSFETs in the Drivers unit of the motors (Figure 4.5). The PWM signal is a periodic signal with a duty cycle. Rotating the motor with different speed values is achieved by adjusting the

duty cycle of the signal to switch on the MOSFET to apply the 24VDC to the motor for a specific time period. The duty cycle is adjusted by changing the pulse width of the signal which results the average voltage supplied for the motors to be set to a desired value.

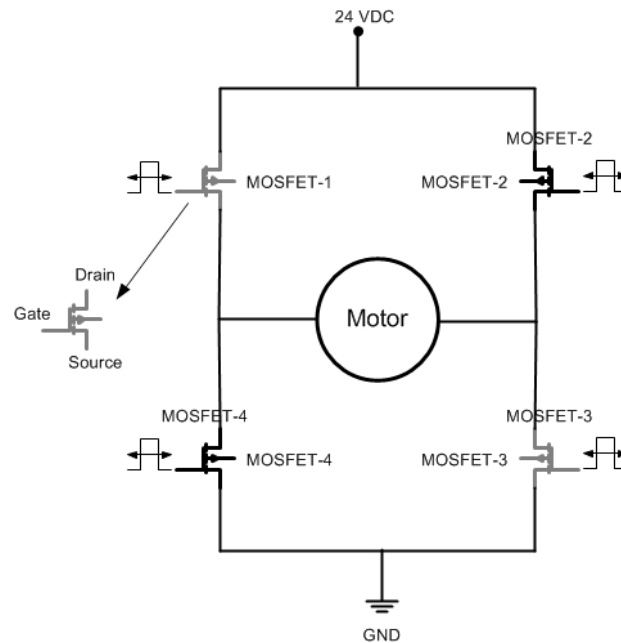


Figure 4.5 Driving the motor by MOSFETs

The motors can run in both directions by switching the proper MOSFETs. The motor is driven in forward direction by switching on the MOSFETs 1 and 3, and in backward direction by switching on the MOSFETs 2 and 4.

4.3.1.3 Driving The Laser Light Source

Laser light source is also switched on or off by the Control unit according to *laser on* bit from the computer as shown in Figure 4.3a in order to scatter the dot-matrix laser pattern to the environment with the FGD in front of the laser beam. The current state of laser light source is indicated in the packet received by the Computer as shown in Figure 4.3b. The distances between the robot and the laser dots in the images taken by the vision system are determined in stereo vision manner by the software in the Computer.

4.3.2 Navigation Platform

The mobility of the Navigation Platform is obtained by two motors connected to the axes of left and right wheels. The velocity of each wheel is measured by using proximity sensor in order to calculate the location of the platform according to the travel distance during specific time period.

4.3.2.1 Mechanical Properties of The Platform

The omni-directional imaging system, Control unit, Laser/FGD unit and the batteries are fixed in the navigation system. It is shown in Figure 4.6b. The dimensions of the mobile robot platform are shown in Figure 4.6a and Figure 4.6c and the general view of the Navigation Platform is given in Figure 4.6b.

Only the velocities of the wheels actuated by the motors are used in calculation of robot localization. The actuator wheels are fixed in front side of the platform and are shown in Figure 4.6c. The platform is kept in balance and easily rotates with the help of the free wheels located at the back side. The Laser/FGD unit is fixed to a metal pole at a specific height (Figure 4.6a) to be able to scatter the laser light beams to the front of the mobile robot for imaging of the environment.

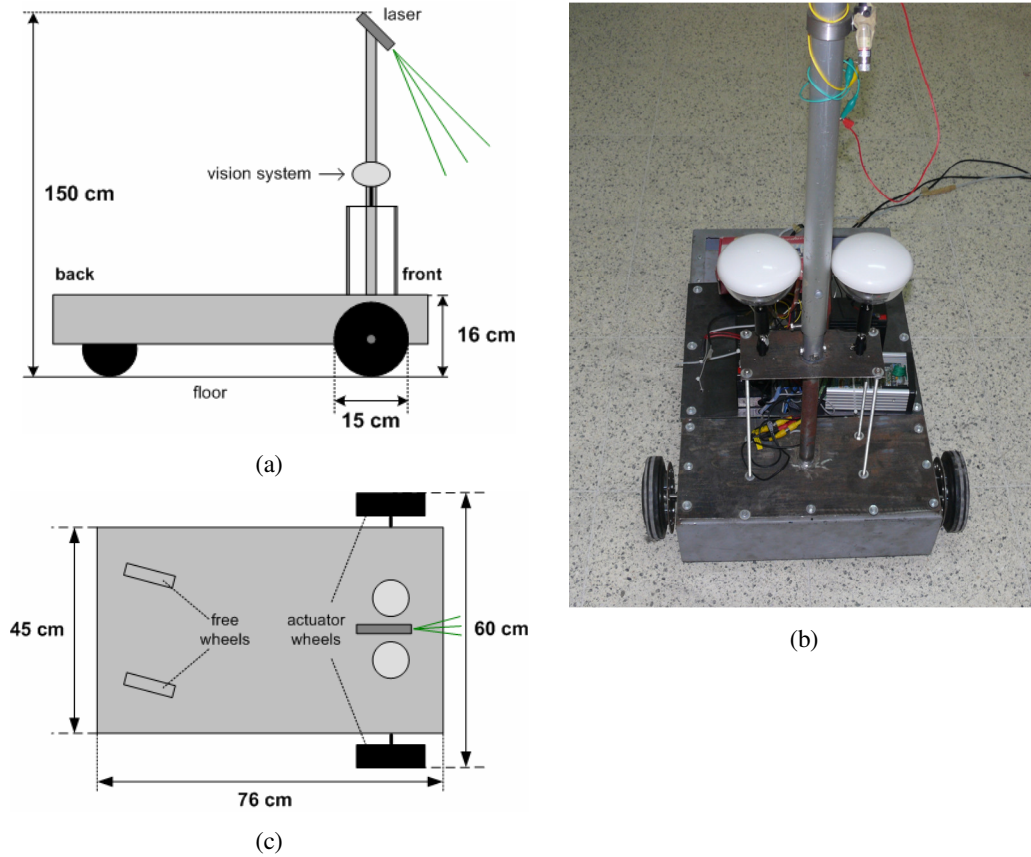


Figure 4.6 Drawings of mobile robot with dimensions: vertical (a), horizontal (c) views; and developed mobile robot (b)

4.3.2.2 Motors

Each wheel is being actuated by two separate 24 VDC electric motors (Figure 4.7). In order to be able to get more accurate movements especially in narrow routes through the obstacles, it is possible to let the wheels to be rotated with different speeds. The technical specifications of the DC electric motor are shown in Table 4.3.

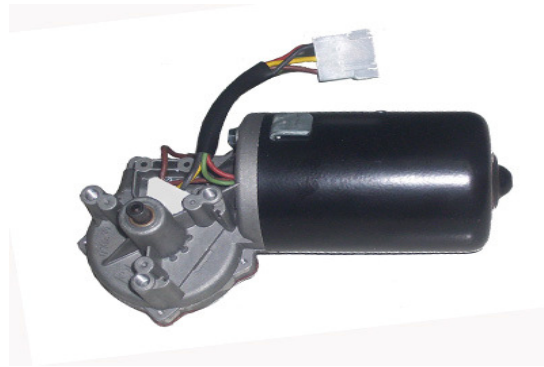


Figure 4.7 Motor used to rotate the wheels

Table 4.3 The specifications of the motor

Type	DC	
Voltage	24 VDC	
Mode	I	II
Current	2 A	2.5 A
Power	18 W	20 W
Rotation	27 rpm	32 rpm
Torque	6 Nm	
Breaking Torque	30 Nm	
Direction	CW	
Class	S1	
Weight	2.720 kg	

4.3.2.3 Proximity Sensors

Two proximity sensors are used for counting the holes in the disk connected to each wheel to measure the speed of the wheel (Figure 4.8). The number of holes counted by the Control unit by signal changes in the output of the proximity sensor is called *clock* of the wheel. The clock decreases while the direction of the robot is backward; and increases during the forward movement. The performed route of the wheelchair can be determined by examining the clock changes frequently. Each disk has 15 holes and the circumference of the wheel is 47.1 cm so each interval between two holes represents:

$$\frac{47.1}{15} = 3.14 \text{ cm}$$

on the floor. The proximity sensor and the disk connected to the wheel are shown in Figure 4.8.

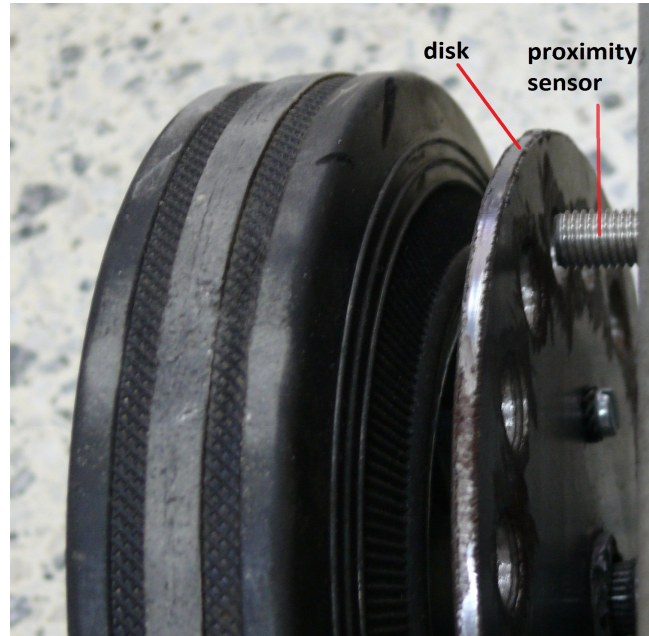


Figure 4.8 Proximity sensor and the disk connected to the wheel

4.4 Vision System

It is necessary that a mobile robot should determine at first the obstacles in the environment in which it is located, and then depending on its dimensions, the free areas between the obstacles. For this aim, determination of the position of mobile robot is necessary. In the scope of this study, an omni-directional stereo vision system, which can be used for mobile robots and was intended to determine both the obstacles in the environment and the places through which a mobile robot can pass, by sensing the environment in a three dimensional manner, was developed (Çebi et al., 2009).

4.4.1 Basic System

The basic system consists of mainly a laser source with a FGD, two rectilinear (omni-directional) mirrors and two Charge Coupled Device (CCD) cameras

(Figure 4.9). In the vision system, rectilinear mirrors are aligned in a horizontal line and the CCD cameras having refractive lenses are fixed at a certain distance in front of the mirror. Both the mirrors and the cameras are aligned with the distance D between their central (focal) points.

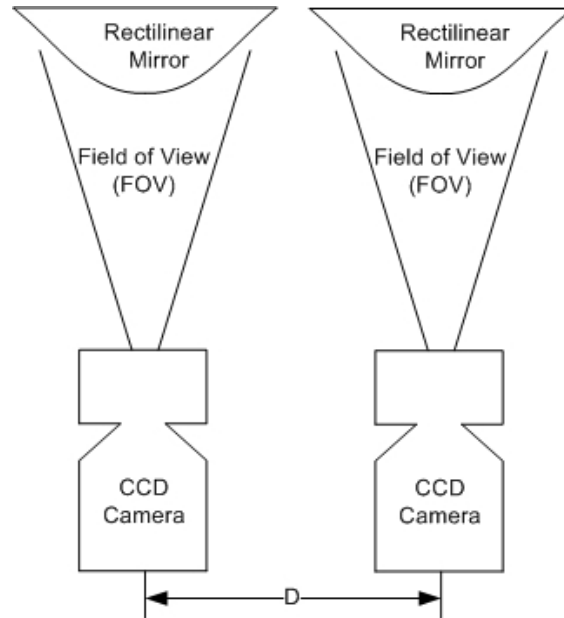


Figure 4.9 Omni-directional stereo vision system

By using a dot-matrix laser pattern with the omni-directional vision system, the 3D structure of obstacles in the environment is constructed and the distances of the obstacles from the vision system is found. The pattern is obtained by passing a laser beam through a FGD (Figure 4.10).

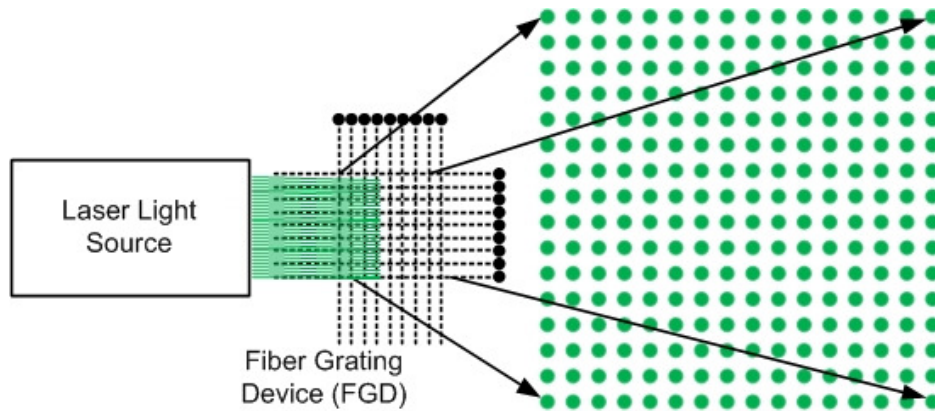


Figure 4.10 Construction of a dot-matrix laser pattern (Tamagawa et al., 2002)

A laser point $P(X_p, Y_p)$ on the real world can be seen on two different mirrors as two different image points having angles δ_1 and δ_2 (Figure 4.11).

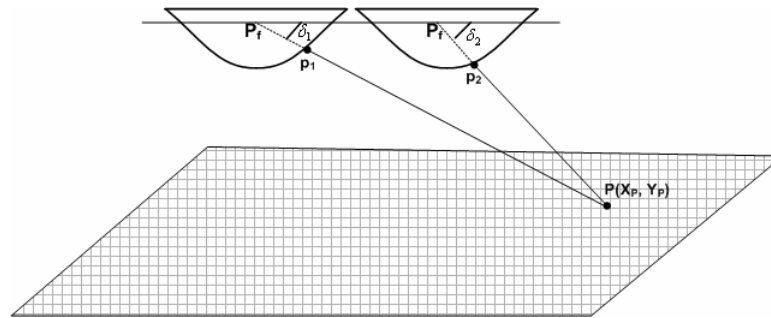


Figure 4.11 Imaging of a laser dot on the environment

The projection principles of rectilinear mirror and the details of the localization and mapping of the environment were given in Chapter 3.

4.4.2 System Components

The experiments were carried out by using the vision system developed by combining two CCD cameras, two curved mirrors and one laser source with FGD. The technical specifications of the hardware are:

- Curved mirrors: They have rectilinear reflection and circular base with diameter of 60mm. The field of view of the mirror was 360° horizontally and 151° vertically (Figure 4.12a). The mathematical formulas for rectilinear reflection were supplied by the manufacturer.

- CCD cameras: They have 410k pixel resolution and 1/3" CCD sensor with analog output. The type of the connection between cameras and lenses was Hitachi M12 (Figure 4.12b).
- Other Accessories: Two plastic domes were used to fix the cameras at a specific distance from the mirrors with the same alignment (Figure 4.12c), and a 5 VDC power supply was also used.
- Also the green laser source with power of 30mW and 532nm wavelength was used with a FGD device which constructs dot-matrix laser pattern (Figure 4.12d and Figure 4.12e).



(a)



(b)



(c)



(d)



(e)

Figure 4.12 Hardware of the vision system: rectilinear mirror (a), CCD Camera (b), plastic dome (c), laser source with FGD (d); and dot-matrix laser pattern (e)

A metal holder was constructed to be able to adjust the optimum distance between two camera-mirror pairs, the horizontal level of the system parallel to the floor and to fix the final installed hardware. The camera-mirror pairs were installed on the holder as the faces of the mirrors towards the floor and the cameras across them

(Figure 4.13). The cameras, mirrors and domes onto which above mentioned hardware was built, were manufactured by Nanophotonics Co. Ltd. of South Korea.

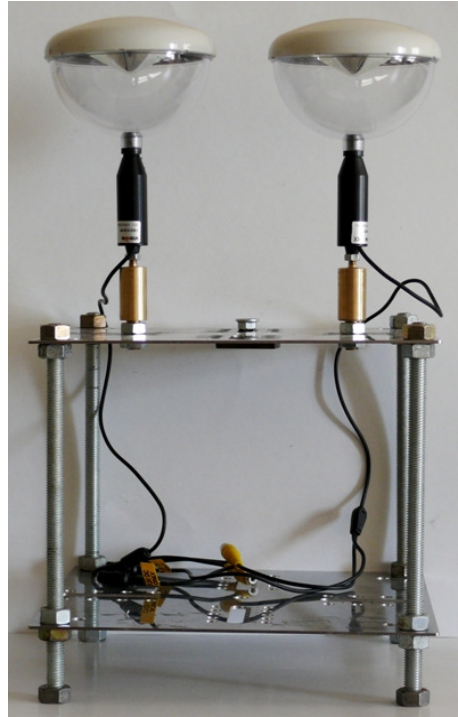


Figure 4.13 The vision system

The camera is placed in the external focal point at which the reflected lights from the mirror surface intersect. Since the mirror and the camera are inserted in the plastic dome (Figure 4.12c) and fixed in front of the dome respectively, the camera is set up in the external focal point. The image contrast is adjusted by screwing the camera to the dome by using an assembly in front of the dome. The distance between the external focal point and the peak point of the mirror on the vertical axis is 42 mm.

CHAPTER FIVE

DETECTION OF LASER DOTS IN 2D IMAGE

The dot-matrix laser pattern is used as a structured light in order to reduce the image processing cost and possible errors encountered in matching the pixels between two images in stereo vision (Çebi et al., 2009). The accuracy of the vision system in sensing the environment is strictly dependent on the accuracy in determining the center locations of the laser dots in 2D image.

5.1 Separation of Laser Dots from The Background

For determining the structure of the environment, two images are taken by using constructed omni-directional vision system. The images obtained before and after scattering the dot-matrix laser pattern by using the vision system is shown in Figure 5.1a and Figure 5.1b, respectively.

The background details of the scene are eliminated by subtracting the first image from the second image. The image taken before scattering the dot matrix laser pattern is called *mask*, the image taken after scattering the laser pattern is called *base* and the resultant image after subtraction is called *subtracted* (Figure 5.1c). After the subtraction process, a grayscale image of the environment is obtained (Figure 5.1d).

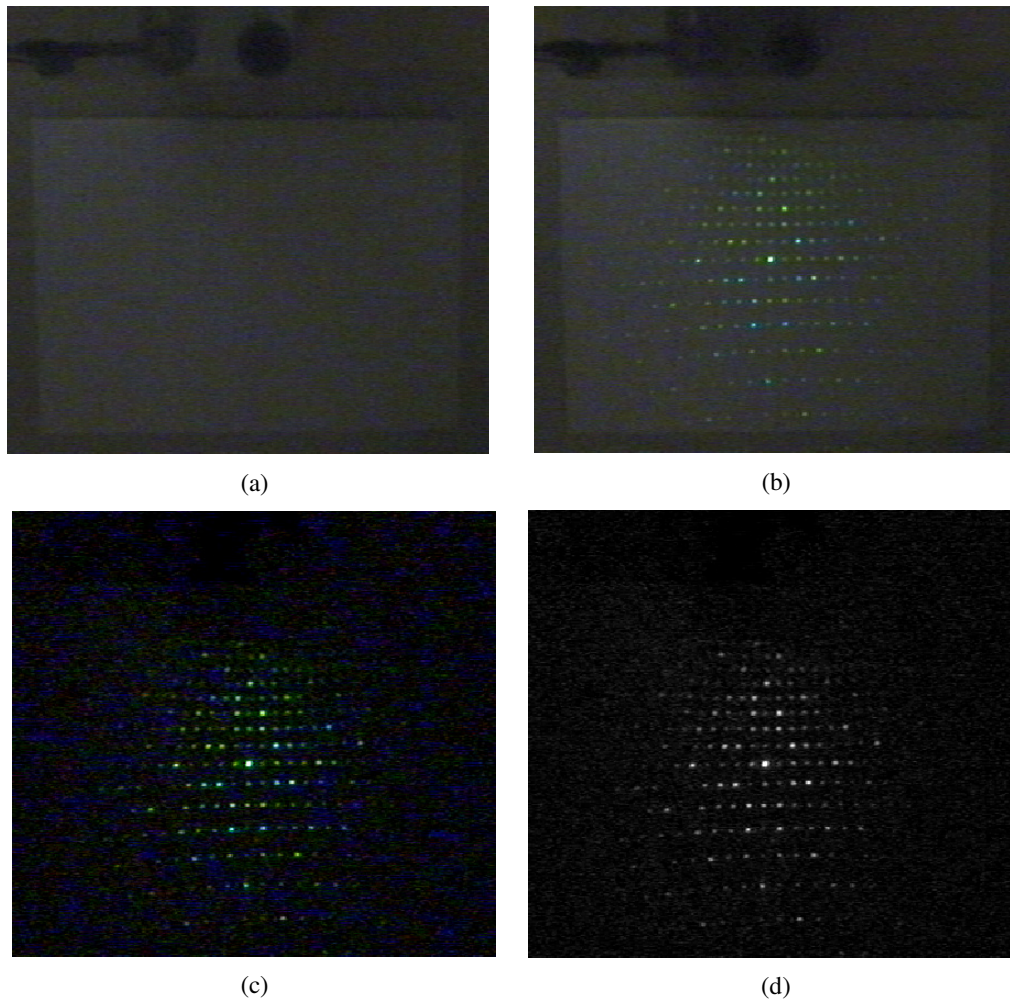


Figure 5.1 Isolating the laser dots by eliminating background. *Mask* (a), *base* (b), *subtracted* (c) and *grayscale subtracted* (d) images

There is a grayscale in the region between the laser points in the gray scaled *subtracted* due to the sparkles of the laser light. The determination of laser points may be difficult due to this region. To eliminate the undesired grayscale,

- The grayscale of each pixel in the subtracted is smoothed by assigning an average value of 3x3 pixels of neighbor around. Therefore the real dots of the lasers are separated from other regions by reducing the grayscale of the pixels on the region caused by the sparkles by smoothing operation. The close view for the result of the smoothing the grayscale subtracted image (Figure 5.1d) is shown in Figure 5.2a.
- The smoothed *subtracted* is enhanced by 21x21 pixel window. The image is scanned by the window with 21 pixels step. The average grayscale for 21x21 window of the subtracted is calculated for each step of the scanning. In order to determine a

threshold grayscale, the average grayscale is multiplied by an experimentally found coefficient. The pixel with the grayscale value less than the threshold value is considered as the point not belong to the laser dot and grayscale value of 0 is assigned to the pixel. So the pixels which are not part of a real laser dot are eliminated and the rest of the points are considered as a part of laser area of the image. The 21x21 pixel window is shifted by 21 pixels step to prevent overlapping and to obtain the enhanced image with low cost. The close view of enhanced subtracted image is shown in Figure 5.2b.

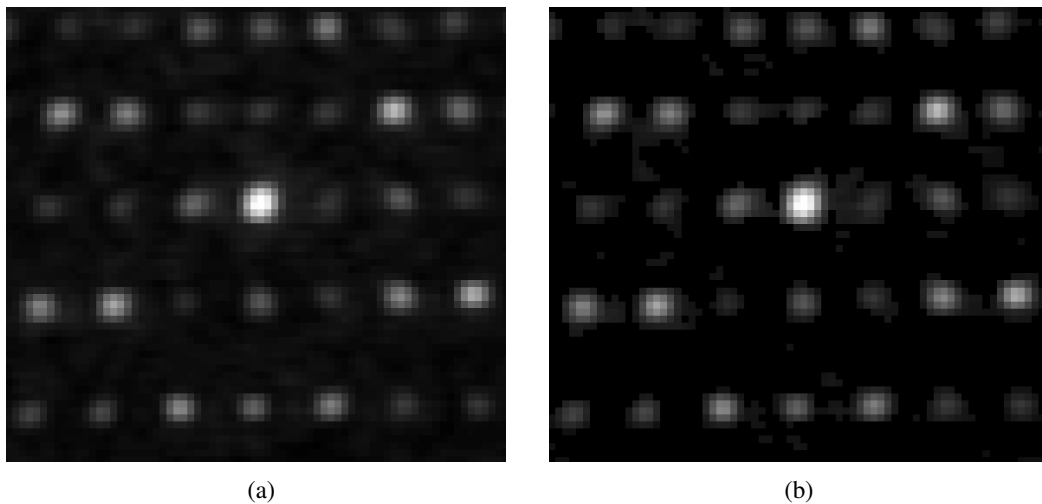


Figure 5.2 Enhancement of laser dots (close view): smoothed (a) and enhanced (b) images

5.2 Finding The Locations of Laser Dots

Although the enhancement of the laser dots have been achieved by eliminating the grayscale pixels below the threshold value, there are still grayscale pixels remained above the threshold value which belong to the region of sparkles of the laser. In this case it is not aimed to eliminate these pixels anymore, however a modal structure of a laser dot is determined in order to detect the real laser dots in the *subtracted* by searching the dots resembled to the modal. After the search operation, not only the dots resembled to the modal are found, but also the bright pixel which has the highest grayscale value of each laser dots found are marked as the center of the laser dot as well (Figure 5.3).

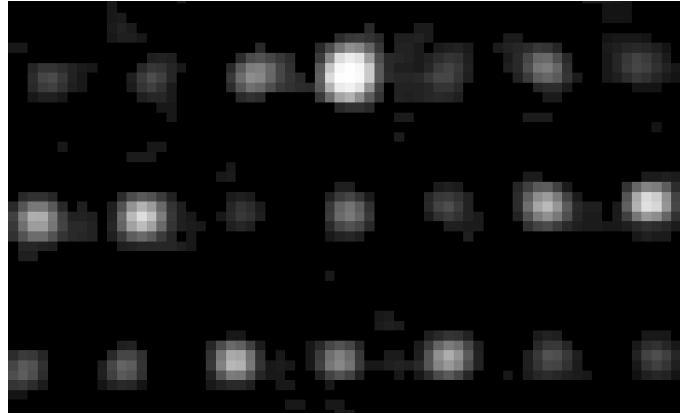


Figure 5.3 Enhanced laser dots (close view)

5.3 Circular Neighborhood Structure of Laser Dots

The laser dots are seen to have a particular structure in which the nearer the pixel to the center of the dot the brighter the pixel. The distance of a real point in the environment from the vision system is determined by the places of image dots of the real point in both images obtained from two mirrors. The matching pixels in two mirrors must be belonged to the same point of the real laser dot in the environment. Therefore the brightest points in the image dots in two images are considered to be suitable for matching in order to calculate the distance of the laser point from the vision system with low error rate.

As the laser dots in Figure 5.3 are examined, the first remarkable point is the brightest pixels with highest grayscale value are seen to be placed around the center of the dots and the brightness (grayscale value) of a pixel is decreasing as the place of the pixel is moving away from the center in any direction. Second noticeable point is the brightness of pixels on the same “*circular neighborhood*” is nearly same. A circular neighborhood modal as seen in Figure 5.4 is proposed as considering the two important common points about the structure of laser dots. Each square in the figure stands for a pixel and the squares with the same color are considered to be in the same circular neighborhood.

In the modal, there are four different circular neighborhoods. The number of pixels in the outer neighborhood is 16 and the number of pixels in the neighborhoods towards the center of the modal is in the sequence of 12, 8 and 4. The laser dots in the *subtracted* are searched according to similarity of the dots with circular neighborhood modal.

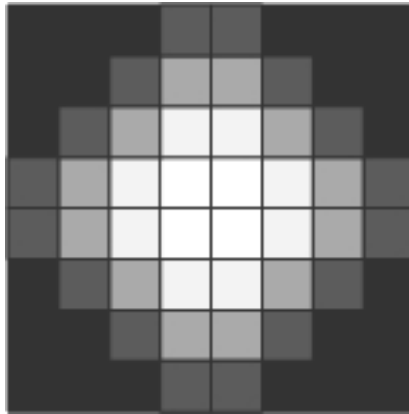


Figure 5.4 Circular neighborhood modal of the laser dot

5.4 Finding The Centers of Laser Dots

An algorithm is developed to find out the laser dots and to determine the centers of the dots in the enhanced *subtracted* (Figure 5.5). A 8x8 pixel window is used for the circular neighborhood modal to find the center of the laser dot with the brightest pixel. The four different circular neighborhoods in the modal are considered as the similarity criteria while scanning the enhanced *subtracted* by 1 pixel step shifting for each column and row starting with searching column first.

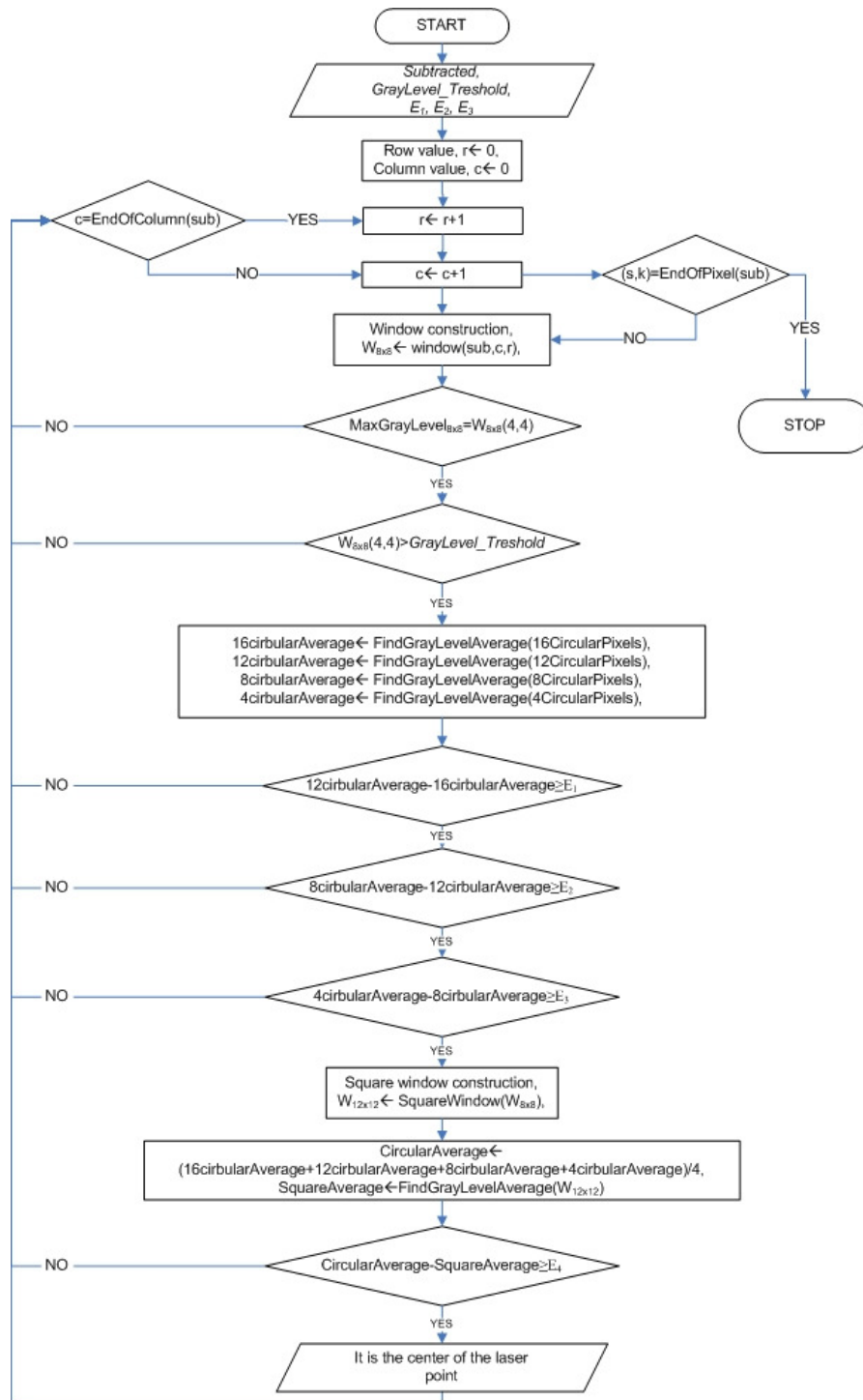


Figure 5.5 The flowchart of the algorithm for finding center of laser dots

The top left pixel is considered as the origin of the window and after each 1 pixel shift, the brightest pixel in the region of interest is checked whether it is in the circular neighborhood with 4 pixels at the center of the window. In other words, the

brightest pixel of the window in the enhanced *subtracted* is the pixel at row and column values of (4, 4).

The brightest pixel found at (4, 4) is also checked to have a grayscale above a threshold. If the pixel of interest is not at (4, 4) or does not have a particular brightness, the window is shifted 1 pixel without any other process. The aims for checking the brightness and the position of the pixel are to be sure that the window is in the region of a laser dot and the window is overlapped exactly on the laser dot in the case of the first criteria is realized respectively. If any control of the criteria is failed, the structure of the window in the image is not checked to suit the modal shown in Figure 5.4 in order to prevent redundant examination of the same laser dot and to speed up the process of the algorithm.

Since the both criteria above are realized, the region in the enhanced *subtracted* searched by the window is checked if it is a laser dot or not. According to the circular neighborhood modal, the brightness of the pixels in the dot must increase towards the center of the region. The arithmetic average of grayscale for each neighborhood in the circular neighborhood modal is calculated to check the brightness of the dot. From the outer to the inner neighborhood, the four averages values of the grayscale of the number of pixels of 16, 12, 8 and 4 are calculated in sequence. The average values are checked to be greater than threshold grayscale values of E_1 , E_2 and E_3 .

$$(12\text{CircularAverage} - 16\text{CircularAverage}) \geq E_1$$

$$(8\text{CircularAverage} - 12\text{CircularAverage}) \geq E_2$$

$$(4\text{CircularAverage} - 8\text{CircularAverage}) \geq E_3$$

After evaluating different threshold values, it was seen that when some values for three thresholds are used, in the determination of laser dots, any considerable failure was found. Therefore all the threshold values are taken to be equal. In the case of three restrictions above are true, the dot of interest is accepted as a laser dot and is checked for the final criterion.

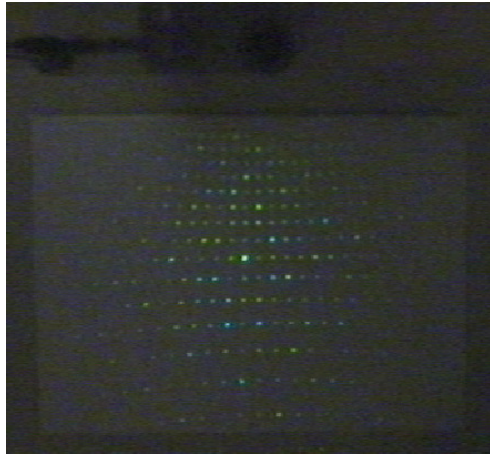
In the final test, the laser dots which have brightness levels with significant difference from the nearest neighbor are selected. The selection is done to eliminate the imaginary laser dots formed by any reflection of other laser dots. Two average values of grayscale are determined to be used for the selection.

A SquareAverage calculated by averaging the grayscale values of pixels of 12x12 pixel region formed by expanding the 8x8 window with 2 pixels in two directions for both axes is subtracted from a general CircularAverage calculated by averaging the four average values of circular neighborhoods. The result of the subtraction is checked if it is bigger than a threshold grayscale value E_4 .

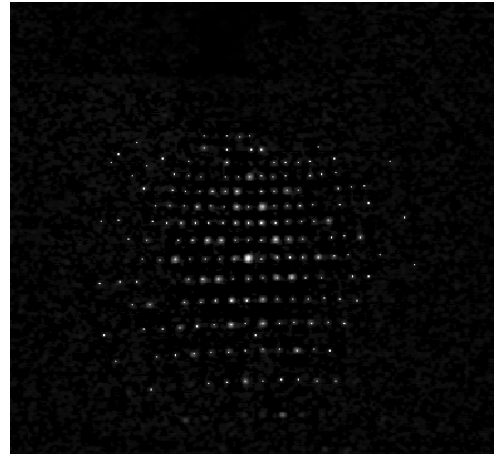
$$(\text{CircularAverage} - \text{SquareAverage}) \geq E_4$$

If the results of checking four criteria with threshold values of E_1 , E_2 , E_3 and E_4 are true, the dot of interest is accepted as the *laser dot* and corresponding pixel in the enhanced *subtracted* with the pixel in the position (4, 4) in the 8x8 pixel window is considered as the brightest pixel and the *center of the laser dot*.

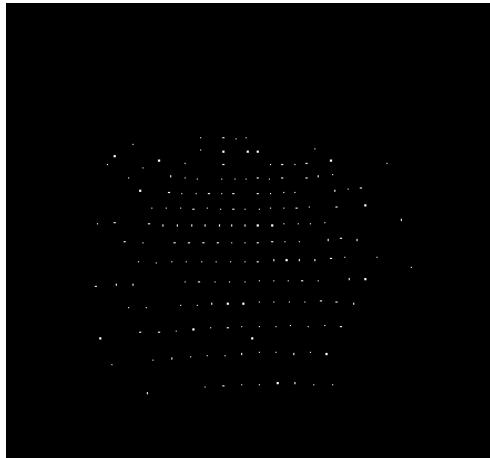
After image processing steps of the algorithm, the laser dot centers in *base* image in Figure 5.6a are found and shown as marked in grayscaled *subtracted* in Figure 5.6 b and purely in Figure 5.6c.



(a)



(b)



(c)

Figure 5.6 *Base* image (a), centers of the laser dots in grayscaled *subtracted* (b) and centers of the laser dots (c)

CHAPTER SIX
OMNI-DIRECTIONAL VISION SYSTEM

The incoming light from a point in real world follows a line between the real point and the focus of the mirror. This light is reflected at the point where it touches the surface of the rectilinear mirror and reaches the image plane of the camera (Figure 6.1) (Kweon et al., 2006). The image plane (CCD sensor) of the vision system is the plane where the light reaches to construct the image after passing the lens of the camera.

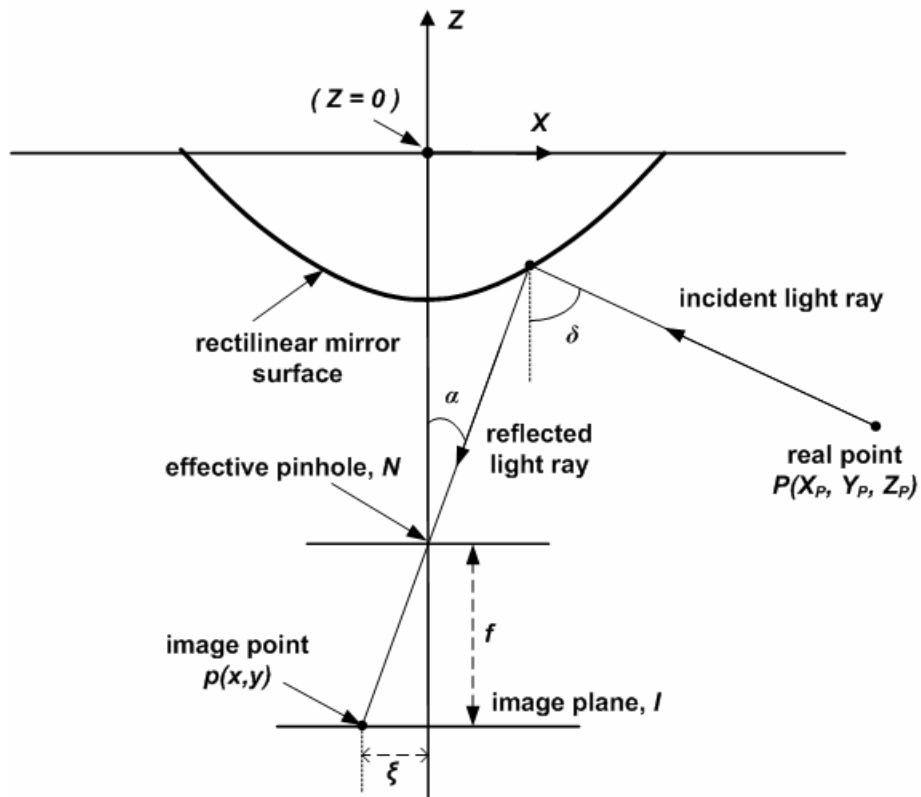


Figure 6.1 Simple projection of rectilinear mirror

In the figure above, α and δ are the zenith and incidence angles, respectively. N is the effective pinhole (nodal point) at which the reflected lights intersect. f is the distance between the nodal point N and the image sensor I . ξ is the pixel distance with respect to the zenith angle α .

6.1 Determination of 3D Locations of Laser Dots in The Environment

Since the stereo vision system includes two mirror-camera pairs, the distance of a point P should be calculated for both of them by using its projections on both mirrors. The geometrical model of the image plane for the constructed vision system is based on triangulation method (Gluckman et al., n.d.) and given in Figure 6.2.

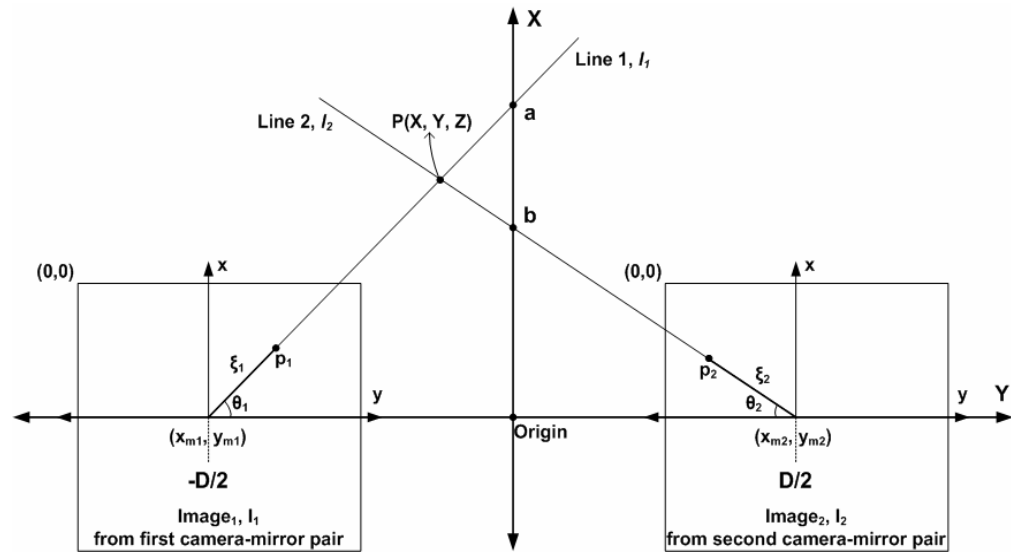


Figure 6.2 Geometric model of image plane for the constructed vision system

The centers of image I_1 and I_2 are (x_{m1}, y_{m1}) and (x_{m2}, y_{m2}) , respectively. Here, x is the row value and y is the column value of a point in the image. The points in the first and second images, which are captured by the first and second camera-mirror pairs, are $p_1(x_{p1}, y_{p1})$ and $p_2(x_{p2}, y_{p2})$, respectively. The θ_1 and θ_2 are the longitude angles. The camera-mirror pairs are placed with a distance D between them.

For finding the horizontal distances between a point in the real world and the vision system, the real world X and Y axes values of point $P(X_P, Y_P, Z_P)$ can be calculated by determining the intersection point of two lines l_1 and l_2 given in the figure. The equations,

$$Y = \frac{D}{2a} X - \frac{D}{2} \quad (6.1)$$

$$Y = \frac{D}{2b} X + \frac{D}{2} \quad (6.2)$$

can be written for lines l_1 and l_2 , respectively. Pixel $p_1(x_{p1}, y_{p1})$ and real world point $(a, 0)$ on X axis are on lines l_1 , and pixel $p_2(x_{p2}, y_{p2})$ and point $(b, 0)$ are on line l_2 . The values a and b are found by using the pixel values of images I_1 and I_2 for $Y=0$ as:

$$a = \frac{-Dx_{1p}}{2y_{1p}} \quad (6.3)$$

$$b = \frac{Dx_{2p}}{2y_{2p}} \quad (6.4)$$

where $x_{1p}=(x_{p1} - x_{m1})$, $y_{1p}=(y_{p1} - y_{m1})$, $x_{2p}=(x_{p2} - x_{m2})$ and $y_{2p}=(y_{p2} - y_{m2})$. Substituting equations (6.3) and (6.4) in equations (6.1) and (6.2), respectively and considering right hand sides of the equations (6.1) and (6.2) to be equal for point P , equations (6.5) and (6.6) are derived to calculate the X and Y axes values:

$$X_p = \frac{Dx_{1p}x_{2p}}{x_{1p}y_{2p} - x_{2p}y_{1p}} \quad (6.5)$$

$$Y_p = \frac{D(x_{1p}y_{2p} + x_{2p}y_{1p})}{2(x_{2p}y_{1p} - x_{1p}y_{2p})} \quad (6.6)$$

According to Figure 6.1, the Z axis value of the real point P for a camera located at rotational axis Z can be calculated as:

$$Z_p = \frac{\sqrt{X_p^2 + Y_p^2}}{\tan \delta} \quad (6.7)$$

where H and δ are the height of the vision system from to the floor ($Z=0$ at the mirror base as shown in Figure 6.1) and incidence angle, respectively. The distance between the real point and the floor, h can be calculated as:

$$h = H - Z_p$$

Finally, substituting equation (3.6) mentioned in Section 3.1.2.2 for rectilinear projection into equation (6.7) for angle δ with respect to the zenith angle α and by using the tangential relation of α with pixel distance ζ and focal length f in Figure 6.1

(ξ_1 for first image in Figure 6.2), the Z axis value of the real point P for the first mirror centered on point $(0, -D/2)$ can be calculated as given in equation (19):

$$Z_p = \frac{\sqrt{X_p^2 + (Y_p + \frac{D}{2})^2}}{\tan \left[\tan^{-1} \left(\frac{\tan \delta_r \xi_1}{\tan \theta_r f} \right) \right]} \quad (6.8)$$

The pixel distance of the image point in equation (6.8) is calculated as:

$$\xi_1 = \sqrt{(x_{p1} - x_{m1})^2 + (y_{p1} - y_{m1})^2} = \sqrt{x_{1p}^2 + y_{1p}^2} \quad (6.9)$$

The value of focal length f should be used as its pixel equivalent. δ_r and α_r are the constants reference angles dependent on sensor size as mentioned in Section 3.1.2.2 for rectilinear projection. α_r is the maximum reflection angle that the camera can take reflections from the mirror. The angles δ_r and α_r are 80° and $26,565^\circ$ for the CCD camera of the developed vision system, respectively (Kweon et al., 2006). Therefore mirror constant of tangential ratio of δ_r and α_r is 11.34259 in equation (6.8).

After obtaining the X , Y and Z axes values of sufficient number of real points, the 3D structure of the environment can be constructed.

Each point in the dot-matrix laser pattern has an image on both of the mirrors used. Therefore, each point is represented by two different points on the vision system and these points are called as *pixel pair*. Since the distribution of the laser dots is known according to a reference point, one of the image points in one mirror can be easily matched with the corresponding image point in the other mirror. Hence, the amount of error is minimal. Depending on the localization difference between these points on the mirror, the distance of the laser point from the vision system in the real world can be calculated.

6.2 Error Calculation According to Row and Column Values

The total relative error rate occurred in calculation of the distance on X axis for function $X(x_{p1}, y_{p1}, x_{p2}, y_{p2})$ can be found by equation (6.10):

$$\frac{dX}{F} = \frac{\frac{\partial X}{\partial x_{p1}}}{F} dx_{p1} + \frac{\frac{\partial X}{\partial y_{p1}}}{F} dy_{p1} + \frac{\frac{\partial X}{\partial x_{p2}}}{F} dx_{p2} + \frac{\frac{\partial X}{\partial y_{p2}}}{F} dy_{p2} \quad (6.10)$$

The total error rate dX is dependent on the errors dx_{p1} , dy_{p1} , dx_{p2} and dy_{p2} for locations of matched pixels in first and second images. The partial derivatives of the function X with respect to four variables can be easily derived with chain rules (Swokowski et al., 1994), and are not derived further here for clarity. The partial derivatives and error rates for each independent variable can be positive or negative. The possible maximum relative error rate can be calculated for any function $F(x_{p1}, y_{p1}, x_{p2}, y_{p2})$ as follows:

$$\left| \frac{dF}{F} \right| = \left| \frac{\frac{\partial F}{\partial x_{p1}}}{F} \right| |dx_{p1}| + \left| \frac{\frac{\partial F}{\partial y_{p1}}}{F} \right| |dy_{p1}| + \left| \frac{\frac{\partial F}{\partial x_{p2}}}{F} \right| |dx_{p2}| + \left| \frac{\frac{\partial F}{\partial y_{p2}}}{F} \right| |dy_{p2}| \quad (6.11)$$

The error formula for X , Y and Z are also obtained by substituting related functions (6.5), (6.6) and (6.7) in equations (6.10) and (6.11), and can be derived further, respectively.

6.3 Calculating The Locations, Errors and Calibration

To reduce the errors in distance calculations, a mathematical calibration procedure was generated using the equidistance projection principle. According to the calibration procedure, the stereo vision system was positioned at a particular height in vertical axis of the camera-mirror pairs and some control points which were matched already in two images were used for the calibration.

6.3.1 The Sources and Reasons of Errors

Possible error sources of the vision systems are:

- The alignment problem of the camera and mirror axis,

- Limited resolution of the vision system,
- Image deformation due to the camera and the surface quality of the mirror.

The hardware problems which cannot be solved by mechanical solution are tried to be corrected by software algorithms and the process of correction is called “*calibration*”.

An omni-directional vision system consists of mirrors, cameras, lenses and the platform to combine all the components. The error rates due to the components of the system may be corrected by different methods. In such a method, the classical perspective camera is calibrated alone with the lens used and the calibrated parameters are used to calibrate over all vision system. In other method, the vision system with cameras, lenses and mirrors is calibrated as a whole system. While in the first method, the intrinsic and extrinsic parameters of the camera are calculated; in the second one the calibration is done independent of the parameters.

Since the refractive lens used in the vision system for the study is special purpose lens, the vision system must be calibrated as a whole independent of the camera parameters.

In rectilinear projection, in a horizontal plane at a specific height from the floor, the sequential lights with a constant distance between each other generate image points with a constant pixel distance between corresponding sequential points. Since the mirror has equidistance projection for the lights from the same horizontal plane in contrast to perspective projection, the reflected lights at the external focal point would cause the image taken from the camera to be unperceptive in the case of a standard lens were used in the vision system (Kweon et al., 2004).

The refractive lens used in the vision system reflects the reflected lights from the mirror surface on to the image sensor of the camera in a manner to obtain a perceptible view keeping the equidistance projection principle. The classical

calibration method (Zhang, 2000) done with some calibration patterns such as chequered pattern is no more need since the refractive lens is used with the system.

It is possible to calculate the distances on X , Y and Z axes from the vision system of a real point in the environment corresponding to a particular matched pixel pair in the images by matching of the pixels in two images obtained by using two mirrors and two cameras. However the alignment problem of the axis of the camera and mechanical and electrical differences in the camera-mirror pairs in the stereo vision system, some errors are occurred in matching of the laser dots causing errors in calculations of the distances.

6.3.1.1 Matching The Pixels for Environment Without Obstacle

Acceptable calibration results can only be obtained in the case of acceptable matching procedure for the centers of the laser dots since the distance and height values of a real point according to the vision system are calculated by using the locations of the matched pixel pairs in two images. Therefore a calibration procedure must be followed for matching the pixels in the image obtained from the first camera with corresponding pixels in the image obtained from the second camera.

The row and the column of the image are represented by X and Y axes of the vision system respectively (Figure 6.2). The experiments were done by two camera-mirror pairs installed with an alignment on the Y axis first with 150 mm and then with 200 mm apart from each other (Figure 6.3).

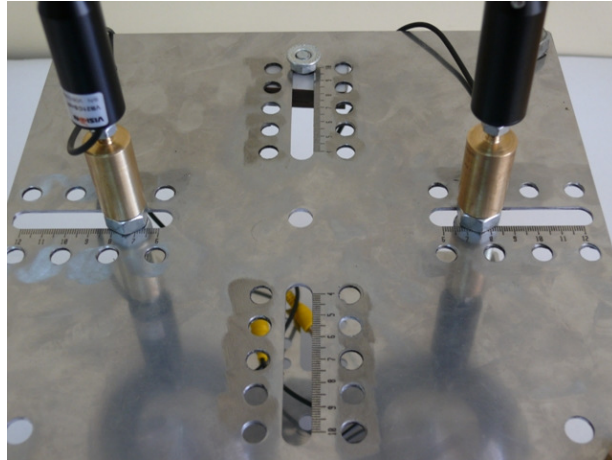


Figure 6.3 The vision system

The image obtained from the camera is considered as a matrix of pixels whose row values are on the vertical axis and the column values are on the horizontal axis. Two polynomials, one has degree of 1 and the other has degree of 4, are used in the mathematical model of matching. The rows of centers of two laser dots are matched by using the polynomial with degree of 1 since the matching is simple because of the alignment of the camera-mirror pairs on the same Y axis on which the row values are represented. The columns of centers of two laser dots are matched by using the polynomial with degree of 4 since the matching is relatively more complex. The flowchart of the matching algorithm is shown in Figure 6.4.

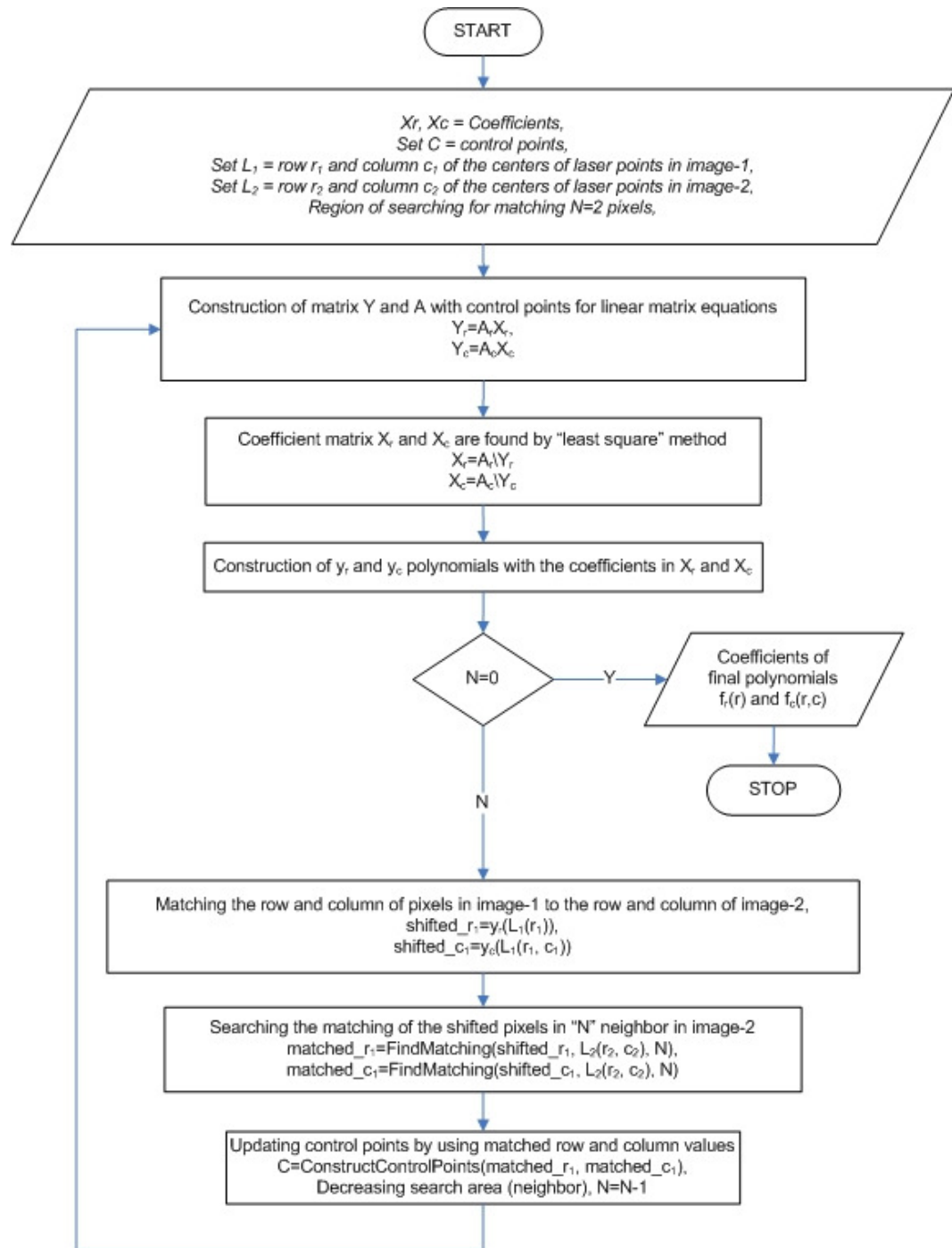


Figure 6.4 The flowchart of the matching algorithm

After the centers of the laser dots in the images obtained from two cameras were found, the equation (6.12) was used to match the rows of the centers:

$$y_r = l_1 r + l_2 \quad (6.12)$$

The equation (6.13) was used to match the columns of the centers:

$$y_c = k_1 r^3 + k_2 c^3 + k_3 r^2 c^2 + k_4 r^2 c + k_5 r c^2 + k_6 r^2 + k_7 c^2 + k_8 r c + k_9 r + k_{10} c + k_{11} \quad (6.13)$$

where r and c are the row and the column values of a pixel in the image respectively. y_r calculated by equation (6.12) and y_c calculated by equation (6.13) are the values of the row and the column values of the corresponding pixel in the second image matched for the pixel in the first image respectively.

The l and k coefficients in both equations are calculated by using Least Squares method. So the equations (6.12) and (6.13) can be written as:

$$Y_r = A_r X_r \quad (6.14)$$

$$Y_c = A_c X_c \quad (6.15)$$

where the equations for the matrices used above can be written as:

$$A_r = [r \quad 1]$$

$$X_r = [l_1 \quad l_2]^T$$

$$Y_r = [y_{1r} \quad y_{2r} \quad \dots \quad y_{nr}]^T$$

$$A_c = [r^3 \quad c^3 \quad r^2 c^2 \quad r^2 c \quad r c^2 \quad r^2 \quad c^2 \quad r c \quad r \quad c \quad 1]$$

$$X_c = [k_1 \quad k_2 \quad k_3 \quad k_4 \quad k_5 \quad k_6 \quad k_7 \quad k_8 \quad k_9 \quad k_{10} \quad k_{11}]^T$$

$$Y_c = [y_{1c} \quad y_{2c} \quad \dots \quad y_{nc}]^T$$

The matrices A_r and A_c , and the solution vectors Y_r and Y_c are to be filled with values in order to solve the linear matrix equations (6.14) and (6.15). The matrices A must be filled with sufficient number of row (r) and column (c) values of some pixels in the first image, and the corresponding values of row y_r and column y_c of the matched pixels in the second image. The pixels used to form the values of A matrices are called “*control pixel pairs*”.

The matching of the control pixel pairs were done manually to determine the row and column values of the pixels in both images to fill the values of A_r and A_c matrices. Matrices A_r and A_c are formed to calculate the row and the column values of the corresponding other pixels in the second image respectively. The X_r and X_c coefficient matrices are calculated by using A_r and A_c matrices in the solution for equation in the form of $(Y=AX)$ with Least Squares sense method in MATLAB. The row and the column values of the corresponding pixels in the second image of the pixels in the first image are calculated by substituting the coefficients in equations (6.12) and (6.13) respectively.

To find the row and column values of the centers of the corresponding laser dots in the second image, the matching of laser dots in both images is achieved by substituting the row and column values of the centers of the laser dots in the first image in equations (6.12) and (6.13) respectively. To check the validity of the calculated row and column values of a pixel, 2 pixels neighborhood of the pixel in the second image is searched to have an center of a laser dot which is already found. In the case of the presence of a laser dot in the specified neighborhood, the pixel in the first image and the center of the laser dot in the second image are considered to be matched to each other. After matching of the laser dots, the matched center pairs are to be used as the second *control pixel pairs*.

In the second step, the control pixel pairs found in the first step are used to calculate the new X_r and X_c coefficient matrices and the procedure followed in the first step is repeated except the neighborhood of 1 pixel is used for search area instead of 2 pixels. The row and column values calculated in second step are again used to calculate the final X_r and X_c coefficient matrices for the calibration process in the third step.

The final coefficients calculated after three steps are used to calibrate the calculations of the distances and the heights of the obstacles in the environment from the vision system and from the floor respectively.

6.3.1.2 Matching The Pixels for Environment With Obstacle

In the case of presence of obstacle in the environment, the rows and the columns of the centers of the laser dots in the first image are matched with the rows and columns of centers of the laser dots in the second image by using the equations (6.12) and (6.13) including the calibrated coefficients with an additional integer n ($n= 1, 2, 3, \dots, m$) determined experimentally in equation (6.13). The equation (6.13) is rewritten as equation (6.16):

$$y_c = k_1 r^3 + k_2 c^3 + k_3 r^2 c^2 + k_4 r^2 c + k_5 r c^2 + k_6 r^2 + k_7 c^2 + k_8 r c + k_9 r + k_{10} c + k_{11} - n \quad (6.16)$$

where n is an integer used only for matching of pixels and determined with the experiments according the resolution of vision system.

It is experimentally seen that, for a particular height of the placement of the vision system, if the column value of corresponding pixel can be found for the n value increased by 1, the height of the real point in the environment is nearly 150 mm from the floor. The n is increased one by one in matching process in order to find the matching centers of the laser dots. For each n value, if any centers are found to be matched, the matched centers are removed from the set of the laser centers to be matched. The n value is increased until all the centers of the laser dots are matched or reached to a predetermined upper limit. The heights of the real laser dots in the environment from the floor are not calculated by the value of integer n . They are calculated by using other parameters used also for calculations of the distances.

For example, while the points which are matched at the value of $n=0$ are considered to be around the level of floor, the ones which are matched at the value of $n=1$ are estimated to be on an obstacle above the floor.

The height of a laser dot on the obstacle varies according to the location of the obstacle. The dimensions of a corresponding real point in the environment of a pixel in the image are dependent on the height of the point from the floor as well as the dimensions of a laser dot. The locations of the rows for matched pixels in two images according to each other move more than the movement of the locations of the

columns as the height of the laser dot on the obstacle increases. Therefore the polynomial for matching the column pixels must calculate the corresponding column value with an additional integer value according to the height of the real point. The location of the corresponding pixel in the second image of the pixel in the first image cannot be found otherwise.

Although the implementation of the algorithm is extremely complex, for a mobile robot using this vision system, determination of the free area to navigate is so simple by matching only the laser dots in the environment for $n=0$.

The unmatched points during the matching procedure are considered to be “noise” and eliminated. However since especially the side of the obstacle is not often the common view of both cameras, some of the eliminated points are seen not to be noise but to be unmatched points due to the presence of them only in one image.

After all the laser dots are matched, by using θ_1 , θ_2 and δ which are already calibrated angles of two pixels matched of two laser centers in the images, the distances in the horizontal plane and the height in the vertical axis of all the laser dots can be calculated. The values of angles which are calculated for the laser dots in the environment without only obstacle are considered as calibrated angle values and do not need to be recalculated until the physical properties and the height of the vision system do not change.

6.3.1.3 Calculating The Distance and Height

To minimize the error rates in calculations of distances and height, the vision system is calibrated by using the images for the horizontal plane (floor) without any obstacle. The vision system is located at a particular height for calibration. The laser dots are scattered to the environment by using laser light source located in the middle of the camera-mirror pairs. The laser dots are all scattered on the floor in absence of any obstacle in the environment and therefore the heights of all the laser dots are to be the same. The values for distances in the horizontal plane and the height are first

calculated by the same image from one camera-mirror pair, then all the pixels in the first image are matched with the second image, finally three angle values are calculated by using known values for the distances and the height for all the matched pixels. The flowchart of the method is shown in Figure 6.5.

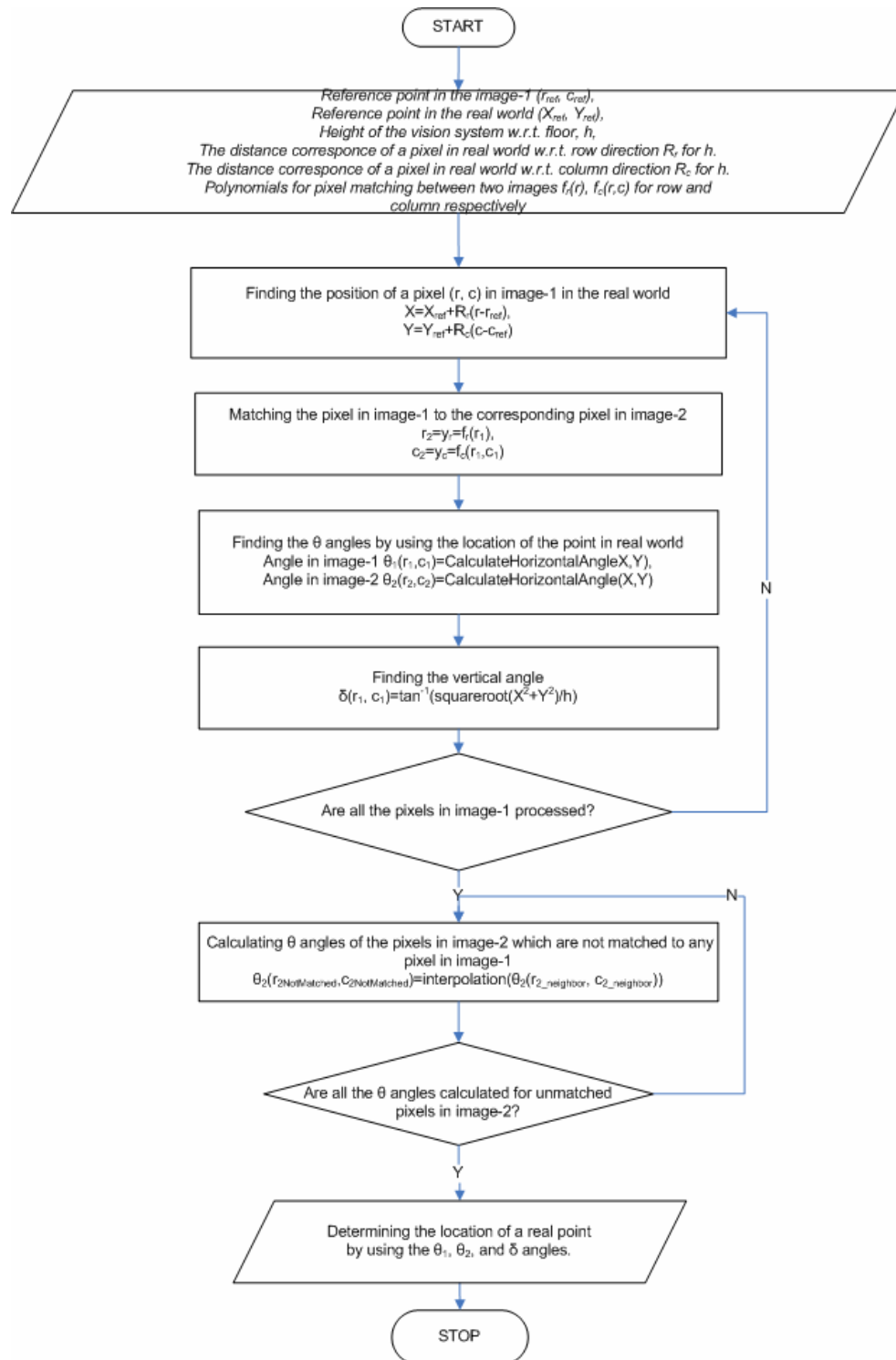


Figure 6.5 The algorithm for calculating horizontal distances and height

The corresponding number of pixels in the image of a particular length on the floor in the environment is already calculated with respect to the calibration

procedure. The distances of the laser dots from the vision system in the environment are calculated by the help of the equidistance principle of the mirrors used. According to the equidistance principle, a pixel in the image represents the same dimensional area in every location in the environment. By using this principle, if the distances in the horizontal plane, X and Y values, of corresponding real point in the environment of a pixel in the image are known, the distances of the real points in the environment of all the pixels in the image can be calculated. The equations (6.17) and (6.18) can be written for the calculations:

$$X = X_{ref} - R_r(r - r_{ref}) \quad (6.17)$$

$$Y = Y_{ref} - R_c(c - c_{ref}) \quad (6.18)$$

Where;

r_{ref} and c_{ref} are the row and column values of a reference pixel in the first image respectively.

X_{ref} and Y_{ref} are the distances of X and Y in the horizontal plane of the corresponding real point in the environment of reference pixel..

r and c are the row and column values of corresponding pixel in the first image of the real point whose distances are to be calculated.

R_r and R_c are the dimensions of corresponding area in the environment of a pixel in the first image.

In addition, angles θ_{irc} for all pixels in both images are also calculated. i represents the interested first or the second camera-mirror pair, r is the row value and c is the column value of the pixel for angle to be calculated.

R_r and R_c values may vary according to resolution of the image and distance of obstacle viewed in the image from the image plane. While the resolution is low the pixel in the image represents wide area in the environment. In contrast, the pixel represents narrow area while the resolution is high. Therefore the dimensions of obstacle in the image vary with respect to the resolution of the image. In addition, though the resolution is constant, the dimensional representative area of a pixel is increasing depending on the height of the vision system from the viewed region and

the accuracy of the image is decreasing. For example, when the vision system was placed at a height of 1,170 mm from the floor for experiments in an environment without obstacle, R_r was seen to be the real dimension of nearly 10.80 mm for each pixel in the image.

Pixel matching method is used to match each pixel in the first image whose horizontal distances of the corresponding point in the environment from the vision system is calculated.

In the case of the environment with an obstacle, the horizontal distances and/or the heights in the vertical axis of the center of the laser dot on the obstacle is different. Therefore the locations and the angles of the laser center in both images are different from the locations and angles of the laser center in the case of the environment without any obstacle (Figure 6.6). The location of the corresponding real point for the laser center is calculated by using angles θ_{irc} which are already determined.

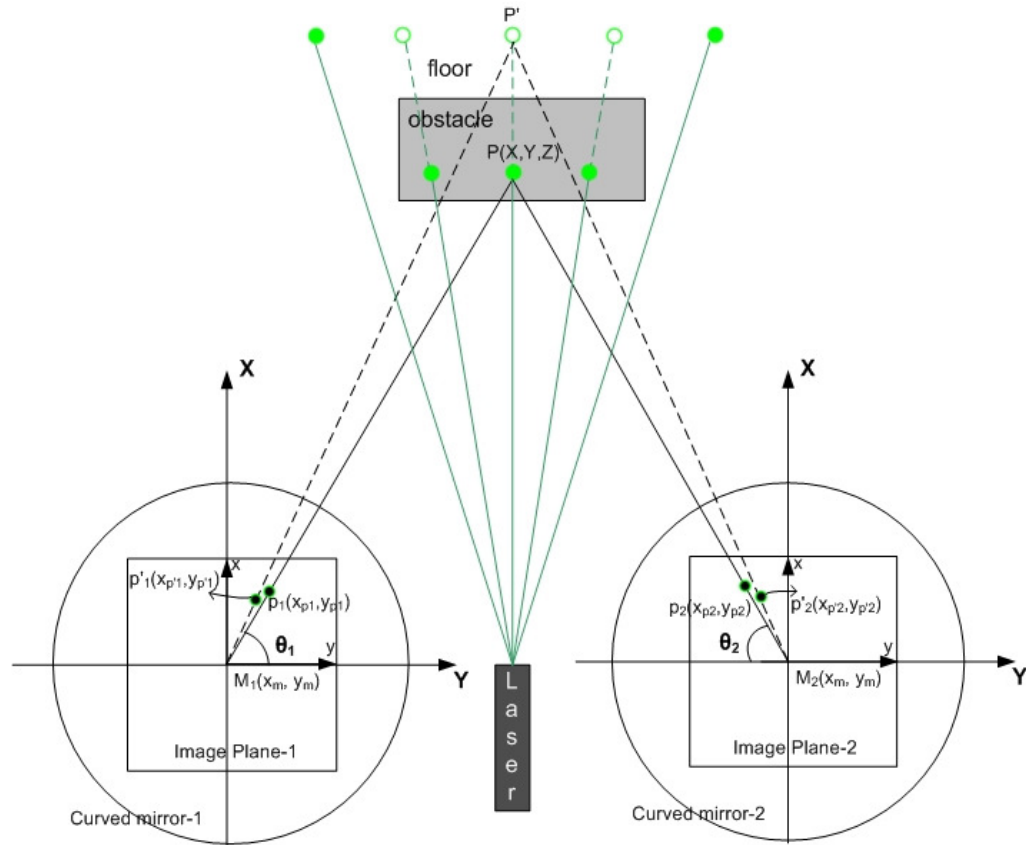


Figure 6.6 Horizontal distances and angle relationship in stereo vision

Where;

P is the real point,

P' is the location of the light in the environment without obstacle,

p_1 and p_2 are the images of the real point in both mirrors,

p_1' and p_2' are the projections of P' in both mirrors,

θ_1 and θ_2 are the angles between the light from point P and the Y axis of the vision system,

M_1 and M_2 are the centers of the mirrors.

The locations of the corresponding pixels in both images for the laser dot in the environment may vary since the real location of the laser dot changes according to the structure of the obstacle. The values of θ_1 and θ_2 for the rows and columns of the pixel are used to find the horizontal location of the laser dot in the environment by

using triangulation method according to geometric model of the vision system in Figure 6.2 easily.

To find the Z axis value of the laser dot in vertical axis, the height of the vision system and the horizontal distances of the dot are used. These values are used first to calculate the δ angle as in equation (6.19), and then the value of δ is substituted in equation (6.7) to calculate the Z axis value of the laser dot.

$$\delta = \tan^{-1}\left(\frac{\sqrt{X_p^2 + Y_p^2}}{H}\right) \quad (6.19)$$

where H is the height of the vision system from the floor.

Since the height of real point in the environment is the same for both camera-mirror pairs, calculating only the values of angle δ for all the pixels in the first image is sufficient.

Since the values of the rows and columns of the pixels in both images are integer, the results of the mathematical equations in matching method must be rounded to integers. Therefore some pixels in the second image may not be matched with any pixels in the first image. The error rates of the polynomial, whose coefficients are calculated, are relatively high in the border areas of the laser dots region. Because of these reasons, matching of the laser dots in the first image with the laser dots in the second image is a problematic process.

In the case of the presence of unmatched pixels in the second image, the angle value of each unmatched pixel is determined by calculating the arithmetic average of all the angle values known of pixels neighbor to the interested unmatched pixel.

CHAPTER SEVEN

EXPERIMENTS

The experiments done for the vision system can be classified into two main categories. The first category includes the experiments carried out by using synthetic data. By using the synthetic data, it is possible to test the vision system with more data and analyze the robustness of the vision system to noisy locations of the image pixels. In the second category, the experiments were done with real data representing the real laser dots. In the latter case, the experiments can be analyzed as the ones before and after the vision system improvement.

The vision system was improved by correcting the camera-mirror alignment and using the distance between two camera-mirror pairs as $D = 200$ mm instead of 150 mm which was used in the experiments done before the improvement of the vision system. In the experiments carried out after the improvement, the calibration done with the help of matching was not required anymore for calculating the distances of real laser dots from the vision system. Finally the vision system will be installed on the mobile robot and tested the whole system in terms of detecting the obstacles in the environment.

7.1 Preliminary Work

The preliminary experiments were done in two ways. In the first way, the applications were carried out with manual matching of the pixels in stereo images and in the second way, matching algorithm which was developed as detailed in Section 6.3.1.1 and 6.3.1.2, was used for the experiments.

7.1.1 Applications Without Matching Algorithm

Two images called *mask* and *base* were obtained before and after scattering the laser beam to the environment respectively by using both camera-mirror pairs of the

vision system. After the images obtained, by using the algorithms developed the laser dots in the environment were detected (Figure 7.1).

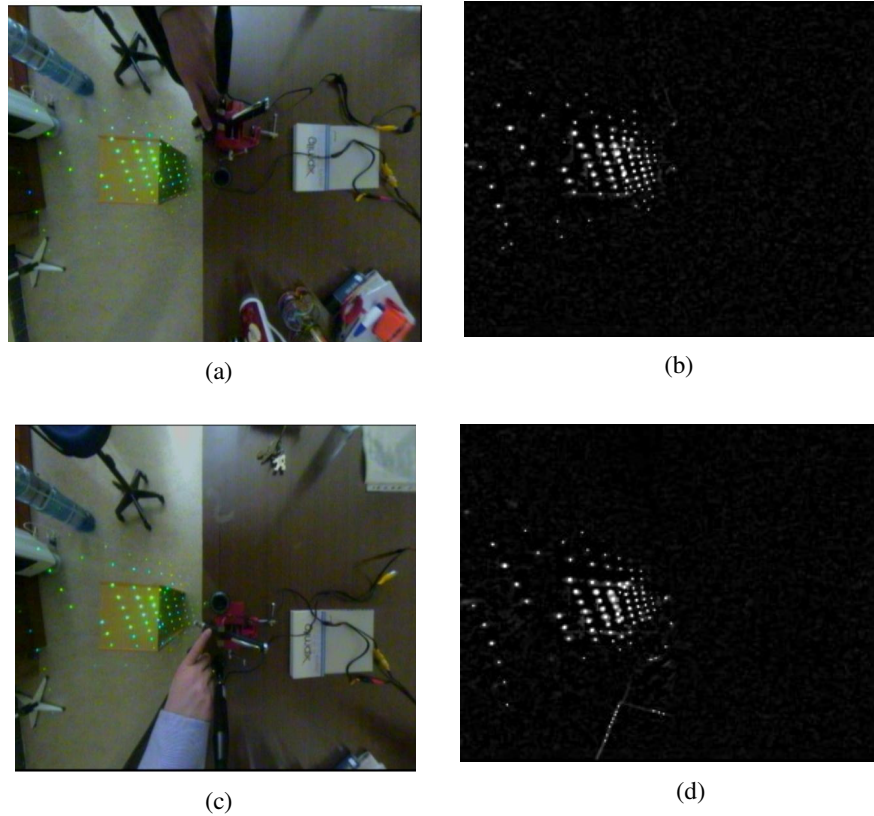


Figure 7.1 Stereo images *base1* for mirror-1 (a), *base2* for mirror-2 (c); and the laser dots in the base images are shown in (b) and (d), respectively.

Before the algorithm for matching of the laser dots in both image pairs was developed, some control laser dots in the image were marked to figure out the error rates in distance calculation and the locations of the dots on the X , Y and Z axes were measured manually according to the vision system.

By using software developed, the locations of the control dots in the environment were calculated. With the row and column values (x , y) for locations of dots in both mirrors which were determined manually. The results were compared with the measured locations and the error rates were calculated (Table 7.1).

Table 7.1 Locations on axes before matching

# of Point	Locations in the image, pixel				Calculated distances in the environment, cm			Measured distances in the environment, cm			Error rate, \pm (%)		
	Mirror-1		Mirror-2		CX	CY	CZ	MX	MY	MZ	EX	EY	EZ
	x	y	x	y									
1	238	242	271	239	3.00	-44.00	48.00	3.00	-46.00	55.00	0.00	-4.35	-12.73
2	243	260	263	256	2.00	-60.00	81.00	2.00	-63.00	95.00	0.00	-4.76	-14.74
3	276	235	309	232	-15.00	-49.00	49.00	-15.50	-51.50	55.00	-3.23	-4.85	-10.91
4	273	170	306	166	-13.00	-79.00	49.00	-13.50	-84.00	55.00	-3.70	-5.95	-10.91
5	189	170	222	168	25.00	-75.00	46.00	26.00	-80.00	55.00	-3.85	-6.25	-16.36
6	182	74	202	72	46.00	-194.00	76.00	48.00	-215.00	92.00	-4.17	-9.77	-17.39

CX, CY, CZ: Calculated Distance; MX, MY, MZ: Measured Distance; EX, EY, EZ: Error Rate

While the real points near the center of the vision system have almost no error, the ones which are far on the line perpendicular to the axis of the vision system have relatively higher error rates.

The absolute values of error rates on vertical Z axis for all points were seen to be higher than 10% and the highest error rate is on the 6th point with the value of -17.39%.

7.1.2 Applications With Matching Algorithm

Three experiments with different obstacle and obstacle locations were carried out. After capturing *mask* and *base* images and determining the centers of laser dots, by using the algorithm described in Section 6.3.1.1 and 6.3.1.2 for matching, the pixel correspondences in stereo images were found. Then the longitude angles θ_1 and θ_2 and incidence angle δ calibrated according to the procedure in Section 6.1.1.3 were used to calculate the distances of the laser dots, whose locations were already known, from the vision system.

The implementations included not only detecting the obstacles in the environment, but also finding the free area on the floor for a mobile robot to pass. For detecting the free area, the real points which were located on the floor level were used.

In the first experiment, a single obstacle was placed exactly across the vision system. The stereo *base* images captured from first and second camera-mirror pairs are shown in Figure 7.2a and 7.2b, respectively. In the second experiment, two obstacles were placed on both side of the line perpendicular to the axes of the vision system each with the same distances from the line (Figure 7.2e and 7.2f). In the third experiment, the single and small obstacle was placed symmetrically on the line perpendicular to the axis of the vision system (Figure 7.2i and 7.2j).

For each experiment, after the matching of laser dots in the two images, the matched pixel pairs were used to calculate the 3D distance of related real laser point from the vision system. According to the *Z* axis location within a threshold value, the point was marked if it was on the floor level. The points which were not on the floor level were considered to be on the obstacle and eliminated in the image. Therefore rest of the points in the image represents the free area in the environment.

The images including matched pixel pairs in three experiments are shown in Figure 7.2c, 7.2g and 7.2k, respectively. The related images for free area including the points on the floor level are shown in Figure 7.2d, 7.2h and 7.2l.

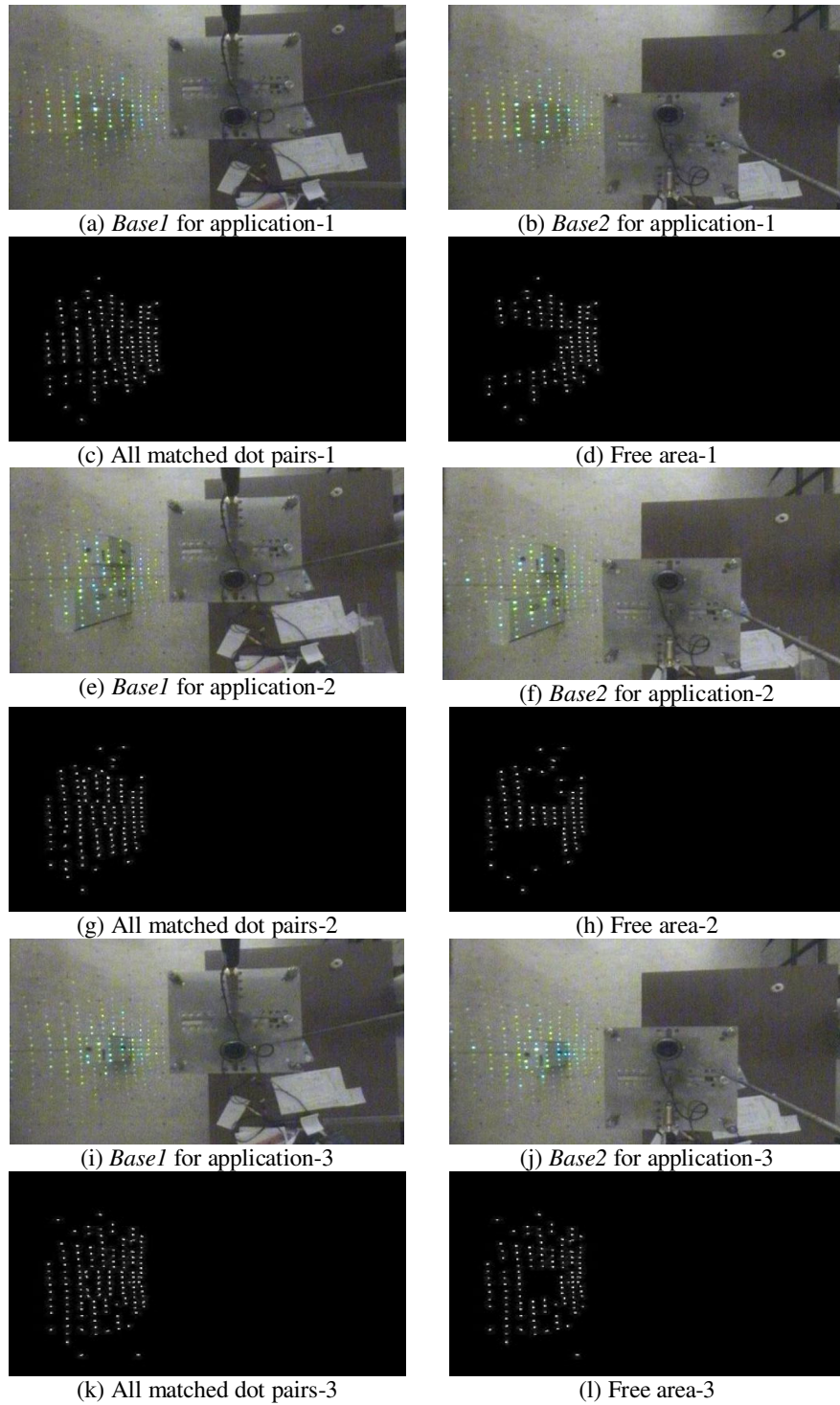


Figure 7.2 Images indexes through (a) – (l) for three applications

The relative error rates were analyzed especially for the Z axis values of the points on the floor level since the real distance value is the same for all the points.

Therefore error rates were relatively simple to calculate. The absolute error rates for the related axis were mostly lower than 10% but still high due to incorrect alignment of the camera-mirror pairs.

7.1.3 Problems and System Improvements

Possible error sources are some mechanical problems in the platform on which the vision system stands, the alignment problem of camera and mirror, and the horizontal alignment of the vision system.

As a result, especially to achieve better alignment, the vision system was improved mechanically and extensive experiments were done to test the vision system as described in the next section. The next experiments were carried out by adjusting the distance (D) between the camera-mirror pairs 200 mm instead of 150 mm used in the preliminary work, to achieve better accuracy in distance calculation.

7.2 Experiments After Vision System Improvement

Synthetic and real data were used after improvement of the vision system. The vision system can be tested with more experiments by using synthetic data. The synthetic corrupted data were used to simulate the robustness of the vision system to the noise. After improvement of the system, the vision system was tested by using real laser points.

7.2.1 Experiments With Synthetic Data

For implementation with synthetic data, the equations (3.1) through (3.7) explained in Section 3.1.2.2 for rectilinear projection, were used to obtain the synthetic images for two mirrors consisting of image points corresponding to the points in the environment assumed to be located 100 mm apart from each other as a

matrix pattern in the same horizontal plane. This simulation process was repeated for the horizontal plane locations of 8 different vertical distances (Z axis) (Figure 7.3).

The distance (D) between the camera-mirror pairs was 200 mm. The first and the second camera-mirror pairs were assumed to be located at $Y = -100$ mm and $Y = +100$ mm, respectively for stereo imaging.

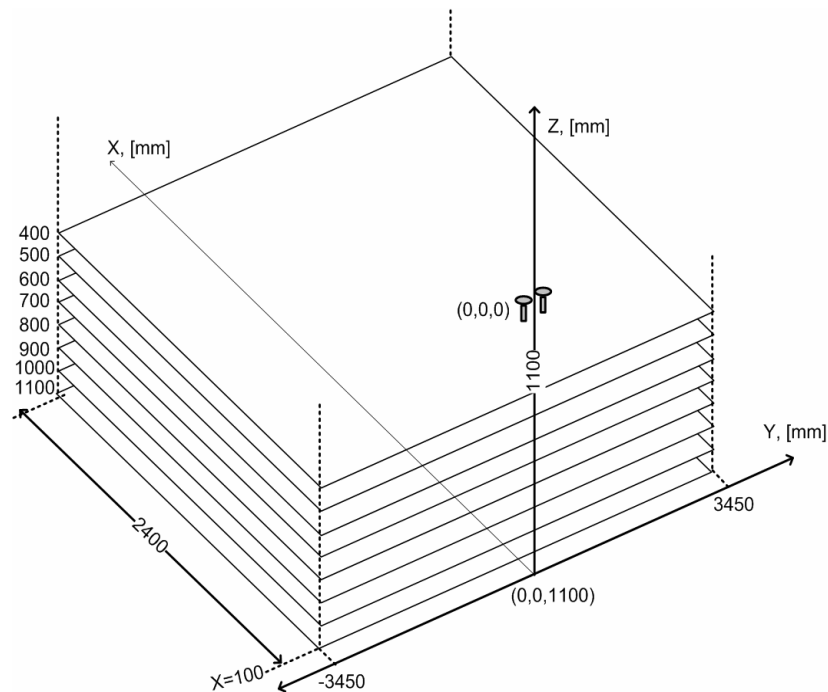


Figure 7.3 Horizontal plane locations for simulation

The simulated images obtained for horizontal plane locations of vertical distances 1100 mm, 800 mm, 600 mm and 400 mm are shown as samples in Figure 7.4. The closer the horizontal plane to the vision system, the smaller will be the number of points to be viewed as seen in the figure. For each horizontal plane, the above and the below images of stereo pair were constructed for the first and second camera-mirror pairs, respectively.

There are some missing image pixels at the same vertical line on the border area of the stereo images in the figure because the imaginary real points are out of view of

the vision system and there may be some calculation errors during the processing of the fraction numbers resultant of the rectilinear projection equations.

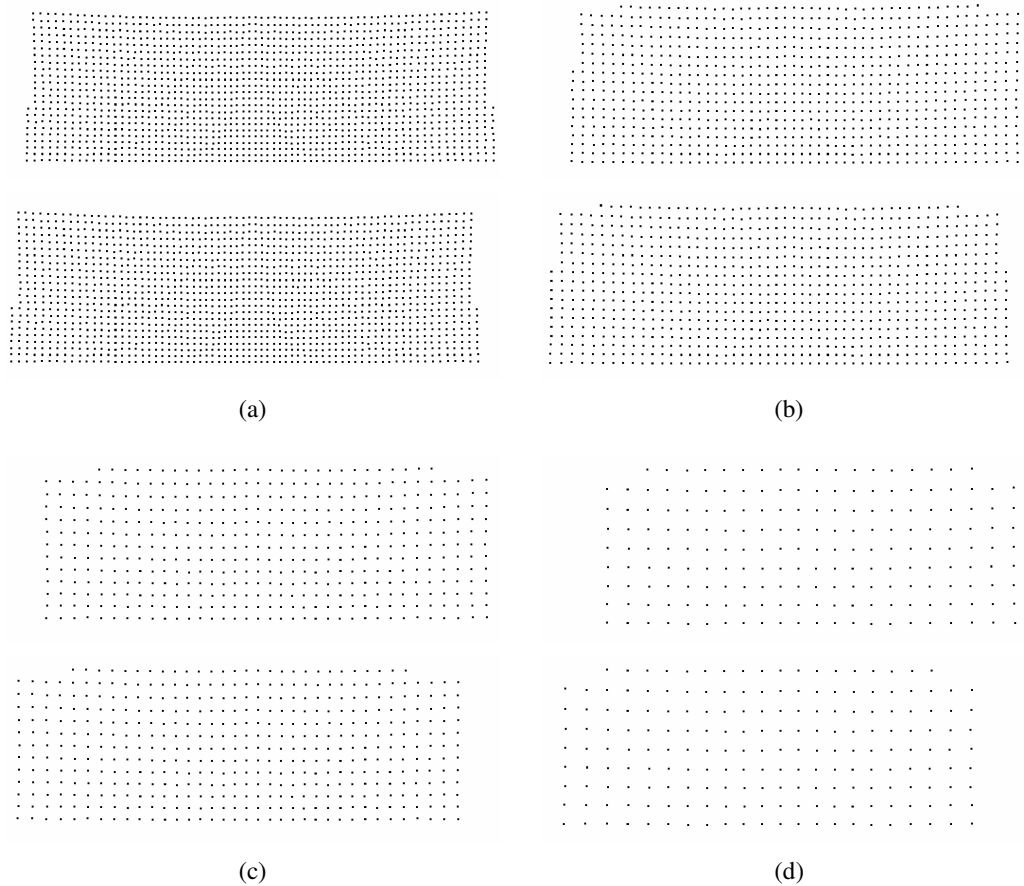


Figure 7.4 Synthetic stereo images for horizontal planes at vertical distances of 1100 mm (a), 800 mm (b), 600 mm (c) and 400 mm (d)

For each pixel in the first image, there is a corresponding pixel in the second image. The locations of the matched pixels in two images for two mirrors were used for back projection to calculate the related 3D distances of the points in the environment whose locations were already known. The calculated distances and the correct locations were used to determine the average relative error rates for all the horizontal planes located in different vertical distances (shown as *without distortion* column in Table 7.2).

Table 7.2 Horizontal Plane locations and error rates for image points

Vertical Distance from Vision System, [mm]	# of points	Distances	Error Rates, [%]				
			without distortion	r1	r1-c1	r1-c1-r2	r1-c1-r2-c2
400	194	X	1.24	1.48	1.96	2.65	2.54
		Y	1.26	1.45	2.02	2.54	2.59
		Z	7.62	7.86	7.58	7.86	8.01
500	302	X	1.66	1.92	2.45	3.10	3.72
		Y	1.68	1.88	2.50	3.10	3.81
		Z	5.33	5.55	5.47	5.88	6.54
600	460	X	1.78	2.32	2.89	3.69	3.79
		Y	1.76	2.30	2.93	3.69	3.97
		Z	3.96	4.55	4.56	5.20	4.82
700	650	X	2.42	2.75	3.40	4.45	4.82
		Y	2.49	2.71	3.43	4.39	4.96
		Z	3.66	4.05	4.23	5.16	5.56
800	878	X	3.04	3.65	4.18	5.50	6.69
		Y	3.14	3.63	4.21	5.53	6.84
		Z	3.74	4.50	4.67	6.01	7.03
900	1130	X	3.27	4.14	5.15	7.57	7.08
		Y	3.30	4.13	5.22	7.63	7.21
		Z	3.72	4.68	5.41	7.83	7.29
1000	1386	X	3.45	4.14	5.12	7.00	7.28
		Y	3.52	4.11	5.19	7.05	7.47
		Z	3.77	4.50	5.31	7.19	7.35
1100 (floor level)	1582	X	3.97	5.10	6.02	8.62	8.60
		Y	4.03	5.08	6.09	8.71	8.82
		Z	4.27	5.42	6.20	8.81	8.73
Weighted Averages for all points	6582	X	3.12	3.86	4.68	6.50	6.69
		Y	3.18	3.84	4.73	6.53	6.86
		Z	4.07	4.86	5.37	7.15	7.26

r1, r2, c1, c2: Distorted row and column for pixels of points in first and second images, respectively

The calculated row and column values were rounded to integer to simulate the effect of the image sensor resolution on error rate. Hence the error rates in the table for distortion free data are due to the limitation of the image resolution.

The error distributions along perpendicular (X) and lateral (Y) directions for horizontal plane 1100 are shown in Figure 7.5. The nearer the points to the vision system in perpendicular direction, the higher will be the error rates since the points are viewed in the lower resolution part close to the of center of the mirror (Figure 7.5a). The far the points from the center axis of the vision system in lateral direction, the higher will be the error rates (Figure 7.5b).

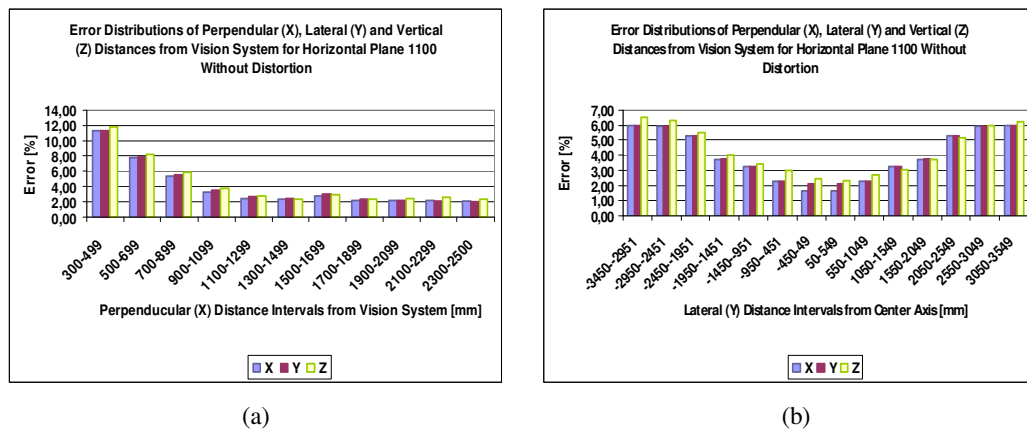


Figure 7.5 Error distributions of horizontal plane 1100 for X (a) and Y (b) intervals for synthetic data without distortion

Then randomly generated real value of interval $(-1, 1)$ with zero mean was added to the row and column values of pixel locations in order to see the effect of corrupted pixel locations on the relative error rate of the system. The random generator was run separately to add distortion to the row and column locations. The distortion corresponds to value of dx_{p1} , dy_{p1} , dx_{p2} and dy_{p2} in equation (6.10) for rows and columns in first and second images, respectively. The results of error rates obtained for all axes with distorted pixel locations are also shown in Table 7.2. The notations $r1$, $r2$, $c1$ and $c2$ are used for the distorted row and column for pixels of points in first and second images, respectively.

In Table 7.3, the average error rates extracted for almost the same region with the experiments done with real laser points after the improvement of the vision system (Section 7.2.2), (Figure 7.6a) are given. The simulation results are seen to be lower than or close to the real data results.

Table 7.3 Error rates for a specific region in the environment

Perpendicular (X) Interval : (+450) – (+2500) mm Lateral (Y) Interval : (-1400) - (+1400) mm				
Vertical Distance of Horizontal Plane from Vision System, [mm]	# of points	Error Rates, [%] (without distortion)		
		X	Y	Z
700	332	1.31	1.42	3.18
800	390	1.62	1.77	2.71
900	468	1.63	1.67	2.39
1000	540	1.89	2.11	2.39
1100	546	2.08	2.26	2.56

7.2.2 Experiments With Real Data

For the experiments carried out with real data, two different environment models were used. In the first model, a horizontal plane and in the second model, a vertical plane was used. In order to see the effects of vertical distance between the horizontal plane locations and vision system, horizontal plane was located at four vertical distances (height) from the vision system with the near most side from the Z axis of the vision system at perpendicular distance of 450 mm. Besides, for perpendicular distance effect, vertical plane was located at 6 different locations. The locations and the dimensions of horizontal and vertical planes are seen in Figure 7.6a and 7.6b.

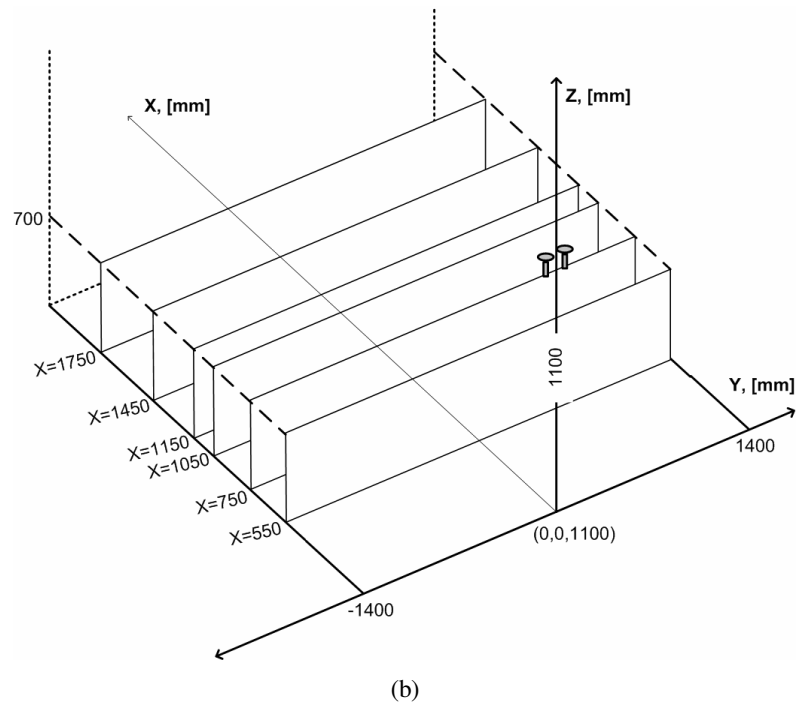
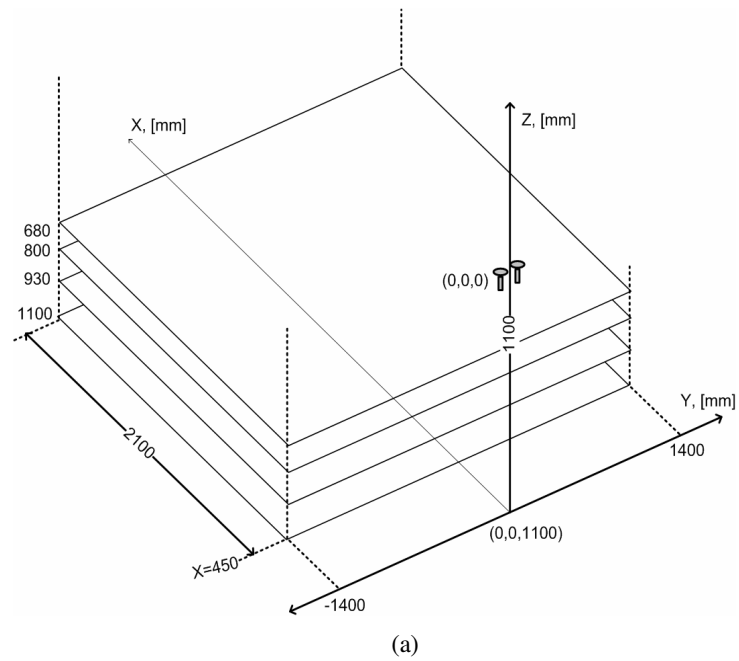


Figure 7.6 Experiment layouts for horizontal (a) and vertical (b) plane locations for real laser dots

The *base* images of horizontal plane locations captured by the omni-directional vision system are shown in Figure 7.7. The *base* images of horizontal plane located

at vertical distances (Z axis) of 1100 mm, 930 mm, 800 mm and 680 mm are shown in Figure 7.7a through 7.7d, respectively.

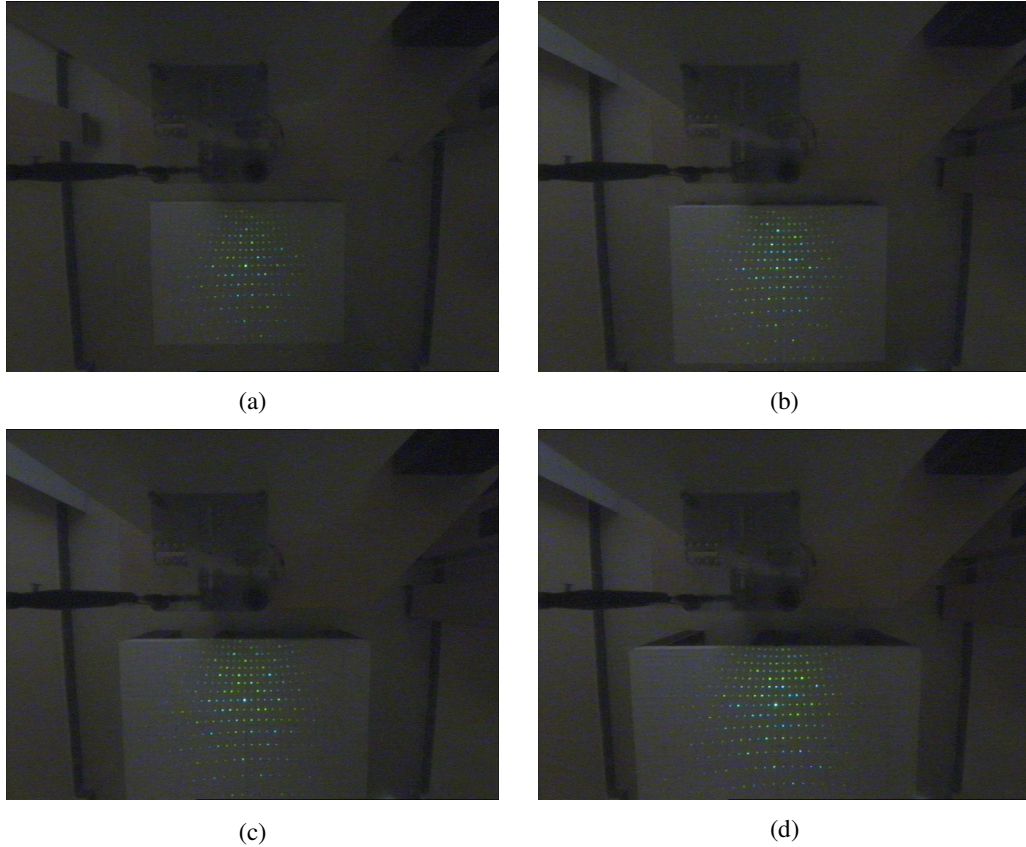


Figure 7.7 *Base* images for horizontal plane locations of vertical distances 1100 mm (a), 930 mm (b), 800 mm (c) and 680 mm (d)

The *base* images of vertical plane located at perpendicular distances (X axis) of 550 mm, 750 mm, 1050 mm, 1150, 1450 and 1750 mm are shown in Figure 7.8a through 7.8f, respectively.

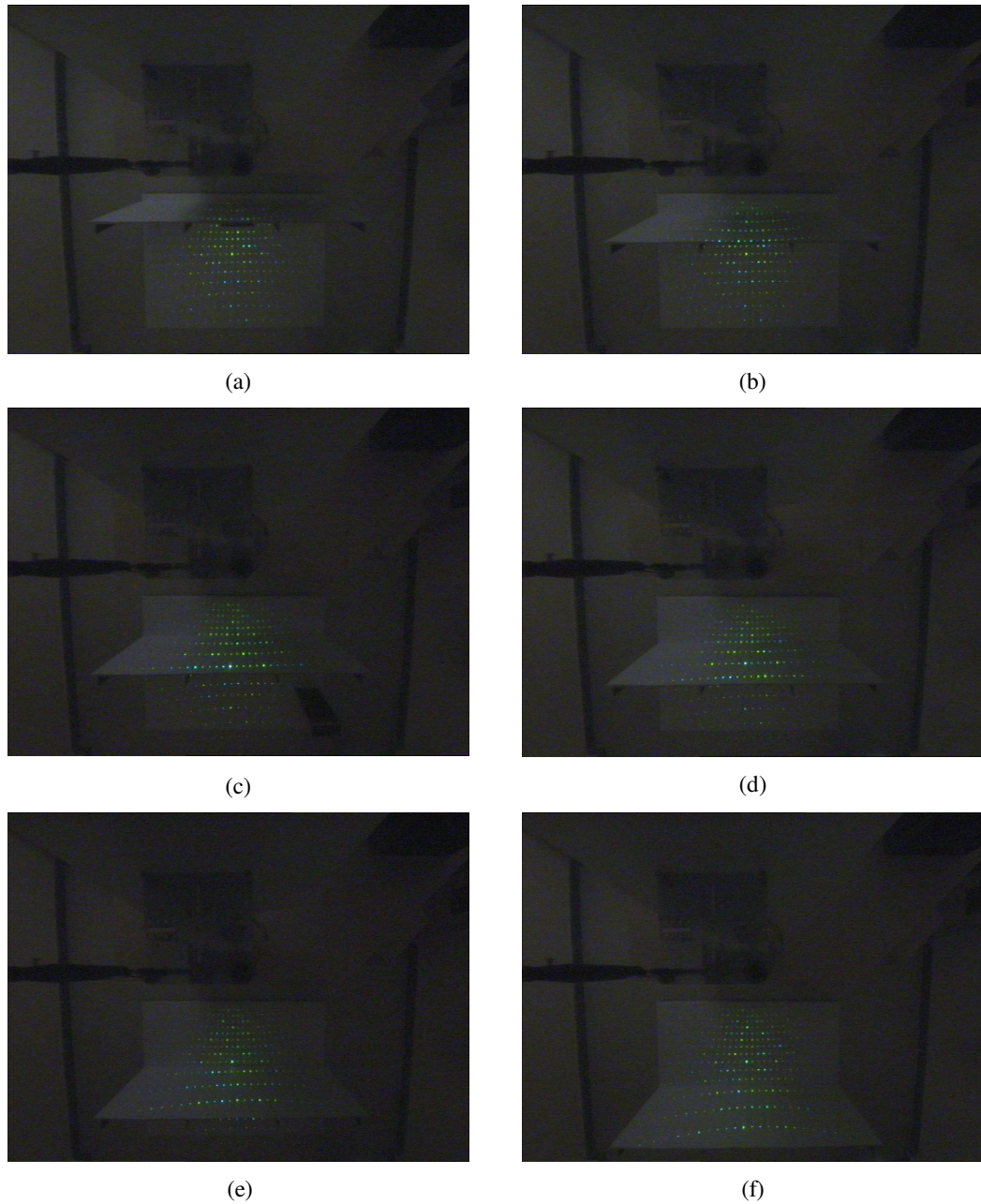


Figure 7.8 *Base* images for vertical plane locations of perpendicular distances 550 mm (a), 750 mm (b), 1050 mm (c), 1150 mm (d), 1450 mm (e) and 1750 mm (f)

The error details of horizontal and vertical planes are given in Table 7.4.

Table 7.4 Plane locations and error rates for vertical and perpendicular distances of detected real points

Error Distributions, [%]	Horizontal Planes				Vertical Planes					
	Vertical Distance (Z)				Perpendicular Distance (X)					
Distance from Vision System, [mm]	680	800	930	1100	550	750	1050	1150	1450	1750
# of data points	200	192	161	159	19	46	56	56	51	37
Minimum	0.03	0.02	0.01	0.00	0.00	0.01	0.03	0.00	0.05	0.00
Lowest 25%	1.38	1.68	1.15	1.53	1.30	0.64	1.06	1.19	0.89	0.82
Median	3.29	3.14	3.02	2.76	2.27	1.41	1.72	2.24	1.95	1.60
Lowest 75%	5.90	5.57	4.96	4.30	3.62	2.34	3.40	3.03	2.98	3.12
Maximum	17.45	14.26	13.28	11.03	5.57	5.95	8.16	6.67	5.11	7.16
Mean	4.13	3.91	3.51	3.14	2.41	1.78	2.26	2.18	2.17	2.02
Standard Deviation:	3.57	2.98	2.81	2.28	1.53	1.44	1.72	1.39	1.41	1.59

Depending on error rates, it can be said that, with the increasing distance from the vision system the mean error of the vertical distance decreases from 4.13% at level 680 to 3.14% at level 1100 which is the floor level. At the same situation also occurs for the perpendicular distance calculations. The mean error decreases from 2.41% at plane 550 to 2.02% at vertical plane 1750. Also, most of the errors (75%) were located under 4.30% for horizontal (1100) and 3.12% for vertical (1750) planes.

In order to see the error distributions of all axes together, including lateral (Y axis) distance errors with respect to distance intervals of all axes, the results of horizontal plane at vertical distance of 1100 mm and vertical plane at perpendicular distance of 1450 mm are analyzed. The related average error rates for different distance intervals and the error details are shown in Figure 7.9 and Table 7.5, respectively.



Figure 7.9 Error distributions of horizontal plane 1100 for X (a) and Y (b) intervals; and of vertical plane 1450 for Y (c) and Z (d) intervals

Table 7.5 Plane locations and error rates for all axes distances of detected real points

Error Distributions, [%]	Horizontal Plane			Vertical Plane		
	X	Y	Z	X	Y	Z
Distance from Vision System, [mm]	1100			1450		
# of data points	159			51		
Minimum	0.00	0.04	0.00	0.05	0.06	0.01
Lowest 25%	0.73	1.45	1.53	0.89	1.09	0.82
Median	2.05	2.73	2.76	1.95	2.38	2.24
Lowest 75%	3.60	4.38	4.30	2.98	3.49	3.53
Maximum	6.80	10.81	11.03	5.11	8.24	6.87
Mean	2.31	3.10	3.14	2.17	2.71	2.37
Standard Deviation	1.78	2.23	2.28	1.41	1.92	1.71

The minimum and maximum average error rates are 2.17% and 3.14%, respectively for both plane locations. According to Table 7.5 and the graphs in Figure 7.9, the average error rates for lateral Y axis are generally higher than the ones for X axis. The average error rates for all axes (Figure 7.9c and 7.9d) generally

follow each other for vertical plane. The average error rates for horizontal plane experiment (Figure 7.9a and 7.9b) are not so regular with respect to each other. Besides, the corresponding error rates for axes of vertical plane are lower than the ones for horizontal plane.

Another experiment was also carried out with three obstacles located on the floor plane. The dimensions and locations of the obstacles are given in Figure 7.10. In this experiment, all obstacles on the floor were determined and their heights were also approximately calculated. It was seen that the average error rates for the points on the obstacles are 2.20%, 3.21% and 3.55% for X, Y and Z axes, respectively.

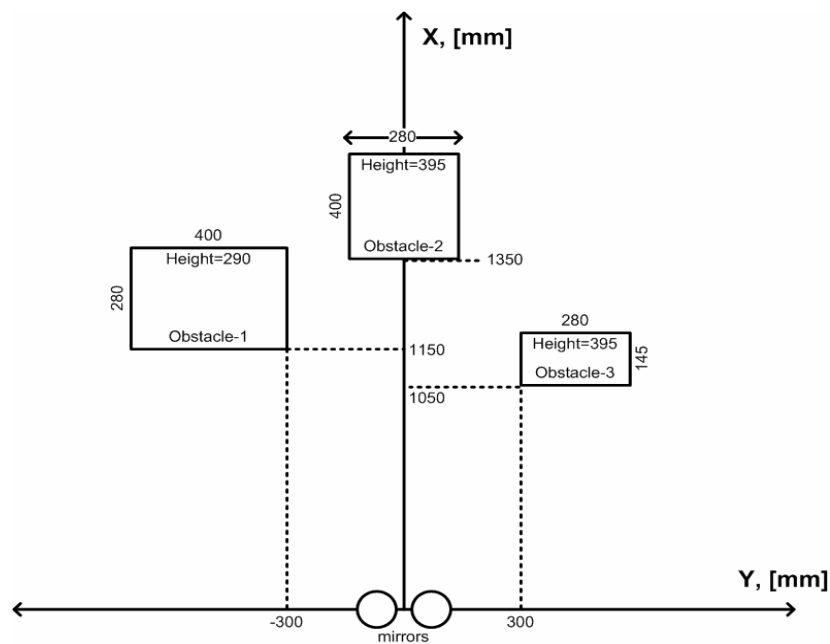


Figure 7.10 Dimensions and locations of three obstacles

When the points which are close to the floor level ($Z \cong 1100$) are extracted from the dot image 2, then the free area through which passing is allowed can be obtained. At the same time, after the extraction process, the exact location of the obstacle can also be determined. The stereo views of environment with obstacles imaged by vision system and the dot image showing the free area are shown in Figure 7.11a, 7.11b and 7.11c, respectively.

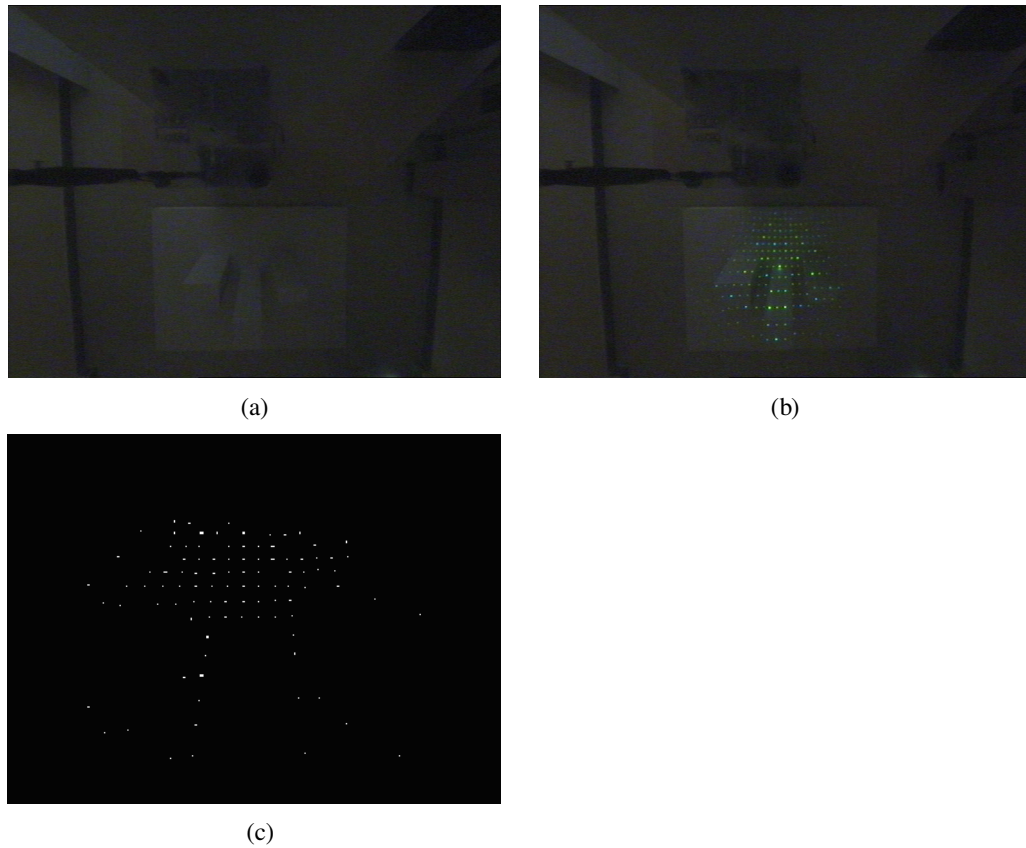
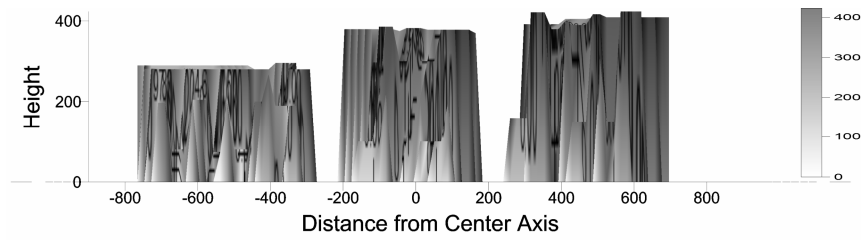
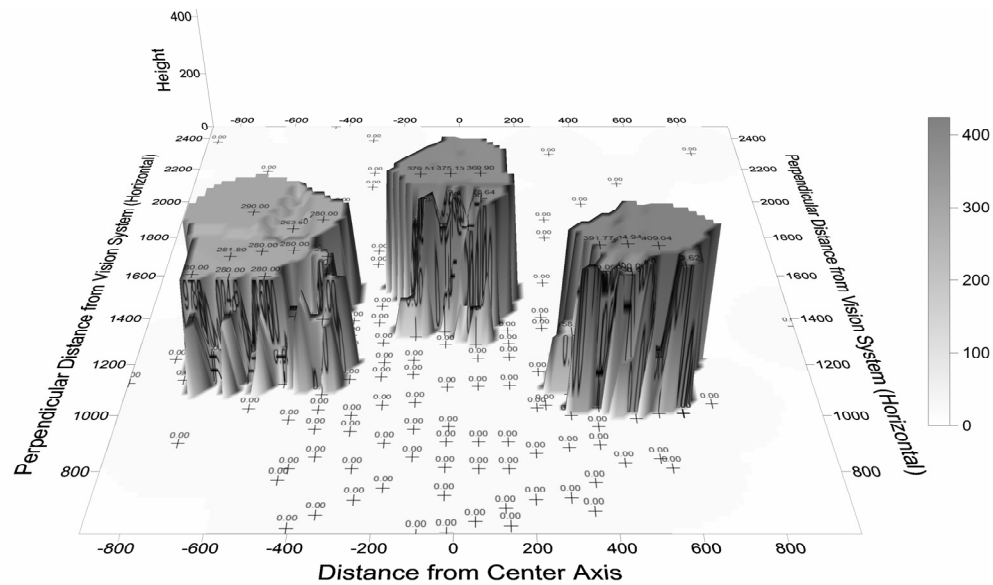


Figure 7.11 *Mask* (a), *base* (b) and close view of *free area dot* (c) images for environment with three obstacles

The approximate shapes and locations of the obstacles are given in Figure 7.12a and 12b). The shape construction was realized by a construction software package by using Nearest Neighbor method using the 3D points.



(a)



(b)

Figure 7.12 3D structure for experiment with three obstacles: front (a) and perspective (b) views

7.3 Experiments for Mobile Robot

The integrated mobile robot consists of tilt sensor and joystick (keyboard) as HCIs and omni-directional vision system to achieve behavior of safe navigation in the environment by sensing the environment and making decision of route without any obstacle.

First, some experiments were implemented for the mobile robot with tilt sensor and joystick options and without omni-directional vision. After achieving sufficient control of the robot with the HCIs, the omni-directional vision system will be included in the robot and the experiments for the whole integrated system will be carried out.

The direction of the robot and the velocities of the motors will be determined by using kinematics mentioned in Section 3.3 according to the obstacle information obtained by using omni-directional vision system.

After the experiments carried out, a calibration procedure for both of the motors is seen to be necessary in order to get the mobile robot to follow the desired route and to overcome the errors arisen in the estimation of path length.

CHAPTER EIGHT

CONCLUSIONS

In this study, an autonomous mobile robot was constructed to enhance the mobility of disabled people by integrating a mobile platform including two actuator wheels with an omni-directional vision system, tilt sensor and joystick. The omni-directional vision system consists of two mirror-camera pairs and a laser light source with a fiber grating device to sense the environment with wide field of three dimensional view. The tilt sensor and the joystick are the options of human computer interface to control the wheelchair movement with the user command. The locations of the obstacles in the environment which are obtained by processing the stereo images captured by the vision system are used for safe navigation in the determined route to the target area.

8.1 Omni-directional Vision System

In order to localize and map the obstacles in the environment with a wide field of view imaging, the stereo omni-directional vision system of the mobile robot with two curved mirrors having rectilinear projection and two CCD cameras was developed.

For obtaining the obstacles in the environment, a dot matrix laser pattern, which is obtained by a FGD with diffracted green laser light, was projected to the environment. The locations of the laser dots were found by using a mathematical model developed for constructing approximate 3D structure of the environment including the obstacles. The model was based on the locations of matched pixels in stereo images for calculating the distance of the laser dot from the vision system.

The constructed vision system was tested by two ways, manual and polynomial matching of the pixels in the images. The errors obtained after the experiments done with manual matching were found to be high. Especially the error rates in Z axis were mostly higher than 10%. In order to find the correspondences in the stereo images and to calibrate the longitude and incidence angles to reduce the error rates, a

polynomial based matching algorithm was developed. The vision system was tested again with the developed matching model. Although the average of error rates was reduced, it was still higher than expected. The matching based calibration can be used especially for curved mirror with indefinite surface profile and stereo vision system including mirrors which are not similar physically.

After the preliminary studies carried out, the vision system was improved by achieving better alignment of camera-mirror pairs and the distance between the pairs was increased in order to obtain better accuracy in distance calculations. An error estimation model in terms of pixel locations in the images was also developed to see the effect of corrupted row and column values of the pixels on the error rates. The experiments for testing the improved vision system were carried out with synthetic data and real data.

During the experiments, it was seen that errors were occurred depending on the limitation of the image sensors for the pixels in the images without noisy locations. After the pixel locations were distorted by adding randomly generated value to their row and column values, the resultant errors were increased. When the pixel locations in both images had distortion effect, then the errors were reached to significant values. Due to the decreasing resolution to the center of the mirror, the errors for the pixels closer to the center of the mirror were found to be high. The errors were decreased for the horizontal planes with the decreasing vertical distance from the vision system. It was also seen that the error rates were also increased with the increasing distance from the center axis (Y).

After the experiments done with real data, it was seen that the error rates for all axes were dependant to the distance between the vision system and laser dots which are on the same horizontal or vertical plane in the environment. However, the average error rates for X (range) and Z (height) were decreased to 2.02% and 3.14% from 2.41% and 4.13%, respectively with the increasing distance between the vision system and horizontal/vertical planes. Since the Z (height) value is calculated by the equation using the X and Y values, it is directly affected from their error rates. By

using the vision system developed in this study, it was found that wider area in the environment can be sensed and the error rates are lower when compared with the other omni-directional camera system (Orghidan et al., 2005 and Orghidan et al., 2007). Besides, the error rates obtained in different studies were strictly increased with the increasing distance from the vision system, however, in the developed system, the error rates were decreased with the increasing distance.

Since the center axis (Y) is taken as reference for calculating lateral error, for the dots nearby the axis, the lateral errors have relatively higher values than the errors of the perpendicular axis (X). The comparison of X and Y axes errors was meaningful since they were calculated with the same mathematical relations. The trends of error rate were almost similar for the vertical plane location on which the vision system can detect the laser dots with better view than the ones for horizontal plane.

The error rates determined for the common region in the environment for both experiment types done for synthetic and real data were lower than the rates for real data, as expected.

The variation in accuracy is dependant mainly on the size of the laser dots and the viewpoint of the vision system. The smaller the size of the laser dot and the better the view point of the vision system to image the laser dot, higher will be the accuracy of detecting the laser center.

The accuracy was affected by the limitation of the image resolution, alignment of the mirror-camera pairs, reflection errors on the mirrors due to the roughness of the surface profile and sensitivity of the refractive lens used in the system.

By using the developed system, when sufficient number of laser dots on the obstacle can be obtained, the 3D structure of an obstacle can easily be constructed. However, greater the number of laser dots reflecting from the objects, greater will the quality of the constructed 3D image. Also, the computational cost will increase with the increase in the number of dots.

8.2 Integrated Mobile Robot

The navigation platform of the wheelchair was equipped with the omni-directional vision system for sensing the environment and tilt sensor and keyboard (for joystick option) as HCIs to control the movement of the mobile robot.

After testing each component of the system independently, components were assembled and tested. The movement control of the mobile robot according to the kinematics and the experiments for the whole system integrated with the other components were realized in the environment including obstacles.

During the studies done with the integrated system, it was seen that the obstacles could be detected and the mobile robot could be directed according to the free area in the environment.

8.3 Future Work

In order to minimize the error rates in distance calculations, the resolution of the mirror camera pairs should be increased and the alignment system of the mirror-camera pairs will be improved. The accuracy can also be improved by emitting more focused and similar sized laser dots from laser light source with Fiber Grating Device. Since the developed system includes only one Fiber Grating Device which scatters laser points only in front of the vision system, an additional optical system will be developed to scatter the laser dots around the vision system to obtain the whole scene information. However, the visible laser has some problems on the working environment; the usage of infrared lasers will be investigated for vision systems.

The sensing area of the environment is limited since the dot-matrix laser pattern can be scattered to a particular field of the environment. Therefore construction of an optical system to scatter the laser pattern to the whole surrounding of the wheelchair can be the solution for the limited field of view problem.

A new study including only one mirror-camera pair can be proposed for sensing the environment.

The omni-directional vision study may include analyzing the resolution of the mirror with respect to the location of the pixel on the mirror surface with a non-equidistance mirror type such as hyperbolic mirror.

A mobile robot, which is able to follow the shortest and safe route towards the target area decided by the user, in the structurally known environment can be developed. Another study can also be carried out in order to develop a mobile robot which is controlled by the user and able to navigate through the obstacles in the structurally unknown environment by considering its dimensions.

REFERENCES

- Adachi, Y., Tsunenari, H., Matsumoto, Y., & Ogasawara, T. (2004). Guide robot's navigation based on attention estimation using gaze information. *Proceeding of the IEEE/RSJ International Conference on Intelligent Robots and Systems (IROS 2004), 1*, 540.
- Aizawa, K., Sakaue, K., & Suenaga, Y. (2004). Omnidirectional Sensing and Its Applications. *Image Processing Technologies: Algorithms, Sensors, and Applications*, (116-141). New York Basel: Marcel Dekker Inc.
- Azevedo, T., Tavares, J.M.R.S., & Vaz, M.A.P. (2009). 3D Object Reconstruction from Uncalibrated Images Using an Off-the-Shelf Camera. *Advances in Computational Vision and Medical Image Processing, Computational Methods in Applied Sciences, 13*, 117-136.
- Azevedo, T., Tavares, J.M.R.S. & Vaz, M.A.P. (2010). Three-dimensional reconstruction and characterization of human external shapes from two-dimensional images using volumetric methods. *Computer Methods in Biomechanics and Biomedical Engineering, 13* (3), 359-369.
- Baker, S., & Nayar, S. (1999). A theory of single-viewpoint catadioptric image formation. *International Journal of Computer Vision, 35* (2), 175-196.
- Barea, R., Boquete, L., Mazo, M., Lopez, E., & Bergasa, L.M. (2000). EOG guidance of a wheelchair using neural networks. *Proceeding of the 15th IEEE International Conference on Pattern Recognition, 4*, 668-671.
- Bastanlar, Y., Temizel, A., Yardimci, Y., & Sturm, P. (2010). Effective Structure-from-Motion for hybrid camera systems. *20th IEEE International Conference on Pattern Recognition*, 1654-1657.

- Bauckhage, C., Kaster, T., Rotenstein, A. M., & Tsotsos, J. K. (2006). Fast learning for customizable head pose recognition in robotic wheelchair control. *Proceeding of the 7th IEEE International Conference on Automatic Face and Gesture Recognition*, 311-316.
- Biber, P., Fleck, S., & Duckett, T. (2005). 3D Modeling of Indoor Environments for a Robotic Security Guard. *IEEE Computer Society Conference on Computer Vision and Pattern Recognition – CVPR Workshops*, 124-130.
- Chang, Y., Kuwabara, H., & Yamamoto, Y. (2008). Novel Application of a Laser Range Finder with Vision System for Wheeled Mobile Robot. *IEEE/ASME International Conference on Advanced Intelligent Mechatronics*, 280-285.
- Charles, J.R. (1997). *Wide Angle Eclipse Photography*. Retrieved September 13, 2010, from <http://www.eclipsechaser.com/eclink/image/widetechn.htm>.
- Chen, Y. L., Chen, S. C., Chen, W. L., & Lin, J. F. (2003). A head orientated wheelchair for people with disabilities. *Disability and Rehabilitation*, 25 (6), 249-253.
- Correa, F.R., Guizilini, V.C., & Junior, J.O. (2006) Omnidirectional stereovision system with two-lobe hyperbolic mirror for robot navigation. *ABC M Symposium Series in Mechatronics*, 2, 653-660.
- Court, H. (2008). *Chrysler Museum Wedding Photography*. Retrieved April 9, 2011, from <http://www.ononblog.com/wedding/chrysler-museum-wedding-photography-huber-court-photos/>
- Çebi, Y., Gürkahraman, K., & Ünsal, E. (2009). *Eğrisel ayna ve matris desenli lazer noktalar kullanarak çevrenin üç boyutlu yapısını oluşturan tümyönlü (omni directional) bir görüntüleme sisteminin geliştirilmesi*. TÜBİTAK Proje Sonuç Raporu, Proje No: 108E156.

- Dellaert, F., Seitz, S.M., Thorpe, C.E. & Thrun, S. (2000). Structure from Motion without Correspondence. *Proceedings. IEEE Conference on Computer Vision and Pattern Recognition*, 2, 557-564.
- Dual axis tilt sensor, (n.d.). Retrieved March 21, 2011, from <http://news.thomasnet.com/fullstory/Dual-Axis-Tilt-Sensor-acts-as-stand-alone-inclinometer-450765>.
- Duan, Z., & Cai, Z. (2008). Robust simultaneous localization and mapping based on laser range finder with improved adaptive particle filter. *Control and Decision Conference, (CCDC)*, 2820-2824.
- Edlinger, G., & Guger, C. (2005). Laboratory PC and mobile pocket PC brain-computer interface architectures. *Proceeding of the 2005 IEEE Engineering in Medicine and Biology 27th Annual Conference*, 5347-5350.
- Faria, P. M., Braga, R. A. M., Valgode, E., & Reis, L. P. (2007). Interface Framework to Drive an Intelligent Wheelchair Using Facial Expressions. *IEEE International symposium on Industrial Electronics*, 1791-1796.
- Faugeras, O. (1993). *Three-dimensional computer vision: A geometric viewpoint*. MIT Press.
- Gasparri, A., Panziera, S., Pascucci, F., & Ulivi, G. (2007). A hybrid active global localization algorithm for mobile robots. *IEEE International Conference on Robotics and Automation*, 3148-3153
- Gluckman, J., & Nayar, S. K. (1999). Planar catadioptric stereo: geometry and calibration. *IEEE Conference on Computer Vision and Pattern Recognition (CVPR)*, (1), 22-28.

- Gluckman, J., & Nayar, S. K. (2002). Rectified catadioptric stereo sensors. *IEEE Transactions on Pattern Analysis and Machine Intelligence*, 24 (2), 224-236.
- Gluckman, J., Nayar, S. K., & Thoresz, K.J. (n.d.). *Real-Time Omnidirectional and Panoramic Stereo*. Retrieved April 19, 2011, from http://www1.cs.columbia.edu/CAVE/publications/pdfs/Gluckman_IUW98_2.pdf
- Habib, M. K. (2007). Fiber-grating-based vision system for real-time tracking, monitoring and obstacle detection. *IEEE Sensors Journal*, 7 (1), 105- 121.
- Hartley, R. & Zisserman, A. (2003). *Multiple View Geometry in Computer Vision*. Cambridge University Press, 2nd Edition.
- Hashimoto, M., Takahashi, K., & Shimada, M. (2009). Wheelchair Control Using an EOG- and EMG-Based Gesture Interface. *IEEE/ASME International Conference on Advanced Intelligent Mechatronics*, 1212-1217.
- Hu, Z., Li, L., Luo, Y., Zhang, Y., & Wei, X. (2010). A novel intelligent wheelchair control approach based on head gesture recognition. *IEEE Conference on Computer Application and System Modelling (ICCASM)*, 6, 159-163.
- Joseph, T., & Nguyen, H. (1998). Neural network control of wheelchair using telemetric head movement. *Proceeding of the 20th Annual International Conference of IEEE Engineering in Medicine and Biology Society*, 20 (5), 2731-2733.
- Kang, S., & Katupitiya, J. (2004). A hand gesture controlled semi-autonomous wheelchair. *IEEE Conference on Intelligent Robots and Systems (IROS 2004)*, 4, 3565-3570.

- Karray, F., Alemzadeh, M., Saleh, J.A., & Arab, M.N. (2008). Human-Computer Interaction: Overview on State of the Art. *International Journal on Smart Sensing and Intelligent Systems*, 1 (1).
- Kim, J., & Suga, Y. (2007). An Omnidirectional Vision-Based Moving Obstacle Detection in Mobile Robot. *International Journal of Control, Automation, and Systems*, 5 (6), 663-673.
- Komiya, K., Morita, K., Kagekawa, K., & Kurosu, K. (2000). Guidance of a wheelchair by voice. *Proc. IECON*, 102-107.
- Kriegman, D.J., Triend, E., & Binford, T.O. (1989). Stereo vision and navigation in buildings for mobile robots. *IEEE Transactions on Robotics and Automation*, 5, 792-803
- Kweon, G., Hwang-Bo, S., Kim, G., Yang, S., & Lee, Y. (2006). Wide-angle catadioptric lens with a rectilinear projection scheme. *Applied Optics*, 45 (34), 8659-8673.
- Kweon, G., Kim, K., Choi, Y., Kim, G., Kim, H., & Yang, S. (2004). A catadioptric double-panoramic lens with the equi-distance projection for a rangefinder application. *Proceedings of SPIE, Bellingham, WA*, 5613, 29-42.
- Lakany, H., & Conway, B. A. (2005). Classification of wrist movement using EEG-based wavelets features. *Proceeding of the 2005 IEEE Engineering in Medicine and Biology 27th Annual Conference*, 5404-5407.
- McInerney, T. & Terzopoluos, D. (1996). Deformable Models in Medical Image Analysis: A Survey. *Medical Image Analysis*, 1 (2), 91-108.

- Montesano, L., Diaz, M., Bhaskar, S., & Minguez, J. (2010). Towards an Intelligent Wheelchair System for Users With Cerebral Palsy. *IEEE Transactions on Neural Systems and Rehabilitation Engineering*, 18 (2), 193-202.
- Moon, I., Lee, M., Ryu, J., & Mun, M. (2003). Intelligent robotic wheelchair with EMG-, gesture-, and voice-based interfaces. *Proceeding of the IEEE/RSJ International Conference on Intelligent Robots and Systems (IROS 2003)*, 3, 3453-3458.
- Murata, A. (1991). An experimental evaluation of mouse, joystick, joycard, lightpen, trackball and touchscreen for Pointing – Basic Study on Human Interface Design. *Proceedings of the Fourth International Conference on Human-Computer Interaction 1991*, 123-127.
- Nakazawa, K., & Suzuki, C. (1991). Development of 3-D robot vision sensor with fiber grating: fusion of 2-D intensity image and discrete range Image. *International Conference on Industrial Electronics, Control and Instrumentation, (IECON '91)*, 3, 2368-2372.
- Nanophotonics. (n.d.). *Fisheye lens*. Retrieved September 13, 2010, from http://www.nanophotonics.kr/html_shop/en_shop_list_fisheye.htm
- Nayar, S. K. (1997). Catadioptric omnidirectional camera. *Proceeding of IEEE Conf. On Computer Vision and Pattern Recognition*, 482-488.
- Nene, S. A., & Nayar, S. K. (1998). Stereo with Mirrors. *Proceedings of the 6th International Conference on Computer Vision*, 1087-1094.
- Orghidan, R., Mouaddib, E.M., & Salvi, J. (2005). Omnidirectional Depth Computation from a Single Image. *Proceedings of the 2005 IEEE International Conference on Robotics and Automation*, 1222-1227.

- Orghidan, R., Mouaddib, E.M., Salvi, J., & Serrano, J.J. (2007). Catadioptric single-shot rangefinder for textured map building in robot navigation. *IET Computer Vision*, 1 (2), 43-53.
- Ronzhin, A., & Karpov, A. (2005). Assistive multimodal system based on speech recognition and head tracking. *Proceedings of 13th European Signal Processing Conference, Antalya*.
- Shimizuhira, W., & Maeda, Y. (2003). Self-Localization method used multiple omnidirectional vision system. *SICE Annual Conference, Fukui, Japan, 1*, 324-327.
- Siebert, J.P. & Marshall, S.J. (2000). Human Body 3D Imaging by Speckle Texture Projection Photogrammetry. *Sensor Review*, 20 (3), 218-226.
- Simpson, R. C., & Levine, S. P. (2002). Voice control of a powered wheelchair. *IEEE Transactions on Neural Systems and Rehabilitation Engineering*, 10 (2), 122–125.
- Southwell, D., Basu, A., Fiala, M., & Reyda, J. (1996). Panoramic stereo. *In Proceedings of International Conference on Pattern Recognition, 1*, 378-382.
- Spacek, L. (2007). *Catadioptric image of Praque*. Retrieved September 13, 2010, from <http://cswww.essex.ac.uk/mv/images.html>.
- Su, L., Luo, C., & Zhu, F. (2006) Obtaining obstacle information by an omnidirectional stereo vision system. *IEEE International Conference on Information Acquisition*, 48-52.
- Svoboda, T., Pajdla, T., & Hlavac, V. (1998). Epipolar Geometry for Panoramic Cameras. *Fifth European Conference on Computer Vision*, 218-232.

- Swokowski, E.W., Olinick, M., & Pence, D. (1994). *Calculus* (6th edition). PWS Publishing Company.
- Tamagawa, K., Ogawa, K., & Nakajima, M. (2002) Detection of respiratory movement during SPECT/PET data acquisition. *IEEE Nuclear Science Symposium Conference Record*, 3, 1571-1574.
- Tanaka, K., Matsunaga, K., & Wang, H. O. (2005). Electroencephalogram-Based control of an electric wheelchair. *IEEE Transactions on Robotics*, 21 (4), 762-766.
- Tilt sensors, (n.d.). Retrieved September 13, 2010, from <http://www.sysacom.com/Products/USBDualAxisTiltAcellSensor/GS311USB-00.pdf>
- Ukida, H., Yamato, N., Tanimoto, Y., Sano, T., & Yamamoto, H. (2008). Omnidirectional 3D measurement by hyperbolic mirror cameras and pattern projection. *Proceedings of IEEE on Instrumentation and Measurement Technology Conference (IMTC)*, 365-370.
- Wang, J.H., & Hsiao C.P. (1996). Stereo matching by neural network that uses Sobel Feature data. *IEEE International Conference on Neural Networks*, 3, 1801-1806.
- Yagi, Y., & Yachida, M. (1991). Real-Time generation of environmental map and obstacle avoidance using omnidirectional image sensor with conic mirror. *Proc. CVPR*, 160-165.
- Yagi, Y. (1999). Omnidirectional Sensing and Its Applications. *IEICE Transactions on Information and Systems*, E82-D (3), 568-579.

- Yagi, Y., & Yachida, M. (2002). Omnidirectional sensing for human interaction. *Proceeding of the Third IEEE Workshop on Omnidirectional Vision (OMNIVIS'02)*, 121-127.
- Yamaguchi, J., & Nakajima, M. (1990). A 3D shape identification system using a fiber grating vision sensor. *Industrial Electronics Society, IECON '90, 16th Annual Conference of IEEE, 1*, 507-511.
- Zhang, Z. (1998). Determining Epipolar Geometry and Its Uncertainty: A Review. *International Journal of Computer Vision*, 27 (2), 161-195.
- Zhang, Z. (2000). A flexible new technique for camera calibration. *IEEE Transactions on Pattern Analysis and Machine Intelligence*, 22 (11), 1330-1334.
- Zhao, G. (2005). *Serial communication with GS311 series of sensors*. Retrieved September 13, 2010, from <http://www.sysacom.com/Products/DualAxisSensor/03028APN01-01.pdf>